Mitochondrial localization and function of the lysosomal enzyme glucocerebrosidase

Dissertation

zur Erlangung des Grades eines
Doktors der Naturwissenschaften

der Mathematisch-Naturwissenschaftlichen Fakultät
und
der Medizinischen Fakultät
der Eberhard-Karls-Universität Tübingen

vorgelegt
von

Pascale Baden
aus Ettelbrück, Luxemburg

2023

Tag der mündlichen Prüfung: 07.06.2023

Dekan der Math.-Nat. Fakultät: Prof. Dr. Thilo Stehle

Dekan der Medizinischen Fakultät: Prof. Dr. Bernd Pichler

1. Berichterstatter: Prof. Dr. Dr. Michela Deleidi

2. Berichterstatter: PD Dr. Christian Johannes Gloeckner

Prüfungskommission: Prof. Dr. Dr. Michela Deleidi

PD Dr. Christian Johannes Gloeckner

Prof. Dr. Thomas Gasser

Prof. Dr. Doron Rapaport

Erklärung / Declaration:

Ich erkläre, dass ich die zur Promotion eingereichte Arbeit mit dem Titel: „Mitochondrial localization and function of the lysosomal enzyme glucocerebrosidase“ selbständig verfasst, nur die angegebenen Quellen und Hilfsmittel benutzt und wörtlich oder inhaltlich übernommene Stellen als solche gekennzeichnet habe. Ich versichere an Eides statt, dass diese Angaben wahr sind und dass ich nichts verschwiegen habe. Mir ist bekannt, dass die falsche Abgabe einer Versicherung an Eides statt mit Freiheitsstrafe bis zu drei Jahren oder mit Geldstrafe bestraft wird.

I hereby declare that I have produced the work entitled “Mitochondrial localization and function of the lysosomal enzyme glucocerebrosidase”, submitted for the award of a doctorate, on my own (without external help), have used only the sources and aids indicated and have marked passages included from other works, whether verbatim or in content, as such. I swear upon oath that these statements are true and that I have not concealed anything. I am aware that making a false declaration under oath is punishable by a term of imprisonment of up to three years or by a fine.

Tübingen, den ....

Datum / Date Unterschrift /Signature

Content

Statement of contribution

Most data of the thesis were included in a manuscript submitted to Nature Communications. The preprint entitled: “Glucocerebrosidase, a Parkinson´s disease-associated protein, is imported into mitochondria and regulates complex I assembly and function” was published on Research Square (doi.org/10.21203/rs.3.rs-1521848/v1). The paper was resubmitted after major revision with the title: “Glucocerebrosidase, a Parkinson´s disease-associated protein, is imported into mitochondria and preserves complex I integrity and energy metabolism”. Resubmission was accepted and published under a CC-BY 4.0 license (Baden et al., 2023). Part of the data was already presented in Anna-Lena Katja Krines’ (ALK) Bachelor thesis with the title: “Characterization of tagged glucocerebrosidase overexpression in HEK and neural precursor cells”. The data consist of Fig. 5-1 A and Fig. 5-3 A-B.

Personal contribution

I performed most experiments and collected most data shown in the thesis. I designed experiments and analyzed the data with help from Michela Deleidi (MD). I wrote and prepared the first draft of the manuscript and figures. For the following figures, I had support: For Fig. 5-9, Fig. 5-10 cloning and site directed mutagenesis were done by Stefanie Kalb (SK). The immunoblots in Fig. 5-4 D, Fig. 5-15, Fig. 5-18 E, Fig. 5-22 C and Fig. 5-27 were performed with support from SK. The endogenous co-IP of GCase with LONP1 (Fig. 5-12 C) was performed by SK with my support. Gabriele Di Napoli supported the characterization of iPSC lines, Fig. 5-17 E. Sorting of nucleofected cells in Fig. 5-21 was done together with Kristin Bieber. Claudio Giuliano helped with the immunofluorescent staining and imaging in Fig. 5-19 and Fig. 5-24. The volcano plots (Fig. 5-4 A-C, Fig. 5-6) were generated based on initial LC-MS data analysis by Frank Stein (FS). The analysis of LC-MS results using String V.11 in Fig. 5-5 D was performed with the help of María José Pérez.

Further contributions from others to my thesis

MD supervised the PhD thesis, obtained the funding for the PhD position and experimental work, and reviewed the thesis. The Proteomic Core Facility (EMBL) processed and labelled the eluates and lysates for LC-MS analysis and did the measurements (Mandy Rettel and Per Haberkant). FS did the initial bioinformatic analysis and was involved in the initial discussion of the LC-MS data. Fibroblast from MIGAP study were provided by Thomas Gasser and Kathrin Brockmann. Christian Johannes Gloeckner provided the pcDNA^{TM}3 plasmid. Empty T-Rex HEK cells and necessary plasmids were provided by Manuela Neumann. Chiara Valori supported with advice on cloning and inducible T-Rex HEK cell line generation. Initial discussion of GCase trafficking into mitochondria was done with Johannes Martin Herrmann. The plasmids from the Mission library were gifted by Joachim Täger. Blue native gel from figure 5-28 was generated by Maria Illescas Garcia (Cristina Ugalde’s lab).

1 Summary

1.1 Zusammenfassung

Biallelische Mutationen im Gen *GBA1*, welches das lysosomale Enzyme Glukozerebrosidase (GCase) codiert, führen zu unzureichendem GCase Proteinlevel in der Gaucher-Krankheit (GD). Vor kurzem wurden Mutationen in *GBA1* zum größten Risikofaktor für die Parkinson-Krankheit (PD) und andere Synucleinopathien identifiziert. Im Lysosom, katalysiert GCase die Hydrolyse von Glucosylceramid (GlcCer), einem Glycosphingolipid (GLS) der Membran, zu Ceramid und Glukose, sowie von Glucosylsphingosine zu Glukose und Sphingosine. Interessanterweise wird eine Reduktion der GCase Aktivität auch bei sporadischer PD und beim Altern beobachtet. Bislang ist der Mechanismus, der in Trägern von *GBA1* Mutationen zur Neurodegeneration führt, noch nicht aufgeklärt worden. Um diesen Mechanismus zu untersuchen, haben wir das Interaktom von Wildtyp (WT) und mutiertem GCase untersucht. Hierfür haben wir ein induzierbares T-Rex HEK Zellen Model für die Überexpression von V5-Flag-Tag gekennzeichnetem WT, p.E326K, oder p.L444P GCase erstellt. Wir haben diese beiden Mutationen ausgewählt, da einerseits die p.L444P eine schwerwiegende Mutation ist, welche zu einer neuropathischen Form von GD führt und eine der häufigsten *GBA1*-PD Mutationen ist. Andererseits, weil die p.E326K zu den weitverbreitetsten *GBA1*-PD Mutationen gehört, jedoch im Gegensatz zu anderen *GBA1* Mutationen, führen p.E326K homozygote Mutationen nicht zu GD. Das GCase Modell wurde auf Basis der Analyse der GCase Expressions- und Aktivitätslevel, sowie der Colokalisation mit dem lysosomalen Marker, LAMP1, validiert. Wir führten eine Ko-Immunpräzipitation vom Flag-Tag durch und analysierten die Eluate mit quantitativer Tandem Mass Tag Flüssigchromatographie mit Massenspektrometrie. Interessanterweise sind 13.3% der Interaktoren von GCase mitochondriale Proteine. Da die mitochondriale Dysfunktion schon zuvor im Zusammenhang mit *GBA1* Mutationen stand, haben wir einen direkten Zusammenhang zwischen den *GBA1* Mutationen und der mitochondrialen Dysfunktion untersucht. Als Erstes haben wir die mitochondriale Lokalisation von GCase durch Split-GFP Experimente bestätigt. Hierbei führt die Interaktion zwischen Matrix gezieltem GFP1-10 und WT oder mutiertem GBA1-GFP-S11ß zu einem grün fluoreszierendem Signal. Wir zeigen, dass GCase mit Hilfe von HSC70, dem Translokase der äußeren mitochondrialen Membrane (TOM)- und Translokase der inneren mitochondrialen Membrane (TIM)-Komplex, in die Mitochondrien importiert wird. Die Entfernung der internen Mitochondrien Matrix Targeting ähnlichen Sequenz (iMTS-ls) verhindert den Import von GCase in Mitochondrien. Außerdem haben wir eine erhöhte Interaktion zwischen LONP1 und HSP60 mit dem mutierten GCase Protein nachgewiesen. Dies deutet darauf hin, dass das mutierte Protein in Mitochondrien neu gefaltet oder abgebaut wird. Des Weiteren gibt es eine reduzierte Interaktion zwischen mutiertem GCase und TIMMDC1, welches in Mitochondrien in der Komplex I (CI) Zusammensetzung involviert ist,

sowie NDUFA10, einer CI Untereinheit. Um diese Resultate in einem relevanten Modell für *GBA1*-PD zu validieren, haben wir induzierte pluripotente Stammzellen (iPSC) von p.L444P und p.E326K heterozygoten PD Patienten Fibroblasten generiert. Als nächstes haben wir mithilfe von Genome Editing (Zinkfingernuklease und CRISPR-Cas9) die dazugehörigen isogenen gen-korrigierten Kontrollen erzeugt. Die Gen-Korrektur hat das Proteinlevel und die Aktivität von GCase verbessert. Das Differenzierungspotential zu Mittelhirn-Dopaminergen (mDa) Neuronen unterschied sich nicht zwischen mutierten Zellen und Gen korrigierten isogenen Kontrollen. Die Interaktion zwischen HSP60 und LONP1 mit endogenem GCase wurde per Ko-Immunpräzipitation im Lysate von neuronalen Vorläuferzellen (NPCs) verifiziert. Präliminäre Daten deuten darauf hin, dass es Defekte im CI Zusammenbau in *GBA1* mutierten und Knockout NPCs und mDa Neuronen gibt. Die Migration von GCase in die Mitochondrien zu verbessern, könnte ein therapeutisches Ziel darstellen, da die Überexpression von GCase die mitochondriale Funktion in T-Rex HEK Zellen verbessert hat. Unsere Daten liefern erste Beweise für eine neue Rolle von GCase in Mitochondrien, und zeigen seine potentielle Rolle in der Erhaltung der CI Integrität, möglicherweise durch die Stabilisation von TIMMDC1.

1.2 Summary

Biallelic mutations in the *GBA1* gene, which encodes the lysosomal enzyme glucocerebrosidase (GCase), cause the lysosomal storage disease Gaucher's disease (GD). These mutations have been recently identified as the strongest risk factor for Parkinson's disease (PD) and other synucleinopathies. In the lysosome, GCase catalyzes the hydrolysis of glucosylceramide (GlcCer), a membrane glycosphingolipid (GSL), to ceramide and glucose and of glucosylsphingosine to glucose and sphingosine. Interestingly, a reduction in GCase activity has also been observed in sporadic PD as well as with ageing. The mechanisms leading to neurodegeneration in *GBA1* carriers remain unclear. To explore the mechanisms involved in *GBA1*-linked neurodegeneration, we assessed the interactome of wild-type (WT) and mutant GCase. To this end, we developed an inducible T-Rex HEK cell model overexpressing V5-Flag-tagged WT, p.E326K, or p.L444P mutant GCase. We chose these two mutants as p.L444P is a severe mutation leading to a neuropathic form of GD and as it is one of the most common severe *GBA1*-PD mutations. p.E326K is another common mutation in *GBA1*-PD. However, unlike most other *GBA1* mutations, p.E326K homozygous mutations on their own are not linked to GD. The overexpression model was validated by the analysis of GCase expression and protein level, as well as co-localization with the lysosomal marker LAMP1. We performed Flag co-immunoprecipitation and analyzed the eluates by quantitative tandem mass tag liquid chromatography mass spectrometry. Interestingly, we found that 13.3% of GCase interactors are mitochondrial proteins. As mitochondrial dysfunction has previously been linked to *GBA1*, we further explored a potential direct link between GCase and mitochondrial dysfunction. First, we validated the mitochondrial localization of GCase by split-

GFP experiments, in which the interaction between mitochondrial matrix targeted GFP1-10 and WT and mutant GBA1-GFP-S11ß lead to green fluorescence. We demonstrated that the import of GCase into the mitochondrial matrix is HSC70, translocase of outer mitochondrial membrane (TOM)-, and translocase of inner mitochondrial membrane (TIM)-complex dependent. Removal of the internal mitochondrial targeting like sequences prevented import of GCase into mitochondria. In addition, we found an increased interaction between HSP60 and LONP1 with mutant GCase, suggesting their potential role in the refolding or degradation of mutant GCase in mitochondria. Furthermore, we found a decreased interaction of mutant GCase with the complex I (CI) assembly factor TIMMDC1 and the CI subunit NDUFA10. To validate these results in a model relevant to *GBA1*-PD, we generated induced pluripotent stem cells (iPSCs) from p.L444P and p.E326K heterozygous PD patients' fibroblasts. Next we employed genome editing (zinc finger nucleases and CRISPR-Cas9) to generate corresponding isogenic gene-corrected controls. Gene-correction rescued GCase protein level and activity. Mutant and isogenic controls did not show differences in midbrain neuron differentiation potential. The interaction with HSP60 and LONP1 was validated by co-immunoprecipitation with endogenous GCase in neural precursor cell (NPC) lysates. Preliminary data point towards CI assembly defects in mutant and *GBA1* KO NPCs as well as midbrain neurons. These data confirm the potential involvement of GCase in CI assembly. Improving GCase trafficking to mitochondria could be a potential therapeutic target as overexpression of GCase improved mitochondrial dysfunction in T-Rex HEK cells. Our data provide evidence for a novel mitochondrial role of GCase, showing its potential involvement in the maintenance of CI integrity by modulating the stability of the assembly factor TIMMDC1.

2 Introduction

In the following section, an introduction to Parkinson's disease (PD) is provided and the mechanisms by which glucocerebrosidase (GCase) mutations contribute to PD with a special consideration for its effect on α-synuclein aggregation and mitochondrial dysfunction are described. Then an overview of GCase deficiency models is presented.

2.1 Parkinson's disease

Parkinson's disease (PD) belongs to the group of Lewy body (LB) disorders (Clark *et al*, 2009) and is one of the most common neurodegenerative diseases (Poewe *et al*, 2017). In the population over 65 years of age about 2-3% of the adults are affected by PD (Poewe *et al.*, 2017), with more males than females being affected (Pavelka *et al*, 2022; Wooten *et al*, 2004). Before diagnosis, some evidence of motor and non-motor symptoms might already be indicative for the risk of developing PD (Alarcón *et al*, 2020). In a small cohort, it was observed that people that were later on diagnosed with PD already showed signs like tremor of a limp, action dystonia or non-motor symptoms like depression or anxiety before the diagnosis (Alarcón *et al.*, 2020). These are partially characteristic symptoms of PD. The motor symptoms of PD include resting tremor, difficulties in the initiation of movement called akinesia, and rigidity (Caligiore *et al*, 2016; Dauer & Przedborski, 2003). Furthermore, movements are carried out more slowly which is called bradykinesia (Dauer & Przedborski, 2003). Higher motor symptom severity correlates with later age at onset (Pavelka *et al.*, 2022). Some patients show more severe tremor and others experience a more severe impact on gait and postural stability (Gong *et al*, 2018). Both patient groups present decreased GABA levels in the basal ganglia compared to control, whereas the GABA level is the most reduced in the group suffering more from tremor (Gong *et al.*, 2018). Furthermore, higher Hoehn and Yahr score within the first 5 years after diagnosis correlated with faster progression of motor and cognitive decline and was linked to the development of postural instability (Skidmore *et al*, 2022). There is a wide spectrum of non-motor symptoms. Surveys show that non-motor symptoms have a high prevalence in PD patients (Hermanowicz *et al*, 2019). Among the non-motor symptoms are constipation (Edwards *et al*, 1993; Garrido-Gil *et al*, 2018; Vascellari *et al*, 2021) and problems with swallowing and nausea (Edwards *et al.*, 1993). According to one survey, the most significant non-motor symptoms are sleep disorders and tiredness as well as cognitive deficits (Hermanowicz *et al.*, 2019). Furthermore, psychiatric symptoms like hallucinations, depression and anxiety are other motor symptoms encountered by a majority of PD patients (Hermanowicz *et al.*, 2019; Rana *et al*, 2018). Another important non-motor symptom is acute and chronic pain (Defazio *et al*, 2008; Nègre-Pagès *et al*, 2008). Non-motor symptoms might appear early on, within 3 years of diagnosis (Hermanowicz *et al.*, 2019). However, the frequency of non-motor symptoms increases with the duration of PD (Hermanowicz *et al.*,

2019). Early onset of cognitive symptoms might correlate with later age at onset (Pavelka *et al.*, 2022), low education and male gender (LaBelle *et al*, 2017). Not only do the non-motor symptoms impact the quality of life of the PD patient, but these symptoms impact even to a higher degree the care partners (Hermanowicz *et al.*, 2019). Non-motor symptoms often co-occur. A study has shown that poor sleep quality often went along with anxiety, depression, and pain (Rana *et al.*, 2018). There might be a link between severity of motor and non-motor symptoms. A small study in a Chinese cohort correlated bradykinesia with defects in the visuospatial and memory related tasks (Wang *et al*, 2017).

2.1.1 PD brain pathology

Pathologically, brains of PD patients present LBs and Lewy dendrites, which are mainly formed by α-synuclein aggregates but contain many other components as well as lipids, ubiquitin, enzymes and neurofilaments (Shahmoradian *et al*, 2019; Wakabayashi *et al*, 2013). In addition, mainly dopaminergic neuron degeneration is observed in the midbrain region called substantia nigra pars compacta (SNpc) (Caligiore *et al.*, 2016; Dauer & Przedborski, 2003), but it is not limited to degeneration of dopaminergic neurons (Dauer & Przedborski, 2003). Furthermore, pathology is not only limited to the central nervous system, but as well in the peripheral nervous system including α-synuclein deposition, reduction in nerve fibers and neuroinflammation (Ma *et al*, 2021). At the PD diagnosis, only approximately 30-50% of functional SNpc dopaminergic neurons are left (Dauer & Przedborski, 2003; Wen *et al*, 2020).

2.1.2 Genetics of PD

Familial PD counts only for 10-15% of PD patients (Ross *et al*, 2008). Already in 1997, an α-synuclein mutation leading to the exchange of the alanine to a threonine at position 53 (p.A53T) was discovered as cause for familial PD (Polymeropoulos *et al*, 1997). Triplication and duplication of the *SNCA* gene, coding for α-synuclein were next linked to PD (Chartier-Harlin *et al*, 2004; Singleton *et al*, 2003). Familial PD originating from α-synuclein mutations or multiplication causes early onset PD (Chartier-Harlin *et al.*, 2004; Polymeropoulos *et al.*, 1997; Singleton *et al.*, 2003). Some SNCA mutations are linked to cognitive decline (Puschmann *et al*, 2009). In individuals with a multiplication of SNCA, there seems to be a dosage effect between copy number and PD severity (Ross *et al.*, 2008). Some of the proteins associated with familial PD participate in the endocytic pathway. Mutations in LRRK2, like p.G2019S, p.R1441C, p.I2020T, p.I2012T, have been linked to autosomal dominant familial PD (Tomiyama *et al*, 2006; Zimprich *et al*, 2004). A mutation causing the change of an aspartate to an asparagine at position 620 in *VPS35* is linked to autosomal dominant late-onset PD (Zimprich *et al*, 2011). VPS35 is part of the complex responsible for the transport from endosomes back to the trans-Golgi network (Zimprich *et al.*, 2011). Furthermore, a point mutation in the gene encoding synaptojanin-1, important for the recycling of vesicles after

endocytosis, is linked to a recessive form of early onset PD (Quadri *et al*, 2013). Another protein causing hereditary recessive PD is ATP13A2, which is important for lysosomal function (Ramirez *et al*, 2006). In this case, the mutant protein is most likely retained in the ER and then undergoes proteasomal degradation (Ramirez *et al.*, 2006). Proteins that are important for mitochondrial function are as well linked to hereditary PD. Two of these proteins associated with autosomal recessive PD, are PINK1 (Hatano *et al*, 2004) and Parkin (Lücking *et al*, 2000). Homozygous deletion and point mutation in DJ-1 lead to early-onset familial PD (Bonifati *et al*, 2003). It was observed that the DJ-1 point mutation p.L166P results in a disturbed localization of cytosolic DJ-1 (Bonifati *et al.*, 2003). The DJ-1 p.L166P mutant is associated mainly with mitochondria (Bonifati *et al.*, 2003).

Not only are mutations in certain genes related to familial PD, many mutations are as well observed to increase the risk for PD (Chang *et al*, 2017; Simón-Sánchez *et al*, 2009). A genome wide association study on sporadic PD patients showed a correlation between variability in the SNCA, LRRK2, MAPT and PARK16 loci and increased risk for PD (Chang *et al.*, 2017; Simón-Sánchez *et al.*, 2009). LRRK2 mutations are observed in familial but as well in sporadic PD (Tomiyama *et al.*, 2006). In cellular models these mutations were shown to cause lysosomal dysfunction (Schapansky *et al*, 2018). In addition, mutations in lysosomal genes are associated with a higher risk to develop PD (Robak *et al*, 2017). Furthermore, different genes linked to lysosomal function or autophagy have as well been linked to higher risk for developing PD (Chang *et al.*, 2017). Among these are genes like *TMEM175*, *CTSB*, *ATP6V0A1*, *GALC* and *KAT8* (Chang *et al.*, 2017). Mutations in *TMEM175*, which encodes a protein involved in the acidification of lysosomes, have been linked to increased risk or protection to develop PD (Wie et al, 2021). The loss-of-function mutation of TMEM175 prevents proper lysosomal acidification (Wie *et al.*, 2021). Loss-of-function in murine primary TMEM175 heterozygous and homozygous knockout (KO) neurons leads to the accumulation of undigested autophagosomes, accumulation of α-synuclein and loss of tyrosine hydroxylase (TH) positive neurons along with deficits in tasks requiring coordination (Wie et al., 2021). p.M393T TMEM175 mutant PD patients seem to have a faster cognitive and motor decline progression (Wie et al., 2021). Genes belonging to certain lysosomal storage disorders are as well linked to PD. First example is Nieman's Pick disease which is caused by homozygous or compound heterozygous mutations in *NPC1* or *SMPD1* (Gan-Or *et al*, 2013; Kluenemann *et al*, 2013). Carriers of mutations in the lysosomal *NPC1* gene have been diagnosed with PD (Kluenemann *et al.*, 2013). Furthermore, analysis of 2 cohorts from Ashkenazi Jewish showed that the p.L303P mutation of SMPD1, which breaks down phosphocholine, increases the risk to develop PD by 9-fold (Gan-Or *et al.*, 2013). The second example is Fabry disease. The p.D313Y in the *GLA* gene, which encodes α-galactosidase A, is causing Fabry disease and seems to increase the risk for developing PD (Lackova et al, 2022). The lysosomal storage

disorder Sandhoff disease is caused by a deficiency of ß-hexosaminidase (Brekk et al, 2020). It was shown that overexpression of ß-hexosaminidase in an α-synuclein overexpression rat model, can rescue two main pathological hallmarks of PD, degeneration of dopaminergic neurons and accumulation of α-synuclein (Brekk et al., 2020). The most common mutations associated with increased risk for PD are located in the *GBA1* gene and are associated with the lysosomal storage disorder Gaucher Disease (GD) (Robak *et al.*, 2017; Sidransky *et al*, 2009).

2.2 GBA1, Gaucher Disease and the link to PD

2.2.1 Glucocerebrosidase (GCase)

GCase is a lysosomal hydrolase encoded by *GBA1*. 96% of the *GBA1* sequence is identical to the sequence of the pseudogene, *GBAP* (Horowitz *et al*, 1989). GCase is trafficked from the endoplasmic reticulum (ER) through the Golgi apparatus to the lysosome. GCase trafficking to the lysosome is facilitated by LIMP2 (Reczek *et al*, 2007). Both enzymes associate in the ER at neutral pH and as this interaction is pH-dependent, it dissociates when reaching the acidic pH in the lysosome (Reczek *et al.*, 2007). N-linked glycosylation of GCase starts already in the ER (Leonova & Grabowski, 2000). Along this migration pathway, the oligosaccharides are processed (Bergmann & Grabowski, 1989). Trafficking is not affected by glycosylation status of GCase (Leonova & Grabowski, 2000). However, it affects its activity (Berg-Fussman *et al*, 1993). Four of the five possible glycosylation sites are glycosylated in mature GCase (Berg-Fussman *et al.*, 1993; Bergmann & Grabowski, 1989; Erickson *et al*, 1985; Grace & Grabowski, 1990). In the lysosome, Saposin C facilitates the activity of GCase (Atrian *et al*, 2008), which breaks down glucosylsphingosine (GlcSph) and glucosylceramide (GlcCer) into glucose and sphingosine or glucose and ceramide respectively (Rocha *et al*, 2015a).

2.2.2 Gaucher Disease (GD)

GD is the most frequent lysosomal storage disorder (Neumann *et al*, 2009). It is caused by homozygous or compound heterozygous *GBA1* mutations (Sidransky *et al*, 1994). Up to now, 480 mutations have been identified and published in the HGMD database (Stenson *et al*, 2003). Characteristic of GD are the Gaucher cells, which are macrophages in which glucosylceramide, one of the GCase substrates, accumulates (Parkin & Brunning, 1982). Based on the age of onset and presence or absence of neurological symptoms, GD is classified into 3 different types (Malini *et al*, 2014). Type 1 is a mild form, which was initially described as non-neuronopathic (Malini *et al.*, 2014). However, type 1 patients anyway have an increased risk of developing PD (Sidransky *et al.*, 2009). Type 2 is the most severe and lethal form (Stone *et al*, 2000). It is associated with brain pathology, skin lesions, hepatosplenomegaly, and respiratory problems (Tayebi *et al*, 1998). The onset of type 2 GD is usually latest within the first few months of life (Tayebi *et al.*, 1998). Due to the fast

progression of the disease, the majority of patients does not reach 2-years of age (Tayebi *et al.*, 1998). Type 3 is a severe form that presents neurological abnormalities (Malini *et al.*, 2014). However, the disease onset is later, and the progression is slower than in type 2 GD (Malini *et al.*, 2014). GD is a very heterogenous disease (Schmitz *et al*, 2005; Tayebi *et al.*, 1998; Tayebi *et al*, 2003). For example, GD type 2 patient lifespan reaches from prenatal death or few days to survival up to 2.5 years of age (Tayebi *et al.*, 1998). Furthermore, the level of GlcSph cannot be correlated with the genotype (Orvisky *et al*, 2002). Therefore, it is nearly impossible to correlate genotypes with a specific disease manifestation within the different GD types (Tayebi *et al.*, 1998). Different *GBA1* mutations effect GCase activity to different degrees (Malini *et al.*, 2014). The p.N370S is the most common mutation in Ashkenazi (63-71.3% of mutant alleles) and among the most common mutant alleles in non-Jewish GD patients (17-34.3% of mutant alleles) (Koprivica *et al*, 2000; Sidransky *et al.*, 1994). p.N370S homozygous mutations are associated with the mild GD type 1 (Sidransky *et al.*, 1994). Recombinant alleles are very severe and are often associated with GD type 2 (Stone *et al.*, 2000). p.L444P mutation is common in type 3 GD (Sidransky *et al.*, 1994). Nowadays it is known that not all *GBA1* mutations cause GD disease. Patients with only p.E326K mutations in both alleles do not develop GD (Duran *et al*, 2013; Park *et al*, 2002). Therefore p.E326K mutant carrier GD patients always have another *GBA1* mutation on the same allele as the p.E326K mutation (Park *et al.*, 2002). The p.E326K mutation is a mild mutation (Thirumal Kumar *et al*, 2018).

2.2.3 Treatment of GD

Diverse types of treatment are available for GD. These include enzyme replacement therapy, substrate reduction therapy and molecular chaperones. GD type 1 can be treated by enzyme replacement therapy (ERT). Imiglucerase from Genzyme and Taliglucerase alfa, which is produced in plant cells, are recombinant GCase used in ERT (Aflaki *et al*, 2014; Pastores *et al*, 2014). Recombinant GCase is taken up in a mannose receptor dependent fashion in induced pluripotent stem cell (iPSC)-derived neurons (Awad *et al*, 2015). It increased LAMP1 signal, average number of lysosomes and rescued defects in autophagic flux in iPSC-derived neurons from GD type 2 patients (Awad *et al.*, 2015). In a phase III clinical trial, it was shown that a switch from Imiglucerase to Taliglucerase alfa is safe and keeps the GD pediatric and adult patient condition stable (Pastores *et al.*, 2014). ERT of GD type 3 patient leads to and improvement (i.e., decrease in liver and spleen size, increase in hemoglobin) and in long-term stabilization of the peripheral pathology (El-Beshlawy *et al*, 2017; Sechi *et al*, 2014). However, when it comes to brain pathology, the situation looks different. Enzyme replacement therapies cannot cross the blood-brain barrier (BBB). Therefore, in a long-term follow-up study of GD type 3 patients receiving ERT, most patients developed neurological symptoms (Sechi *et al.*, 2014). Only 2 patients did not show overt neurological symptoms yet although their EEG already displayed abnormalities (Sechi *et al.*, 2014). Therefore, the focus is on generating

recombinant GCase that can cross the BBB and promote neuronal uptake (Gramlich *et al*, 2016). Other treatments are as well assessed to overcome this problem. Another kind of treatment is the substrate reduction therapy (SRT). These therapies focus on inhibiting the glucosylceramide synthase and thereby reducing the accumulation of GCase substrates by preventing its synthesis (Marshall *et al*, 2016; Peterschmitt *et al*, 2021; Peterschmitt *et al*, 2022). Genz-682452, also called Venglustat, was successful in decreasing liver and hindbrain accumulation of glucosylceramide after treatment of neuropathic GD model mice (Marshall *et al.*, 2016). Venglustat was tested in healthy patients in the clinic (NCT01674036 and NCT01710826) (Peterschmitt *et al.*, 2021). Both studies were placebo controlled (Peterschmitt *et al.*, 2021). The first study NCT01674036 was only a dose escalation of a single dose study (Peterschmitt *et al.*, 2021). In the second clinical trial, NCT01710826, 3 different doses were administered for 14 days and the outcome was compared to a placebo group (Peterschmitt *et al.*, 2021). Only mild adverse effects were observed and it was shown to effectively decrease GlcCer and ganglioside in the plasma (Peterschmitt *et al.*, 2021). The clinical trial with the number NCT02906020 investigated the safety, pharmacokinetics, and dynamics of Venglustat in *GBA1*-PD patients (Peterschmitt *et al.*, 2022). The study was double-blinded, and a placebo control group was included (Peterschmitt *et al.*, 2022). Decrease of GlcCer levels were as well observed in *GBA-1*-PD patient cerebrospinal fluid (CSF) and plasma (Peterschmitt *et al.*, 2022). Only mild to moderate side-effects were observed, although the Venglustat treated group presented psychiatric symptoms like anxiety with panic attacks and depression (Peterschmitt *et al.*, 2022). Lately another glucosylceramide synthase inhibitor, Benzoxazole 1 was tested in primary mouse cortical neurons with the homozygous p.D409V GCase mutation and successfully reduced GlcCer and GlcSph levels (Cosden *et al*, 2021). Benzoxazole 1 penetrates the BBB and can decrease the GlcCer levels of brain tissue (Cosden *et al.*, 2021). On the other hand, there are the non-inhibitory and inhibitory molecular chaperones, which promote ER folding of mutant GCase, thereby decreasing ER associated degradation (ERAD) and promoting maturation of GCase (Steet *et al*, 2006). Isofagomine is an inhibitor of GCase which is able to penetrate the brain (Steet *et al.*, 2006). The inhibitory effect is stronger at neutral than acidic pH and the p.N370S is less susceptible to the inhibition than WT (Steet *et al.*, 2006). Due to this pH and mutation effect, it has the capability to enhance WT and p.N370S fibroblast GCase activity in a dose-dependent manner (Steet *et al.*, 2006). One negative effect of inhibitory chaperones is that they as well inhibit the activity in the lysosomes (Steet *et al.*, 2006). For this reason, non-inhibitory or chaperones that can be inhibitors or enhancers depending on the condition, are a more attractive solution. One of these non-inhibitory molecules is a pyrazolopyrimidine, NCGC00188758, which was shown to improve GCase trafficking to the lysosome and its activity in fibroblasts from WT, p.N370S heterozygous, p.N370S and p.L444P homozygous subjects (Patnaik *et al*, 2012). Another molecule of this

category is NCGC00188758 (Aflaki *et al.*, 2014). Treatment with NCGC00188758 of iPSC-derived macrophages and macrophages generated from monocytes isolated from blood, lead to an increased GCase trafficking to the lysosome and activity (Aflaki *et al.*, 2014). This resulted in a decrease in the GCase substrate, GlcCer (Aflaki *et al.*, 2014). Similar effect was seen by NCGC607 treatment of iPSC-derived macrophages and neurons (Aflaki *et al*, 2016). Ambroxol belongs to the group of molecular chaperones that can inhibit or enhance GCase activity (Maegawa *et al*, 2009). At neutral pH as in the ER, Ambroxol is an inhibitory chaperone of GCase (Maegawa *et al.*, 2009; Mullin *et al*, 2020). However, the advantage of Ambroxol over other inhibitory chaperones is that at acidic pH it can become an enhancer of GCase activity (Maegawa *et al.*, 2009). Fibroblasts from GD type 1-3 reacted to Ambroxol treatment (Bendikov-Bar *et al*, 2011; Maegawa *et al.*, 2009). Unfortunately, not all cells from p.L444P homozygous mutant GD patients show improved maturation and activity of mutant GCase (Bendikov-Bar *et al.*, 2011; Maegawa *et al.*, 2009). All lines reacted to low concentration of Ambroxol and isofagomine but with higher concentration the inhibitory effect of the chaperones was greater than the beneficial effect on GCase activity (Welsh *et al*, 2020). Removal of Ambroxol for 24 hours prevented the inhibitory effect (Welsh *et al.*, 2020). Ambroxol and to a higher extend isofagomine, are less potent in rescuing pathological effects than recombinant GCase in some patient cells (Maegawa *et al.*, 2009; Panicker *et al*, 2014; Welsh *et al.*, 2020). However, the advantage of molecular chaperones is that they can cross the BBB and improve GCase activity in the brain as demonstrated in mice (Migdalska-Richards *et al*, 2016). Ambroxol was shown to reach the CSF in humans and went along with increasing GCase protein level (Mullin *et al.*, 2020). No severe side effects were observed in *GBA1*-PD or control PD patients after Ambroxol treatment (Mullin *et al.*, 2020).

2.2.4 Link between GBA1 and PD

Initially, it was noted that GD patients -even non-neuronopathic patients- can develop Parkinson's disease (Bembi *et al*, 2003; Goker-Alpan *et al*, 2008; Neudorfer *et al*, 1996; Tayebi *et al*, 2001; Tayebi *et al.*, 2003). Furthermore, a higher incidence of PD was detected in relatives of GD patients (Goker-Alpan *et al*, 2004; Halperin *et al*, 2006). The SN of GD patients showed pronounced dopaminergic neurons loss and LBs were detected in these brains (Tayebi *et al.*, 2003). Subsequent analysis investigating specifically the link between *GBA1* mutations and PD, found that the frequency of *GBA1* mutations is higher in PD patients than in controls (Sidransky *et al.*, 2009). Initially, not all mutations, like the p.E326K, were considered to have a higher risk to develop PD (Sidransky *et al.*, 2009). However, nowadays its recognized that p.E326K mutation increases the risk for PD (Berge-Seidl *et al*, 2017; Duran *et al.*, 2013). In the initial investigation, p.N370S and p.L444P were the most common mutations in non-Ashkenazi Jewish (Sidransky *et al.*, 2009). In a study in a small cohort of early onset PD, in which nearly 26% of the patients had a *GBA1* mutation, the p.E326K

mutation was even the most prominent *GBA1* mutations with about 7.6% (Duran *et al.*, 2013) or 4.5% (Malek *et al*, 2018). In latter, the other non-GD variant p.T369M was present in 1.8% of the analyzed patients, p.L444P accounted for 1.6% and p.N370S for 0.6% of patients (Malek *et al.*, 2018). Penetrance varies based on the severity of the mutation, with the severe p.L444P mutation reaching the highest penetrance of about 15% (Straniero *et al*, 2020). In the *GBA1*-PD patients, the risk of developing PD is even more skewed to male PD patients than females (Neumann *et al.*, 2009). Since there is not a complete penetrance of PD/parkinsonism associated with *GBA1* mutations, the contribution of other genes (modifier genes) to the development of parkinsonism is likely (Tayebi *et al.*, 2003). *GBA1* mutation carriers display an earlier date of motor symptoms onset (Lunde *et al*, 2018; Maple-Grødem *et al*, 2021; Neumann *et al.*, 2009; Straniero *et al.*, 2020). In *GBA1* polymorphisms, to which p.E326K is as well counted in that publication, this is observed to a lesser extend (Lunde *et al.*, 2018; Straniero *et al.*, 2020).

Interestingly, not only mutations of *GBA1* are linked to PD, but as well decreased GCase activity. Decreased GCase activity was observed in dried blood spots (Alcalay *et al*, 2015) as well as in the substantia nigra and the caudate of sporadic PD patients (Chiasserini *et al*, 2015). This reduction in activity was accompanied by a decreased *GBA1* expression in the SN (Chiasserini *et al.*, 2015). Another study observed a decrease in GCase activity in different brain regions, including SN, putamen, hippocampus, and cerebellum in PD patients (Rocha *et al.*, 2015a). However, this decrease evened out during aging between PD patients and controls as GCase activity decreases with aging (Rocha *et al.*, 2015a). iPSC-derived neurons from idiopathic PD patients demonstrate reduced GCase activity too after long-term culture (Burbulla *et al*, 2017). Decreased GCase activity of monocytes (CD14+/CD16-) correlates with a worse Unified Parkinson's Disease Rating Scale (UPDRS)-III score (Hughes *et al*, 2021).

In *GBA1*-PD cases the severity of the PD symptoms correlates with the severity of the *GBA1* mutation (Thaler *et al*, 2018). Non-motor symptoms are more common in *GBA1* mutation carriers than in control PD patients. Cognitive impairment is more common in *GBA1*-PD patients (Brockmann *et al*, 2011), including dementia (Cilia *et al*, 2016; Oeda *et al*, 2015; Winder-Rhodes *et al*, 2013; Zhang *et al*, 2018). Furthermore, psychiatric disturbances like hallucinations (Jesús *et al*, 2016), psychosis (Cilia *et al.*, 2016; Oeda *et al.*, 2015), depression (Brockmann *et al.*, 2011; Zhang *et al.*, 2018) are more common. *GBA1* patients suffer more heavily from constipation as well as urinary dysfunction (Brockmann *et al.*, 2011). Differences have been observed with regard to mutation severity and the likelihood of certain symptoms. For example, hallucination and constipation are symptoms associated more with less severe mutations (Jesús *et al.*, 2016). However, severe *GBA1* mutations correlate with worse hallucinations, sleep disturbances and depression (Thaler *et al.*, 2018). Psychosis is more common in PD patients with a *GBA1* mutation that are associated with GD (Oeda *et al.*, 2015).

Severe mutation carriers have a greater risk of developing dementia (Cilia *et al.*, 2016). With regard to motor symptoms, the UPRDRS-III score is higher in *GBA1*-PD patients compared to non-mutant carriers (Brockmann *et al.*, 2011; Thaler *et al.*, 2018). *GBA1* mutation carriers seem to suffer less from tremor but present an increase in dyskinesia (Jesús *et al.*, 2016). Furthermore increased risk for postural instability gait difficulties are as well linked to *GBA1*-PD (Malek *et al.*, 2018). Progression of cognitive impairment (Brockmann *et al*, 2015; Lunde *et al.*, 2018; Neumann *et al.*, 2009) and motor dysfunction is significantly faster in *GBA1*-PD patients compared to non-GBA1 mutant PD patients (Brockmann *et al.*, 2015; Malek *et al.*, 2018; Maple-Grødem *et al.*, 2021). Furthermore, survival was reduced in mutation carriers (Brockmann *et al.*, 2015; Cilia *et al.*, 2016).

2.2.5 Pathological mechanisms of GBA1 mutations

Two hypotheses, the loss- and the gain-of-function hypothesis exist with regard to the pathological mechanism of mutant GCase. A summary of the mechanism in WT (Figure 2-1 A) and gain- and loss-of-function mechanisms is provided in figure 2-1.

The gain of-function hypothesis is based on the acquired functions of mutant GCase (Figure 2-1 B). A significant portion of mutant GCase is retained in the ER (Kuo *et al*, 2022; Ron & Horowitz, 2005, 2008). Mutant GCase is on one hand degraded by ERAD, as shown by the increased levels of GCase after proteasomal inhibition with MG-132 (Bendikov-Bar *et al.*, 2011; Kuo *et al.*, 2022; Ron & Horowitz, 2005, 2008). On the other hand, treatment with ammonium chloride and leupeptin, which both inhibit lysosomal protein degradation, shows that mutant GCase is as well degraded at the level of the lysosome (Jonsson *et al*, 1987; Kuo *et al.*, 2022). Increased GCase degradation leads to the loss-of-function, decreased GCase levels (Bendikov-Bar *et al.*, 2011; Kuo *et al.*, 2022; Ron & Horowitz, 2005, 2008; Schöndorf *et al*, 2014) and GCase activity (Jonsson *et al.*, 1987; Ron & Horowitz, 2005, 2008; Schöndorf *et al.*, 2014).

In the loss-of function hypothesis the focus is on the consequences of the decreased GCase activity caused by the mutation (Figure 2-1 C). In an overexpression model, p.E326K mutant GCase conserved about 54% of wild-type activity (Malini *et al.*, 2014). Overexpression of p.N370S mutation resulted in a reduction of 62% of activity compared to overexpressed WT GCase (Malini *et al.*, 2014). On the other hand, the p.L444P GCase mutant has only 13% of activity left (Malini *et al.*, 2014). Overall, it seems that a certain level of GCase activity is sufficient to prevent glycosphingolipid accumulation in GCase mutant (Schueler *et al*, 2004). However, there are different results regarding which is the critical level of GCase dysfunction and substrate storage. In a J774 macrophage cell line, a reduction of GCase activity did not result in much GlcCer storage until a threshold of 11-15% of activity is reached (Schueler *et al.*, 2004). GlcSph accumulation has been described in iPSC-derived macrophages from GD type 1, 2 and 3, with a residual GCase activity lower than 5% (Panicker *et al*, 2012).

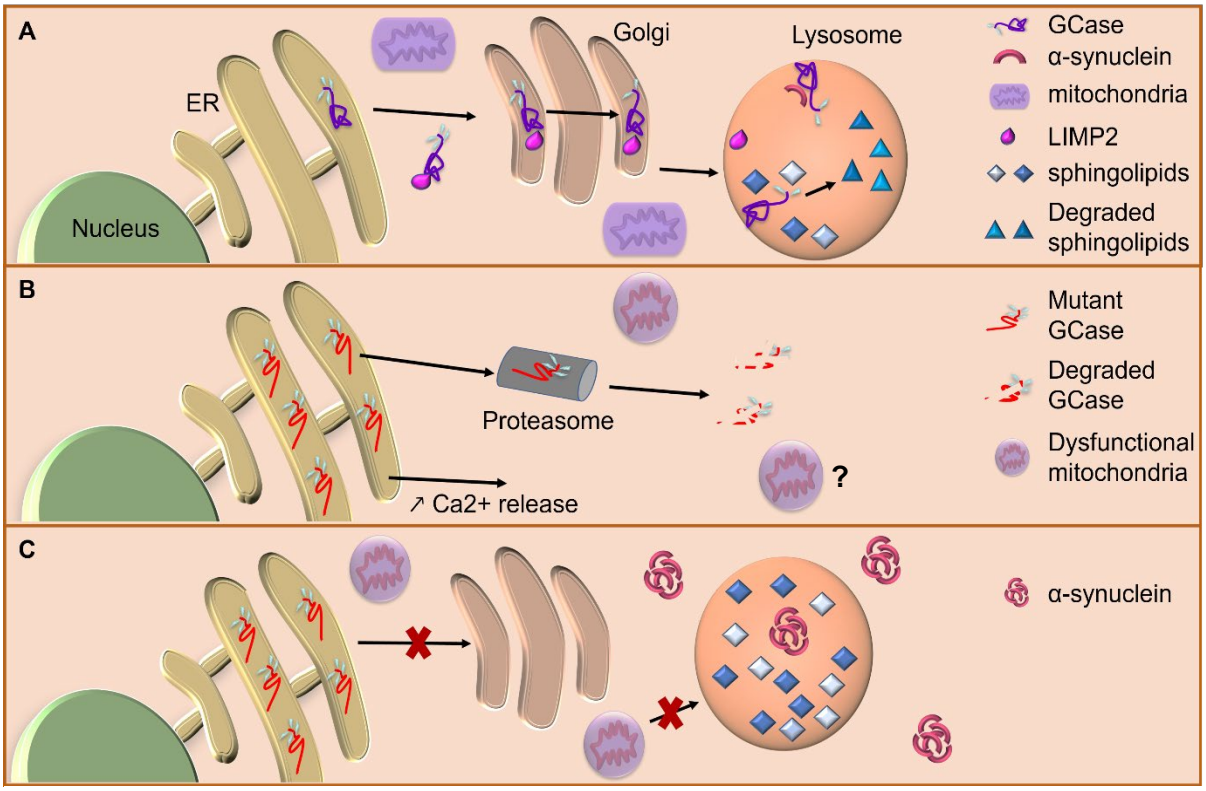

Figure 2-1 Gain-and loss-of-function pathological mechanisms of *GBA1* mutations. A) In healthy cells, *GBA1* mRNA is translated in the endoplasmic reticulum (ER) where GCase gets N-glycosylated. GCase binds LIMP2 for the trafficking through the Golgi apparatus to the lysosome. In the Golgi, N-linked oligosaccharides are trimmed during GCase maturation. In the lysosome, GCase separates from LIMP2. Here it breaks down its glycosphingolipid substrates and indirectly assists through ceramide generation in the degradation of α-synuclein. B) Gain-of-function: Mutant GCase is retained in the ER, where it causes ER stress and increased calcium (Ca^{2+}) release. Misfolded GCase will be exported from the ER to undergo ER-associated degradation (ERAD). If mitochondrial dysfunction is at least partially caused by gain-of-function is not yet understood. C) Loss-of-function: Reduced trafficking of mutant GCase leads to lysosomal dysfunction resulting in accumulation of GCase substrates, sphingolipids (glucosylceramide and glucosylsphingosine). Mitochondrial dysfunction is associated with the membrane lipid change caused by the accumulation of sphingolipids and the dysfunctional mitophagy.

On the other hand, GlcCer and GlcSph were increased in iPSC and iPSC-derived neurons with over 20% GCase activity (Schöndorf *et al.*, 2014; Sun *et al*, 2015). Neural precursor cells (NPCs) and neurons from different patients with similar GCase activity did not have comparable substrate storage levels (Sun *et al.*, 2015). There are several reports, which show elevation of only certain GlcCer species (Fernandes *et al*, 2016; Kim *et al*, 2018a; Kinghorn *et al*, 2016). In a Drosophila KO of the *GBA1* orthologue CG31414, the C16:0, C18:0, C20:0 and C22:0 species of GlcCer were increased (Kinghorn *et al.*, 2016). KO of *GBA1* in HEK cells increased C14:0, C16:0, C18:0 and C24:1 GlcCer (Kim *et al.*, 2018a). In iPSC-derived neurons from p.N370S heterozygous PD patients only the C16:0 and C24:0 GlcCer species were increased, whereas the C20:0 GlcCer species was decreased in the total GlcCer pool (Fernandes *et al.*, 2016). Furthermore, an increase in cholesterol was observed in a severely affected GD patient (Ron & Horowitz, 2008). The mutant sibling that had a milder form of GD did not have elevated cholesterol levels (Ron & Horowitz, 2008). Interestingly, a model

predicted that both the p.E326K and p.L444P can influence the interaction with the co-factor saposin C (Atrian *et al.*, 2008). Lysosomal dysfunction caused by mutant GCase leads to defects in the autophagic flux and causes accumulation of α-synuclein and dysfunctional mitochondria (Schöndorf *et al.*, 2014; Schöndorf *et al*, 2018). As α-synuclein and mitochondrial dysfunction are particularly important in the pathology of PD. The next 2 paragraphs will describe this mechanism more in detail.

2.2.5.1 Mutant GCase and α-synuclein accumulation:

GCase deficiency has been linked to a change in α-synuclein species. Some physiological oligomers (60, 80 and 100kDa) are decreased in primary cortical neurons of p.L444P heterozygous mice, *GBA1* KO SH-SY5Y cells and iPSC-derived dopaminergic neurons from p.N370S heterozygous PD while the monomers are increased (Kim *et al*, 2018b). Others have shown that upon preformed fibrils (PFF) and Conduritol B epoxide (CBE) treatment of mouse cortical neurons and differentiated SH-SY5Y cells lead to elevated high molecular weight α-synuclein species (Gegg *et al*, 2020) and in GD and CBE treated iPSC-derived midbrain neurons (Zunke *et al*, 2018). CBE treatment of different primary brain cell types overexpressing α-synuclein or treated with PFF increased LB-like inclusions in the soma (Henderson *et al*, 2020). The combination of CBE and α-synuclein PFF treatment of mice does not lead to overt tyrosine hydroxylase (TH) positive degeneration in the SN (Henderson *et al.*, 2020). However, motor deficits in the form of reduced forelimb grip strength are observed (Henderson *et al.*, 2020). In primary hippocampal neurons this leads to neurotoxicity (Henderson *et al.*, 2020). Elevated α-synuclein levels were detected in PFF treated p.N370S mutant iPSC-derived dopaminergic neurons (Kim *et al.*, 2018b) or human α-synuclein overexpressing *GBA1* KD mice (Polissidis *et al*, 2022). This observation went along with reduced survival of dopaminergic neurons (Kim *et al.*, 2018b; Polissidis *et al.*, 2022). The importance of GCase for the accumulation of α-synuclein was further underlined as GCase overexpression leads to decrease in α-synuclein pathology in a mouse and even rescues TH positive cells in the SN in a rat model (Rocha *et al*, 2015b). Elevated levels of phosphor Serine129 α-synuclein could be decreased by improving GCase activity using Ambroxol treatment (Migdalska-Richards *et al.*, 2016). Decrease of additional lysosomal hydrolase activity is associated with aggregation of α-synuclein as this effect was not observed when overexpressing α-synuclein lacking the region required for aggregation (Mazzulli *et al*, 2016a).

There are several mechanisms through which GCase deficiency leads to increased accumulation of α-synuclein. The main pathways by which mutant GCase affects α-synuclein aggregation is by causing lysosomal dysfunction (Burbulla *et al*, 2019). KD of GCase primary mouse cortical neurons reduced lysosomal proteolysis of long-lived proteins (Mazzulli *et al*, 2011) and several models show increased levels of α-synuclein (Cleeter *et al*, 2013; Fishbein *et al*, 2014; Mazzulli *et al.*, 2011; Osellame *et al*, 2013; Polissidis *et al.*, 2022; Woodard *et al*,

2014; Yang *et al*, 2020; Yun *et al*, 2018), due to impaired chaperone-mediated autophagy (CMA) (Osellame *et al.*, 2013). Furthermore, decreased turnover of GlcCer to glucose and ceramide by mutant GCase leads to a decrease in ceramide, which is important for cathepsin D to break down α-synuclein (Yang *et al.*, 2020). Treatment with the recombinant GCase, Cerezyme, rescued cathepsin D activity (Yang *et al.*, 2020). This could explain why mice with heterozygous p.L444P mutation display a slower degradation rate of overexpressed α-synuclein (Fishbein *et al.*, 2014). However, not only the loss-of-function of mutant GCase leads to lysosomal and autophagic dysfunction, but as well the gain-of-function of mutant GCase. Unfolded mutant GCase accumulates at the outside of the lysosome and prevents degradation of other CMA targets like α-synuclein (Kuo *et al.*, 2022). This leads to an aggregation and oligomerization of α-synuclein at the outside of the lysosome (Kuo *et al.*, 2022). Incubation of lysosomes with α-synuclein and mutant GCase prevents the LAMP2 multimerization, which is essential for the import of CMA targets and leads to dopaminergic neuron death (Kuo *et al.*, 2022).

An indirect mechanism of how GCase deficiency leads to α-synuclein accumulation, is through the accumulation of its substrates. Several mouse and cell models have shown that GCase deficiency leads to accumulation of GlcCer and GlcSph (Kim *et al.*, 2018a; Polissidis *et al.*, 2022; Schöndorf *et al.*, 2014; Taguchi *et al*, 2017). In the investigated brain regions (cortex from cerebrum and cerebellum) of neuronopathic GC patients levels of GlcCer were elevated (Nilsson & Svennerholm, 1982). In *GBA1*-PD, GlcCer elevation is still under debate, but there might be a slight increase in GlcCer in only certain brain regions (Blumenreich *et al*, 2022). Increase GlcSph levels were observed to accumulate in brains of GD type 2 and 3 and a potential type 1 patient (Nilsson & Svennerholm, 1982; Orvisky *et al.*, 2002; Tayebi *et al.*, 2003). Even more interesting, a correlation between decreased GCase activity in sporadic PD patients in SN correlated with increased levels of GlcSph (Rocha *et al.*, 2015a). In fibroblasts from *GBA1* mutant PD patients changes in lipid composition, i.e., increased total sphingolipid level and decrease of certain phospholipids was observed (Galvagnion *et al*, 2022). The in vitro assessment of the effect of changes in lipid levels showed that α-synuclein accumulates faster in this condition (Galvagnion *et al.*, 2022). Primary motor cortex of *GBA1*-Lewy body dementia patients has as well a reduction in some certain phospholipids (Clark *et al*, 2015). Interestingly, primary cortex changes in sphingolipids levels were observed in LBD patients with and without *GBA1* mutations (Clark *et al.*, 2015). *In vitro* it was shown that incubation of GlcCer and GlcSph lead to the formation of α-synuclein fibrils or oligomers respectively (Taguchi *et al.*, 2017). In a *GBA1* mouse model, GlcCer accumulation correlates with α-synuclein pathology in a linear manner (Taguchi *et al.*, 2017). It was shown that glycosphingolipids directly interact with α-synuclein leading to the formation of insoluble heigh molecular weight α-synuclein species (Zunke *et al.*, 2018). In addition, GlcCer forms fibrils

which stabilize α-synuclein oligomers and increased amyloidogenic aggregation (Paul *et al*, 2021). Reduction of GlcCer levels using Miglustat treatment, reduced the levels of pathological α-synuclein and rescued heterozygous p.N370S mutant iPSC-derived neuronal survival (Kim *et al.*, 2018b).

Not only do GCase mutations lead to an increase in α-synuclein but a whole vicious cycle is kicked off as α-synuclein affects GCase function in turn. In general, WT α-synuclein overexpression in healthy patient iPSC-derived midbrain neurons leads to reduced degradation of long-lived proteins (Mazzulli *et al.*, 2016a). Deletion of the region that allows a α-synuclein aggregation reduced this effect (Mazzulli *et al.*, 2016a). In mice lacking endogenous α-synuclein and overexpressing human α-synuclein, it was shown that GCase activity is decreased in the cortex, striatum, midbrain and brainstem (Migdalska-Richards *et al.*, 2016) and lysosomal specific GCase activity was lower in different cellular models (Gegg *et al.*, 2020; Mazzulli *et al.*, 2011; Mazzulli *et al.*, 2016a; Mazzulli *et al*, 2016b). Furthermore α-synuclein overexpression has negative effects on GCase maturation (Mazzulli *et al.*, 2011; Mazzulli *et al.*, 2016a), as it disrupts maturation of lysosomal hydrolases at the pre-Golgi stage (Mazzulli *et al.*, 2016a), by decreasing COPII vesicle trafficking from ER to Golgi (Credle *et al*, 2015). Furthermore, neurons from iPSC-derived from SNCA triplication PD patients accumulate GlcCer and hexosylsphingosine (Mazzulli *et al.*, 2016b), which can further aggravate the vicious cycle.

2.2.5.2 Mitochondrial dysfunction in PD and defects linked to GBA1 mutations:

Over 30 years ago, decreased protein levels of different subunits of complex I (CI) were shown in the striatum not in the frontal cortex of PD patients leading to a decrease of about 25% of CI activity (Mizuno *et al*, 1989). In the SN of PD patients, a reduction of CI activity without impacting CI protein abundance was also observed (Schapira *et al*, 1990a; Schapira *et al*, 1990b). It is unclear whether the CI deficiency is confined to the SN and PD affected regions. Indeed, it is not clear as there is on one hand evidence that other regions like the frontal cortex present CI deficiency as well (Parker *et al*, 2008). Other studies however did not observe decreased CI activity in other brain regions than SN (Schapira *et al.*, 1990b). Discrepancies in measurement of CI activity can be explained by differences in the experimental setup (Parker *et al.*, 2008). Performing the assay with bovine serum albumin, to increase the measured activity, or on homogenate, not purifying mitochondria, can lead to false negative results (Parker *et al.*, 2008). Another study on a small cohort, detected high variability in oxidative phosphorylation (OXPHOS) protein expression in PD patients using an mass-spectrometry (MS) based approach (Chen *et al*, 2021). Interestingly in this small cohort, the degree of decreased mitochondrial OXPHOS protein levels seemed to correlate with a higher Braak stage of the patient (Chen *et al.*, 2021). A decrease in mitochondrial respiratory chain protein levels went along with a higher mitochondrial mass (Chen *et al.*, 2021).

There is as well genetic evidence that links mitochondria to PD. On one hand, even though the results are partially controversial, mutations in the mitochondrial DNA (mtDNA) region coding for CI proteins, have been linked to decreased CI activity in mitochondria isolated from the frontal cortex (Parker *et al.*, 2008). Furthermore, repopulation of cybrids, cells lacking mtDNA, with mtDNA from PD patients, lead to mitochondrial defects including CI activity, increased reactive oxygen species (ROS) production and sensitivity to MPP+ treatment (Swerdlow *et al*, 1996). Models of PD are often based on chemical models inducing mitochondrial dysfunction. These models were developed based on the discovery that some compounds lead to parkinsonism. For example, in one patient by-products of improper synthesis of 4-propyloxy-4-phenyl-N-methylpiperidine, namely 4-hydroxy-4-phenyl-N-ethylpiperidine and dehydro-4-phenyl-N-methylpiperidine, lead to L-Dopa responsive parkinsonism most likely resulting from the degeneration of SN neurons (Davis *et al*, 1979).

Not only PD is associated with mitochondrial dysfunction but also GCase deficiency. Pharmacological inhibition and GCase KD in SHSY-5Y leads to a reduced adenosine triphosphate (ATP) synthesis due to reduced activity of complex I, II and III after 20 days of CBE treatment and increased oxidative damage (Cleeter *et al.*, 2013). Mitochondrial membrane potential started to decrease within 10 days of CBE treatment as well as in KO primary neurons and astrocytes (Cleeter *et al.*, 2013; Osellame *et al.*, 2013). In cellular models, CBE treatment of SH-SY5Y cells and *GBA1*-PD iPSC-derived midbrain neurons, as well as mouse models display changes in mitochondrial morphology, respiratory defects, and higher ROS production (Cleeter *et al.*, 2013; Osellame *et al.*, 2013; Schöndorf *et al.*, 2018; Yun *et al.*, 2018). The mitochondrial toxin 1-methyl-4-phenyl-1,2,3,6-tetrahydropyridin (MPTP) leads to a reduction in mitochondrial copy number which is exacerbated in p.L444P mutant compared to WT (Yun *et al.*, 2018). *GBA1* KO primary mouse neurons and astrocytes display impaired mitophagy (Osellame *et al.*, 2013). Defective mitophagy is as well detected in iPSC-derived midbrain neurons from PD patients carrying different *GBA1* mutations (Schöndorf *et al.*, 2018). Defective targeting of mitochondria for degradation is caused by lack of Parkin as the membrane potential does not reach the required threshold (Osellame *et al.*, 2013). Nicotinamide riboside (NR) treatment is able to rescue some mitochondrial defects, like mitophagy, ROS production and morphology, in *GBA1*-PD iPSC-derived midbrain neurons (Schöndorf *et al.*, 2018).

Mitochondrial dysfunction and *GBA1* mutations worsen PD related phenotypes. Motor deficits, as demonstrated by increased time to reach the bottom of the pole, were more pronounced in p.L444P heterozygous mice treated with MPTP (Yun *et al.*, 2018). Furthermore, in this model astrocyte activation and TH cell death in the SNpc and striatal fibers was increased upon MPTP treatment compared to untreated Haploinsufficient (*GBA1* p.L444P/WT) mice (Yun *et al.*, 2018). The described pathological observations were only observed after MPTP treatment and

not in untreated *GBA1* p.L444P/WT mice (Yun *et al.*, 2018). However, α-synuclein KO partially prevented the consequences of MPTP treatment in both WT and p.L444P mutant mice (Yun *et al.*, 2018). This is underlining the importance of the interplay between α-synuclein, mitochondria and GCase in PD.

2.2.6 Models of GCase pathology in complex disorders

Models for investigating GCase pathological mechanisms include chemical inhibitors, KO, knockdown (KD), gene-editing, human *GBA1* WT or mutant overexpression, and are used in different model systems like Drosophila melanogaster, zebrafish, mice and cellular models. Several GCase inhibitors exist. The most commonly used one is CBE, which is an irreversible inhibitor of GCase (Kanfer *et al*, 1975; Stephens *et al*, 1978). One of the first mouse models was described in 1975 (Kanfer *et al.*, 1975). As expected GCase activity was reduced and accumulation of GlcCer was observed in spleen and liver and to a lesser extent in the brain of treated infant and adults mice (Kanfer *et al.*, 1975). To recapitulate the higher levels in GlcCer daily injections are required as otherwise GCase activities increases again leading to a decrease in the GlcCer levels (Stephens *et al.*, 1978). Another disadvantage is that CBE is not distributed equally throughout the mouse body (Stephens *et al*, 1981). Lowest concentration was detected in the brain leading to about 37% of residual GCase activity (Stephens *et al.*, 1981), which might not lead to substrate accumulation (Schueler *et al.*, 2004). However, increasing the dose leads to sufficient decrease in GCase activity and accumulation of GlcCer levels in mouse brain (Stephens *et al.*, 1978). Another chemical irreversible inhibitor of GCase is adamantyl-cyclophellitol inhibitor (ME656), which leads to accumulation of GlcCer and GlcSph (Lelieveld *et al*, 2022; Lelieveld *et al*, 2019). Other models, either cellular or based on animals, often rely on KO or disruption of the GCase active site by gene-editing (Kim *et al.*, 2018b; Kinghorn *et al.*, 2016; Lelieveld *et al.*, 2019; Schöndorf *et al.*, 2018; Tybulewicz *et al*, 1992; Westbroek *et al*, 2016). Homozygous KO of the Drosophila *GBA1* brain orthologue leads to reduced survival and decreased locomotor performance (Kinghorn *et al.*, 2016). KO of *GBA1* was as well performed in iPSC, which were differentiated to midbrain dopaminergic neurons (Schöndorf *et al.*, 2018). KO in these different models lead to similar phenotypes like reduced autophagic flux and mitochondrial dysfunction (Kinghorn *et al.*, 2016; Schöndorf *et al.*, 2018), which are as well observed in *GBA1* mutant models (Schöndorf *et al.*, 2014; Schöndorf *et al.*, 2018). In Drosophila *GBA1* KO leads to neurodegeneration (Kinghorn *et al.*, 2016). However, models only focusing on the loss-of-function do not recapitulate the mechanisms related to gain-of-function. For example, it was observed that *GBA1* KO due to absence of misfolding GCase does not lead to ER stress (Kim *et al.*, 2018b; Schöndorf *et al.*, 2018), as it was observed in mutant neurons (Schöndorf *et al.*, 2018). Zebrafish are an interesting model organism for GCase deficiency, as knockout does not lead to death soon after birth (Lelieveld *et al.*, 2019), as observed in homozygous p.L444P or RecNcil mutant mice (Liu *et al*, 1998).

Since the Gaucher macrophages are the main pathological hallmark of GD, one model for the disease are monocytes isolated from patients, which are then differentiated into macrophages (Aflaki et al., 2014). Mouse models have another drawback as they do not have Gaucher cells (Liu *et al.*, 1998), except if the mice present a deletion in exon 8 of prosaposin in addition to the *GBA1* mutation (Sun et al, 2005). These mice showed the hallmark of macrophages filled with GlcCer accumulated in visceral tissues (Sun et al., 2005). Neuropathology started at around 10 weeks of age and showed by gait ataxia, tremor, falling and at later stage hind limp paralysis (Sun et al., 2005). Several interspecies differences between mice and humans make mice a less suitable model to study PD. In mouse cortical neurons, human WT and p.A53T α-synuclein gets degraded twice as fast than mouse α-synuclein (Fishbein et al., 2014). Calcium signaling (Kilpatrick *et al*, 2016; Schöndorf *et al.*, 2014) as well as dopamine metabolism (Burbulla *et al.*, 2017; Woodard *et al.*, 2014) are important players in *GBA1*-PD. This holds as well true in other cellular PD models (Burbulla *et al.*, 2017). However, mouse to human interspecies difference between dopamine metabolism and calcium homeostasis has been shown (Burbulla et al., 2017). Depending on the envisioned outcome this must be considered when assessing whether a mouse model is suitable. Furthermore, human brain tissue is hard to get and usually represents only the later or end stage of diseases like PD. This makes it harder to investigated pathological mechanisms. Therefore, it was a great advance when in 2011 it was published how iPSC can be generated in an easy and reproducible way (Okita et al, 2011). This allowed them to take tissue from patients, reprogram the cells and differentiate them into the cells of interest, like neurons (Reinhardt *et al*, 2013) or macrophages (Aflaki *et al.*, 2014; Gutbier *et al*, 2020). iPSC-derived macrophages express markers associated with macrophages to a similar degree than macrophages isolated from patient blood (Aflaki et al., 2014). They recapitulate the glycosphingolipid accumulation observed in patient macrophages as well as reduced ROS production compared to control (Aflaki *et al.*, 2014). In the beginning, one of the drawbacks of the iPSC-derived models was that proper controls were not used. Often mutant lines were compared to healthy controls. Since complex disorders, such as PD, are multifactorial and the genetic interplay can decide whether one develops PD or not, it is important to generate gene-corrected controls. Here, the genome is identical except for the gene-correction and possible selection cassette. This then allows to investigate the results of a mutation in the given genetic setting. Recently there have been many advances in gene-editing, finally in 2013 a CRISPR-Cas9 based gene-editing protocol was published which makes gene-corrections affordable and easy (Ran et al, 2013) allowing generation of the most adequate controls.

3 Aim

The pathological mechanisms of *GBA1*-related PD are not yet understood. Therefore, the main aim of this work was to assess the GCase interactome to identify novel GCase interactors that may help elucidate *GBA1*-PD. To do so the following intermediate goals had to be achieved: First, the generation and characterization of inducible T-Rex HEK cell lines allowing overexpression of tagged WT, p.E326K and p.L444P mutant GCase. Second, the quantitative analysis of the GCase interactome by co-immunoprecipitation linked with tandem mass tag liquid chromatography mass spectrometry. Third, the generation of iPSC lines and isogenic controls to allow further investigation of the mechanisms.

Based on the initial interactomic results showing the interaction of GCase with mitochondrial proteins, the main aim of this work was to better understand the link between GCase and mitochondria by addressing the following questions:

- Is GCase localized within mitochondria?
- How does GCase reach mitochondria?
- Do *GBA1* mutations impact mitochondrial function?
- What is the potential role of interaction of GCase with proteins involved in mitochondrial proteostasis, namely HSP60 and LONP1, in mitochondrial dysfunction?
- Is GCase potentially involved in CI integrity?

4 Materials and Methods

Some materials are listed in the description of the methods, the detailed list of materials is listed in the Appendix 9.1.

4.1 Cloning constructs into the plasmids

4.1.1 Design of constructs

The cDNA sequence of *GBA1* was obtained from https://genome.ucsc.edu/index.html (Kent *et al*, 2005). For inserting the tag, the leader sequence at the N-terminal of *GBA1* was identified (Tsuji *et al*, 1986). To ensure proper cleavage, the V5-Flag-tag was inserted 9 bp after the cleavage site of the leader sequence, and these 9 bp were repeated after the tag (see Appendix 9.2 V5-Flag-tagged *GBA1*). The V5-Flag-tag was made as short as possible in order to decrease the chance of interfering with the proper folding of GCase. Therefore, instead of using the whole V5 a.a. sequence (GKPIPNPLLGLDST), we went for the smaller form coding for IPNPLLGLD. This allowed us to use the last D as first a.a. of Flag (DYKDDDDK). The amino acid sequence of V5-Flag therefore is IPNPLLGLDYKDDDDK. The nucleotide sequences are shown in Appendix 9.2. The cDNA of wildtype (WT) and N-terminal tagged (V5-Flag-tag) WT *GBA1* as well as V5-Flag-tag only were ordered from IDT (gBlocks Gene Fragments).

4.1.2 Restriction digestion

WT and tagged *GBA1* cDNA were cloned into pcDNA^{TM}3.0 (Invitrogen^{TM}). First both underwent a restriction digest for which the reaction mixes are listed in table 4-1. The pcDNA^{TM}3.0 and later the pcDNA^{TM}5/FRT/TO (Invitrogen^{TM}) plasmids were digested for 2 hours and the constructs for 30 mins at 37°C. Then the plasmid was loaded on a 0.5% Agarose gel and run for 1 hour at 120V. Then the band running at around 5.4 kb, which represented the linearized plasmid, was excised from the gel and the DNA extracted with the QIAquick gel extraction kit (Qiagen) according to manufacturer's protocol. All the following centrifugation steps were performed at room temperature (RT) for 1 min at 13000 RPM and after centrifugation the flow-through was removed from the lower tube. The gel piece was weighted and per 100 mg, 300 µl Buffer QG was added. Then it was incubated for a total of 10 min at 50°C. To better dissolve the gel in the buffer the tube was vortexed every 2-3 min during the incubation. To the yellow buffer 100 µl of isopropanol was added per 100 mg of initial gel. The mixed solution was then added to a QIAquick spin column and spun. Then 500 µl QG was added, and the column was centrifuged again. 750 µl of PE buffer was added and the column spun again. After removal of the flow-through the column was spun empty again. Then the column was placed on a fresh tube and 30 µl Milli-Q H_2O was added. After incubation for 1 min, the column was spun for 1 min at 13000 RPM. The DNA content in the flow-through was measured with the NanoDrop2000^{TM} (Thermo Fisher Scientific Inc.).

	Reagent	Plasmid (3µg/µl)	gBlock DNA (IDT; 10ng/µl)
Cloning construct into pcDNA^{TM}3.0	DNA	1 µl	30 µl
	10x Tango Buffer	2 µl	3,5 µl
	XhoI	1 µl	1 µl
	EcoRI	1 µl	1 µl
	Milli-Q H_2O	5 µl	/
Cloning construct into pcDNA^{TM}5/FRT/TO	DNA	1 µl	28 µl
	10x Buffer O	2 µl	3 µl
	XhoI	1.5 µl	2 µl
	AflII	1.5 µl	2 µl
	Milli-Q H_2O	4 µl	/

Table 4-1: Reaction mixes for the restriction enzyme digests

4.1.3 Ligation

For the ligation of the sequence of interest into the plasmid, different ratios of digested construct to linearized plasmids were incubated over the weekend at 4°C. The following two mixes in table 4-2 were prepared.

Reaction	Material	3:1 construct to plasmid ratio	1:1 construct to plasmid ratio
Ligation of construct with pcDNA^{TM}3.0	Linearized plasmid (100 ng/µl)	0.5 µl (50 ng)	0.5 µl
	Digested construct (8.47 ng/µl)	18 µl	6 µl
	T4 ligase (NEB)	1 µl	1 µl
	Buffer (10x T4 ligase buffer, NEB)	2.5µl	2 µl
	Milli-Q H_2O	3 µl	10.5 µl
Ligation of PCR product with pcDNA^{TM}5/FRT/TO	Linearized plasmid (54 ng/µl)	4 µl	
	PCR product (230 ng/µl)	2 µl	
	T4 ligase (NEB)	2 µl	
	Buffer (10x T4 ligase buffer, NEB)	1 µl	
	Milli-Q H_2O	1µl	

Table 4-2: Mixes prepared for the ligation of the construct into the plasmid of interest.

4.1.4 Restriction enzyme recognition site exchange

To clone V5-Flag-tagged *GBA1* from pcDNA^{TM}3.0 into pcDNA^{TM}5/FRT/TO, the 5' restriction enzyme site of EcoRI had to be exchanged with the AflII restriction site. To this end a long-range PCR was conducted. The master mix was composed of 34 µl Milli-Q H_2O, 10 µl 5x ALLin RPH buffer (highQu), 1µl ALLin RPH polymerase (highQu), 2 µl FW and RV primer and 1 µl pcDNA^{TM}3.0 plasmid (100 ng). After the PCR, the sequence was purified. To do so 250 µl of PB buffer (Qiagen DNeasy Blood & Tissue kit, Qiagen) was added to the PCR product. This mix was added in the spin column and centrifuged. All the following centrifugation steps were done at 13000 RPM and for 1 min. After each centrifugation step, the flow-through was

removed. Then 750 µl PE buffer were added in the column, followed by 2 centrifugation steps. To elute the DNA, the column was put on another tube and 30 µl of Milli-Q H_2O was added. After 1 min incubation the column was centrifuged, and the DNA concentration was measured using the NanoDrop2000™. The construct was then digested with restriction enzymes and ligated into the pcDNA™5/FRT/TO.

4.1.5 Transformation of bacteria

One Shot™ TOP10 chemically competent E. Coli (Thermo Fisher Scientific Inc.) were thawed on ice. 20 µl of E. Coli were transferred into a 1.5 ml tube and 2-4 µl of ligation mix was added. The bacteria with the ligation were incubated on ice for 30 min. Then a 30 second heat shock at 42°C at 1000 RPM was performed. Afterwards, the tubes were put immediately on ice until the Thermocycler (Eppendorf) reached 37°C. 250 µl SOC medium (Invitrogen) was added per tube to the bacteria. The mix was then incubated for 1 hour at 37°C 300 RPM. After 1 hour, the bacteria were plated on LB Agar plates containing Ampicillin (50 µg/ml) for the selection. The LB Agar plates were then incubated upside down overnight (O/N) at 37°C. The next day, colonies were picked and grown in 4 ml LB medium containing Ampicillin (50 µg/ml) shaking O/N at 37°C. The following morning, the pDNA from 3 ml of the bacterial culture were isolated. To this end, the QIAprep Spin Miniprep kit from Qiagen was used according to the manufacturer's protocol. To pellet the bacteria, the culture was centrifuged for 1 min at maximum speed. The LB medium was removed, and the pellet resuspended in 250 µl P1 buffer containing RNase. Next, 250 µl P2 buffer was added, and the tube inverted 6 times to mix the reagents. 350 µl neutralization buffer N3 was added. For mixing, the tube is inverted 6 times. Then the tube is centrifuged for 10 min at 13000 RPM. The supernatant was added on top of the Qiagen column and centrifuged for 1 min at 13000 RPM, which was the centrifugation condition for all the following centrifugation steps. After discarding the flow-through, 500 µl PB buffer was added, followed by another centrifugation step. Next, 750 µl PE buffer was added and the tubes were centrifuged twice. The column was then placed on a new tube and 50 µl of Milli-Q H_2O were added on the membrane. After 1 min incubation at RT, the tube was spun again and DNA concentration of the flow-through was measured.

4.1.6 Neural precursor cell (NPC) nucleofection

To check whether the N-terminal V5-Flag-tag affects GCase localization, *GBA1* KO NPCs (Schöndorf *et al.*, 2018) were nucleofected with pcDNA™3.0 coding for WT or V5-Flag-tagged GCase. To this end, NPCs were detached with Accutase (Sigma-Aldrich) and after 5 min incubation at 37°C, the NPCs were collected and centrifuged for 5 min at 1100 RPM at RT. The NPC pellet was resuspended in PBS to remove medium leftover and counted. $1x10^6$ NPCs were centrifuged again. In the meantime, 100 µl Ingenio (Mirus) solution was mixed with 10 µg of plasmid. After centrifugation, the supernatant was removed, the pellet was resuspended

with the Ingenio solution/plasmid mix and transferred to the Amaxa electroporation cuvette (Lonza). For the nucleofection, the Amaxa nucleofector IIb was used, and the program set to A-033. Next, 500 µl medium was added and nucleofected NPCs were added to wells of a 24-well containing a Matrigel-coated coverslip. 48 hours after nucleofection, the NPCs were fixed for immunocytochemical analysis.

4.1.7 Transfection of 293 HEK cells with WT and V5-Flag-tagged GBA1

The day before the transfection in DMEM+/+ (table 4-3), for each reaction $5x10^5$ cells were split in one well of a 6-well plate. For the transfection, 300 µl of polyethylenimine (Polysciences) were mixed with 300 µl DMEM without phenol red containing 5 µg plasmid coding for either WT or V5-Flag-tagged WT *GBA1*. 48 hours after transfection selection was started by changing the medium to DMEM+/- selection (Table 4-3) containing 500 µg/ml G418. After one week in selection medium, GCase activity assay was assessed.

Medium	Ingredient	Quantity	Manufacturer	Catalogue number
For transfection reaction	DMEM w/o phenol red	300 µl	Gibco	31053028
DMEM +/-	DMEM	500 ml	Sigma-Aldrich	D6546-500 ml
	Fetal bovine serum	50 ml	Gibco	16000044
	GlutaMAX	5ml	Gibco	35050061
For selection	DMEM +/-	/	/	/
	G418 Geneticin	5 µl per ml	InvivoGen	Ant-gn-1
DMEM +/+	DMEM	500 ml	Sigma-Aldrich	D6546-500 ml
	Fetal bovine serum	50 ml	Gibco	16000044
	GlutaMAX	5ml	Gibco	35050061
	Penicillin/Streptavidin	5 ml	Sigma-Aldrich	P0781-100ml

Table 4-3: Medium used for transfection and 293 HEK cell maintenance and transfection

4.1.8 Site-directed mutagenesis to insert the p.E326K or p.L444P mutation in GBA1 sequence

After determining the correct insertion of the V5-Flag-tagged WT *GBA1* sequence into the pcDNA™5/FRT/TO by Sanger sequencing, site-directed mutagenesis (SDM) was performed according to the manufacturer's protocol (SDM kit: QuikChange II XL, Agilent). For each reaction 10 ng of V5-Flag-tagged WT *GBA1* plasmid and 15 picomoles of the primer for the p.E326K mutation or 13 picomoles of the primer for the p.L444P mutation were used. The primers are shown in table 4-4. The concentration of the primers was determined with the following equation, which was suggested by the manufacturer (Agilent): $X\ pmoles\ of\ oligo = \frac{ng\ of\ oligo}{330x\#of\ bases\ in\ oligo}$x1000.

Following the PCR reaction, the original methylated plasmid as well as the synthesized hemi-methylated plasmids were digested with Dpn1 (SDM kit). The PCR product was transformed into bacteria (XL 10-Gold Ultracompetent cells, supplied in SDM kit) according to manufacturer's protocol. Bacteria were thawed on ice. 2 µl of ß-Mercaptoethanol (SDM kit) were added to 45 µl of bacteria. The tubes were swirled and incubated on ice for 8 minutes, after swirling them again, they were incubated for 2 more minutes. 2 µl of PCR product were added to the bacteria and incubated for 30 minutes on ice, followed by a 30 second heat shock at 42°C. 500 µl prewarmed SOC (42°C) medium was added and put on ice for 2 minutes. The mix was incubated for 1 hour at 37°C shaking and then plated on LB agar dishes containing 50 µg/ml Ampicillin and incubated overnight at 37°C. The following day, bacterial colonies were picked and incubated overnight at 37°C in 4 ml LB medium supplemented with 50 µg/ml Ampicillin. 3 ml of the bacterial culture were used for a Miniprep according to the manufacturer's protocol (QIAprep Spin Miniprep Kit, Qiagen).

Primer	Forward (5'->3')	Reverse (5'->3')
p.E326K	GGC GGT GTG TCT TCC CTA GGG TGG C	GCC ACC CTA GGG AAG ACA CAC CGC C
p.L444P	GTG CCA CTG CGT CCG GGT CGT TCT TCT GA	TCA GAA GAA CGA CCC GGA CGC AGT GGC AC

Table 4-4: Primers for site-directed mutagenesis

Plasmids with the correct sequences, which was checked by Sanger Sequencing, were cultured for a Maxiprep (300 ml LB medium containing 50 µg/ml Ampicillin O/N at 37°C). Maxiprep was performed as described in the Manufacture´s protocol (EndoFree Plasmid Maxi kit, Qiagen). The bacterial culture was first centrifuged in 50 ml Falcon tubes at 4°C 6000 RCF for 15 min. The bacterial pellet was resuspended in 10 ml Buffer P1. Next, 10 ml P2 buffer was added, and the tubes were inverted 6 times for mixing and incubated for 5 min at RT for complete lysis.10 ml cold P3 buffer was added and then mixed by inverting the tube 6 times. The mix was filtered through Whatman filter paper. Then for endotoxin removal, 2.5 ml ER buffer was added to the flow-through and incubated for 30 min on ice. In all the following steps, the columns were left to empty by gravity. 10 minutes before the incubation ended, the maxiprep column was equilibrated with 4 ml Buffer QBT. Filtered lysate was added on the column. The columns were washed twice with 10 ml buffer QC, which was added just before the column run empty. After the washes, 5 ml Buffer QN was added to elute the DNA into a 15 ml Falcon tube. Addition of 3.5 ml isopropanol and vortexing allowed precipitation of the DNA. Then the tube was centrifuged for 30 min at 4°C >15000 RCF. The DNA pellet was washed with 1 ml endotoxin-free 70% ethanol and centrifugation for 15 min at 4°C >15000 RCF. The ethanol was removed, and the pellet was left to dry. Last, the pellet was resuspended in 100 µl endotoxin-free water and the DNA concentrations were measured with the NanoDrop2000™ (Thermo Fisher Scientific).

4.2 Polymerase chain reaction (PCR) and Sequencing analysis

4.2.1 DNA extraction with Qiagen kit

DNA from cell pellets was extracted with the DNeasy Blood & Tissue Kit (Qiagen) as described in the manufacture's protocol. 20 µl Proteinase K was put into the tube containing the cell pellets, which were resuspended in 200 µl 1x PBS (Sigma-Aldrich). Before vortexing the tubes, 200 µl AL buffer was added and was followed by an incubation for 10 minutes at 56°C in a heating block (Eppendorf). Subsequently, 200 µl ethanol (VWR Chemicals) was added to the tubes and these were then vortexed. Next the mix was transferred into a DNeasy Mini Spin column and centrifuged. The centrifugation steps were all performed at RT for 1 min at 8000 RPM, except if stated differently. Following the centrifugations, the flow-through was discarded. Then, 500 µl AW1 buffer was added followed by a centrifugation step. Afterwards, 500 µl AW2 buffer was added and this time tubes were centrifuged at 14000 RPM for 3 min. Next, the spin column was put on a new tube and 50 µl of Milli-Q H_2O was added on the filter of the column. After 1 min of incubation, a centrifugation step followed. The flow-through containing the DNA was kept for subsequent analysis.

4.2.2 Quick extraction DNA isolation

Few cells were scraped off the plate, collected together with 5 µl medium and added to a PCR tube. Then 10 µl of QuickExtract DNA extraction solution (Epicentre) was added and the following PCR program: 15 min at 65°C, 15 min at 68°C, 10 min at 98°C and then cooled to 4°C.

4.2.3 PCR and sequencing

1 µl of DNA extracted with the quick extraction method or 50 ng of in Milli-Q H_2O were used. For cDNA sequencing the RNA was isolated and reverse transcribed and 50 ng was used for the PCR. The following PCR master mixes, listed in table 4-5, were prepared per sample depending on the desired PCR.

Reagent	GBA1 exon 8-11 MM µl per reaction	Standard PCR µl per reaction
Milli-Q H2O	9.5	13.3
5X Green GoTaq® Reaction Buffer	4	4
dNTPs (10 mM)	0.4	0.4
FW primer (table 4-6)	0.6	0.6
RV primer (table 4-6)	0.6	0.6
GoTaq® DNA Polymerase	0.1	0.1
DNA (1µl QE extraction or 50ng/µl)	1	1
Q solution	2.4	/
DMSO	1.4	/

Table 4-5: Polymerase chain reaction (PCR) Master Mixes (MM)

During the PCR reaction agarose gels were prepared. To do so SeaKem LE Agarose (Lonza) was dissolved in a 1x TBE buffer to the desired concentration and boiled in the microwave until all the particles were dissolved. When cooled down a bit, 8 µl Midori green (Nippon Genetics) were added per 100 ml. Following the PCR, 5 µl of the reaction were loaded on an agarose gel. To be able to sequence *GBA1* exons or the plasmid, an additional amplification of the individual plasmid segments or parts of the region of interest was required. Therefore, the leftover PCR product was purified. First 50 µl sodium acetate buffer was added, and the samples centrifuged for 45 mins at 3220 RCF 4°C. The supernatant was tapped of and 100 µl of 70% Ethanol (VWR Chemicals) added. A further centrifugation for 15 mins followed. This step was repeated once more. Then the samples were centrifuged upside down without lid for 1 min at 300 RCF. To resuspend the DNA, 15 µl Milli-Q water were added, and the samples were vortexed at the lowest level for 15 minutes. From this sample 1 µl was used to do a standard PCR with the respective primers. Then another sodium acetate purification was performed before the sequencing PCR.

Target	Primer	Forward (5'->3')	Reverse (5'->3')
Genomic *GBA1*	Exon 8-11	TGT GTG CAA GGT CCA GGA TCA G	ACC ACC TAG AGG GGA AAG TG
	Exon 8	TGT GTG CAA GGT CCA GGA TCA G	TTT GCA GGA AGG GAG ACT GG
	Exon 11	CAG GAG TTA TGG GGT GGG TC	GAG GCA CAT CCT TAG AGG AG
***GBA1* cDNA**	Exon 8	CGA GAC TTC ATT GCC CGT GA	TTG GGT CCT CCT TCG GGG
	Exon 10	CGT AAC TTT GTC GAC AGT CC	TTT AGC ACG ACC ACA ACA GC
Construct	CMV-BGH	CGC AAA TGG GCG GTA GGC GTG	TAG AAG GCA CAG TCG AGG
	construct	AAG GGA TTT GGA GGG GCC AT	GTA CTG TTG GCG AGG GTA GG
	CMV-construct	CGC AAA TGG GCG GTA GGC GTG	GTA CTG TTG GCG AGG GTA GG
	Construct-BGH	AAG GGA TTT GGA GGG GCC AT	TAG AAG GCA CAG TCG AGG

Table 4-6: Primers used for sequencing of GBA1 and the constructs

For the sequencing PCR the same primers as used in the previous PCR were used and are listed in table 4-6. For each reaction, either the forward (FW) or reverse (RV) primer was used. In table 4-7 lists the ingredients of reaction mix per sample are listed.

Reagent	µl per reaction
Milli-Q H_2O	2,65
BigDye™ Terminator v3.1 5X Sequencing Buffer	1,65
BigDye™ Terminator v3.1	0,7
Primer (FW or RV)	1
Purified DNA	4

Table 4-7: Master Mix for the sequencing PCR

After the sequencing PCR, the DNA was purified by sodium acetate precipitation. Then the pellet was resuspended in 15 µl Milli-Q H_2O and vortexed in the dark for 15 minutes at the lowest possible level. Then the samples were prepared for the sequencing. 10 µl Hi-Di Formamide (Applied Biosystems) and 7 µl sample were added in a MicroAMP™ optical 96-well reaction plate (Applied Biosystems). The plate was stored at 4°C in the dark until the gene sequencing with the 3130XL 16-capillary array Genetic Analyzer (Applied Biosystem). For sequencing the instrument protocol Pop7 and correct sequencing length was selected. The sequencing files were first loaded into PreGap4 (Staden) for the sequence assembly. Then they were analyzed with Gap4 (Staden).

4.3 T-Rex HEK cell culture and transfection

The composition of the media is listed in table 4-8. Flp-In T-REx 293 cells (called T-Rex HEK cells hereafter) were grown in empty T-Rex DMEM.

Medium	Ingredient	Quantity	Manufacturer	Catalogue number
Empty T-Rex DMEM	DMEM	500 ml	Sigma-Aldrich	D6546-500 ml
	Fetal bovine serum	50 ml	Gibco	16000044
	GlutaMAX	5ml	Sigma-Aldrich	P0781-100ml
	Blasticidin	550 µl	InvivoGen	ant-bl-1
	Zeocin	550 µl	InvivoGen	ant-zn-1
T-Rex DMEM	DMEM	500 ml	Sigma-Aldrich	D6546-500 ml
	Fetal bovine serum	50 ml	Gibco	16000044
	GlutaMAX	5ml	Sigma-Aldrich	P0781-100ml
	Blasticidin	550 µl	InvivoGen	ant-bl-1
	Hygromycin gold	550 µl	InvivoGen	Ant-hg-1

Table 4-8: Media used for T-Rex HEK cells

The day before the transfection, 5x10^5 T-Rex HEK cells were seeded per well of a 6-well plate in empty T-Rex DMEM without Zeocin. This allowed to reach a confluency of 50-80% on the following day. Late afternoon on the next day, the cells were transfected using calcium phosphate for the transfection. In brief, 75 µl of 2x HBS was mixed with 75 µl of a 0.25M $CaCl_2$ solution containing 4.55 µg POG44 plasmid and 0.455 µg pcDNA™5/FRT/TO plasmid containing the sequence of interest. This mix was incubated for 15 minutes at RT and then

added dropwise to a well of a 6-well plate. The medium was changed the following day. 48 hours after transfection the cells were split into T-Rex DMEM to start the selection. From here on, T-Rex HEK cells were grown in T-Rex DMEM until the expression was induced. Colonies were picked and transferred to new wells. The expression of the gene of interest was induced by treating the cells with 50 ng/ml doxycycline hyclate (Sigma-Aldrich) in DMEM+/- for 48 hours. All cells from any cell type used in this thesis were regularly checked for Mycoplasma with the Venor GEM Classic kit (Minerva Biolabs).

4.4 Analysis of the GCase interactome

4.4.1 Flag immunoprecipitation

Cells were detached and washed 2x with ice-cold PBS (Sigma). For the washes, the cells were spined at 4°C 1100 RPM for 5 minutes. Next the cell pellets were snap frozen in liquid nitrogen and frozen at -80°C until the co-immunoprecipitation (co-IP). To-do so, the cell pellets were lysed in lysis buffer for 45 minutes on a spinning wheel at 45 RPM at 4°C, followed by 10 minutes centrifugation at 10000 RCF at 4°C. Lysis buffer is composed of Tris-buffered saline (TBS) supplemented with 0.5 % NP40 (Sigma-Aldrich) and Protease and Phosphatase inhibitor (Thermo Fisher Scientific Inc.). The supernatant was taken off and filtered through a 22 µm filter unit (Millipore). Protein concentration was determined by Bicinchoninic acid (BCA) protein assay (Thermo Fisher Scientific Inc.). Briefly, 10 µl of prediluted cell lysate (1:10) or 10 µl of Albumin standard were mixed with 200 µl BCA working reagent (solution A mixed with solution B 50:1) in a 96-well plate. The assay was incubated for 30 minutes at 37°C. Then the absorbance was measured at 562 nm with the SpectraMax M2e reader (Molecular Devices) using the SoftMax Pro software (Molecular Devices). The protein concentration was calculated based on the equation given by the linear trendline of the standard curve. During the BCA, the anti-Flag M2 Affinity Gel (Sigma) was washed 4x on a spinning wheel (45 RPM) followed by a 30 second centrifugation at 500 RCF 4°C. First, they were washed with TBS, then with lysis buffer and then twice with washing buffer, which was composed of TBS, protease, and phosphatase inhibitor, 0.1% NP40. 10 mg of protein were incubated with 50 µl beads in a total volume of 1.8 ml. The lysate-anti-Flag affinity M2 gel mix is incubated for 2 hours at 4°C, 35 RPM. Next, the beads were transferred to spin columns and washed three times with washing buffer. For the elution of the precipitated protein, the beads where incubated with Flag Peptide (Sigma) for 20 minutes on the spinning wheel (35 RPM, 4°C) followed by a 1-minute centrifugation 1000 RCF. Before the assessment of the eluate with LC-MS, 5% of the sample were probed on a gel. The eluate was further processed for mass spectrometric measurement or subjected to western blot analysis.

4.4.2 Endogenous immunoprecipitation

For endogenous co-IPs, Protein G agarose fast flow beads (Millipore) were washed three times. To this end, the beads were incubated with lysis buffer on the spinning wheel (25 RPM) for 2-5 minutes at 4°C, followed by a 1 min centrifugation at 500 RPM 4°C. After washing the beads, latter were resuspended in wash buffer and distributed equally to the individual tubes. For the pre-incubation with the antibody against GCase, 13 µg of anti-GBA MaxPab antibody (Abnova), or rabbit IgG control (Enzo Life Sciences) were added to the beads. The bead antibody mix was incubated for 2 hours at 4°C and 20 RPM on the spinning wheel. In the meantime, NPCs were lysed as described above and the protein content determined with the BCA protein assay. After incubating the beads with the antibody, these were washed again three times. For the GCase co-IP, 3.5 mg protein was incubated on the spinning wheel for 2 hours with washed antibody decorated beads. Next, the beads were washed three times. Elution was performed by boiling the beads twice with 2x Laemmli buffer. After each boiling step, the beads were spun for 1 min at 10000 RCF and the supernatant collected and subjected to Western blot analysis.

4.4.3 Mass spectrometry analysis

4.4.3.1 Benzonase treatment

0.5 µl Benzonase (Sigma-Aldrich) was added to 40 µg of protein from lysates of cells expressing V5-Flag-tag CT, V5-Flag-tagged WT, p.E326K or p.L444P mutant GCase. The sample volumes were adjusted to 50 µl using HPLC H_2O and incubated for 30 min at 37°C. Digested samples were snap frozen in N_2.

4.4.3.2 Sample preparation for MS measurement and data collection

The samples were sent to EMBL Heidelberg for TMT-labelled mass spectrometric assessment where the samples were processed, measured and the data analysis performed. In brief what was done at EMBL Heidelberg, first the samples were processed for Trypsin digest and TMT11plex labelling with the TMT11plex Isobaric Label Reagent (Thermo Fisher Scientific Inc.). After purification of the samples, the peptides were trapped followed by an elution step. Then the samples were measured on an Orbitrap Fusion™ Lumos™ Tribrid™ Mass Spectrometer (Thermo Fisher Scientific Inc.). For initial data processing isobarQuant (Franken et al, 2015) and Mascot (v.2.2.07) were used together with the UniProt Homo sapiens database (UP000005640). The following criteria lead to exclusion of a peptide: The sequence had more than 2 Trypsin cleavage sites left or was shorter than 7 amino acids. Proteins that were not identified by minimum 2 unique peptides were as well excluded from further analysis. The definition of hit proteins was based on a false discovery rate (FDR) of 0.05 and a fold change (FC) of minimum 2. The FDR of candidate proteins was defined as less than 0.2 and at least a FC of 1.5.

4.4.3.3 Pathway analysis

Enrichment score was calculated using String Version 11.0 (Szklarczyk *et al*, 2019). To analyze the proteome data, lists of hits and candidates compared to V5-Flag-tag CT were generated. The Top10 biological processes with the lowest FDR are represented according to their -log10(FDR) on the graph. For the interactome analysis, a list containing the candidates and hits compared to V5-Flag-tag CT for WT was generated and uploaded on String (Szklarczyk *et al.*, 2019). As ranking value, the log(FC) was used and the FDR was set to 5%. The graph shows the Top10 biological processes with respect to their enrichment score. For the assessment of the proteins shared between the published list of endogenous GCase interactors (Tan *et al*, 2014) and our interactome, the list of gene names of both lists was compared by the Venn diagram platform (https://bioinformatics.psb.ugent.be/webtools/Venn/). For the analysis of the mitochondrial biological processes, the list of WT interactors containing hit and candidate proteins was compared to the MitoCarta 3.0 list (Calvo *et al*, 2016; Pagliarini *et al*, 2008; Rath *et al*, 2021) using the same Venn diagram online platform (https://bioinformatics.psb.ugent.be/webtools/Venn/). For the analysis of the mitochondrial biological processes, proteins shared between the MitoCarta3.0 list and our interactome were analyzed using String Version 11.0 (Szklarczyk *et al.*, 2019).

4.5 Generation and correction of new induced pluripotent stem cells

4.5.1 Generation of induced-pluripotent stem cell lines

Media composition for iPSC generation is listed in table 4-9. Fibroblast from PD patients with heterozygous p.E326K or p.L444P *GBA1* mutation were grown in DMEM+/+. When the fibroblast layer in the T75 flasks was confluent, the cells were washed once with 1x PBS and detached with 1x Trypsin/ETDA (Biochrom) by about 5 min incubation at 37°C. When the cells detached the reaction was stopped by adding fresh DMEM+/+. For the nucleofection, we used the Amaxa nucleofection kit for normal human dermal fibroblasts (NHDF; Lonza). 82µl NHDF solution was mixed with 18 µl Supplement. Then 10 µg of each plasmid, pCXLE-hOct3/4, pCXLE-hSK and pCXLE-hUL (all from Addgene, (Okita *et al.*, 2011)) was added. $7x10^5$ fibroblasts were resuspended with the nucleofection plasmid mix and nucleofected with the program P-022 of the Nucleofector 2b (Lonza). Fibroblasts were plated in a 6-well plate coated with Matrigel (Corning) in fresh DMEM+/- containing 10 µM Rock inhibitor Y-27632 2HCl (Selleckchem). The following day the medium was changed to DMEM+/+ supplemented with 2 ng/ml recombinant basic human fibroblast growth factor (PeproTech). Day 3 or 4 post-nucleofection, the medium was changed to E8 medium, supplemented with 100 µm Sodium butyrate and 0.1% Pen/Strep (Sigma-Aldrich). Colonies started to appear from day 14 onwards and were picked as soon as they were big enough. Induced pluripotent stem cells (iPSCs) were cultured on Vitronectin XF (StemCell Technologies) in E8.

Medium	Ingredient	Quantity	Manufacturer	Catalogue number
E8 medium	DMEM/F-12, HEPES	500 ml	Gibco	31330038
	L-Ascorbic acid (64 mg/L)	1ml	Sigma-Aldrich	A8960
	FGF2 (10 µg/ml)	500 µl	PeproTech	100-18B
	Insulin-Transferrin-Selenium (ITS -G)	5 ml	Gibco	41400045
	Heparin sodium salt from porcine intestinal mucosa (100 mg/ml)	0.5 µl	Sigma-Aldrich	H3149-25KU
	recombinant human TGF-ß1 (100 ng/µl)	10 µl	PeproTech	AF-100-21C
mTeSR	Basic mTeSR	450 ml	StemCell Technologies	85850
	5x mTeSR supplement	50 ml	StemCell Technologies	85850
	Penicillin/Streptavidin	5 ml	Sigma-Aldrich	P0781-100ml

Table 4-9: Medium used for HEK cell maintenance, iPSC generation and maintenance

To confirm integration free reprogramming, PCR reaction was used to confirm absence of the plasmid sequence in the line. As a positive control, the plasmids used for reprogramming or nucleofected cells were used. Untransfected cells were used as negative control. Primers are listed in table 4-10.

Primer	Forward (5'->3')	Reverse (5'->3')
KLF4	CCA CCT CGC CTT ACA CAT GAA G	TAG CGT AAA AGG AGC AAC ATA G
L-Myc	GGC TGA GAA GAG GAT GGC TAC	TTT GTT TGA CAG GAG CGA CAA T
Oct3/4	CATT CAA ACT GAG GTA AGG G	TAG CGT AAA AGG AGC AAC ATA G
Sox2	TTC ACA TGT CCC AGC ACT ACC AG	TTT GTT TGA CAG GAG CGA CAAT

Table 4-10: Primers used to check integration free reprogramming

4.5.2 Gene-correction

4.5.2.1 Gene-correction of GBA1 p.L444P mutation

The gene-correction for the p.L444P mutation was done as previously published (Schöndorf *et al.*, 2014). One hour before nucleofection, 10 µM Rock inhibitor Y-27632 2HCl (Selleckchem) was added to the culture medium. iPSCs were detached as single cells by incubation with Accutase (Sigma-Aldrich) for 5 minutes. $8x10^5$ cells were centrifuged and resuspended in 100 µl Ingenio Electroporation solution (Mirus), containing 3.3 µg linearized homologous construct with a Neomycin resistance and 0.833 µg of each zinc finger nuclease. The iPSCs were nucleofected with program B-016 of the Amaxa Nucleofector 2b (Lonza). After electroporation 500 µl mTeSR (StemCell Technologies) was added and the cells were plated in a Matrigel (Corning) coated 10 cm dish. The selection was started when colonies had formed

by adding 250 µg ml^{-1} of G418 (InvivoGen). Surviving colonies were transferred into 12-wells and sequenced to determine if the clone was gene-corrected.

4.5.3 Gene-correction of p.E326K GBA1 mutation

For the design of guides and the ssODN for the gene-correction, the sequence between GBA1 exon 7 to exon 9 was obtained from https://genome.ucsc.edu/index.html (Kent *et al.*, 2005). This sequence was than analyzed with the tool (http://www.genome-engineering.org/) provided by Ran et al. (2013) to identify potential guides. The guide containing the mutation in the sequence, which allowed to increase the specificity for the mutant allele, was chosen. Furthermore the protospacer adjacent motif (PAM) of this guide was closest to the mutation and therefore increasing the chance for successful gene-correction. To correct the p.E326K mutation, a mix of 3 µl crRNA (5'- CAG GCG GTG TGT CTT CCC TA-3'; 200 µM, IDT) with 6 µl Atto550 labelled tracrRNA (100 µM, IDT) was heated to 95°C for 5 min in the dark. Then they were left to cool down to RT on the bench in the dark. 7.5 µl crRNA: tracrRNA duplex were incubated for 10 minutes at RT with 4 µl Cas9 nuclease (62 µM, IDT, N° 1081058) to form the ribonucleoprotein (RNP) complex. 16 µl single-stranded oligodeoxynucleotides (ssODN; Ultramer DNA Oligo, IDT) were added to the RNP complex. The sequence of the ssODN was the following: 5'-CAT TGC TGT ACA TTG GTA CCT GGA CTT TCT GGC TCC AGC CAA AGC CAC CCT AGG GGA GAC ACA CCG CCT GTT CCC CAA CAC CAT GCT CTT TGC CTC AGA GGC CTG TGT GGG-3'. 1 hour before nucleofection, iPSC medium was supplemented with 10 µM Rock inhibitor Y-27632 2HCl (Selleckchem). iPSCs were incubated with Accutase (Sigma-Aldrich) to obtain single cells. $1.6x10^6$ cells were nucleofected with 13.6 µl RNP complex/ssODN mix in 100 µl Ingenio Electroporation solution (program B-016, Amaxa Nucleofector). Following nucleofection, the cells were spun at 1100 RPM for 5 min. The pellet was re-suspended in FACS buffer (PBS, 1mM EDTA, 2% FBS) filtered through a 40 µm nylon mesh and FACS sorted for Atto550 medium and high positive cells. Sorting was performed with a 100 µm on an ARIA IIIu flow cytometer using the DIVA software. It was done with the support of the Flow Cytometry Core Facility of the Universitätsklinikum Tübingen. 1x10^4 cells were plated per 10 cm dish. Colonies were picked and sequenced by Sanger sequencing to check for successful gene-correction. Furthermore, to confirm no chromosomal aberrations occurred, DNA was sent to Genomics – Life and brain in Bonn. To confirm absence of off-target effects, we used CCTOP (https://cctop.cos.uni-heidelberg.de:8043/; (Stemmer *et al*, 2015), Appendix 9.3) CRISPOR and (http://crispor.tefor.net/crispor.py; (Concordet & Haeussler, 2018), Appendix 9.4) to predict the 5 most likely off-target effects and sequenced the region with the primers listed in table 4-11.

Off-target	Forward (5'->3')	Reverse (5'->3')
NUDCD3	TGC CCC TTC CTC TCT AGA CC	TCA AGG CCA TCT TGT GAC CC
BBS9	CCA CAC GCA CCG AGG G	AGC ACT TAC AAC GGA CGC CA
RP11-576I22.2	GTT TGT GTT AGC GGA AGG CG	TGG CAA CCA GAA GTG AAT GC
WDR1	ACC CCT GGA ACA AAC TGG TG	CAT TTT GTC ACG GAA CCG CA
GBAP1	TCT TTG GTG AGA CTA CTA ATG GG	CAG GGT GAC TTG TTC TTC CTT TG
CDH23	GAG CCA AGA CTA GCA CCC AA	ACG CTG TAG GGC TGA TTG TG

Table 4-11: Primers used for the off-target sequencing

4.6 Differentiation of iPSC into neural precursor cells and dopaminergic neurons

The generation of neural precursor cells (NPCs) and the differentiation to midbrain dopaminergic neurons was done according to Reinhardt et al. (2013) . On day 0, colonies were cut into pieces using a needle (Terumo) and detached from the well to form embryoid bodies (EB) in hESC medium. hESC medium contains Knockout DMEM (Gibco), 20% Knockout Serum replacement (Gibco), 1% Pen/Strep (Sigma-Aldrich), 1% GlutaMAX (Gibco), 1% Non-essential amino acids (Gibco), 500 µM ß-Mercaptoethanol (Sigma) supplemented with 10 µM SB431542 (Selleckchem), 1 µM Dorsomorphin (Sigma), 3 µM CHIR99021 (CHIR, Sigma-Aldrich), 0.5 µM Purmorphamine (PMA; Merck Millipore) and 10 µM Rock inhibitor Y-27632 2HCl (ApoI, Selleckchem). On day 2, the medium was changed to N2B27 medium containing 50% Neurobasal Medium (Gibco), 50% DMEM/F12 (Gibco), 1% Pen/Strep (Sigma-Aldrich), 1% GlutaMAX supplemented with 10 µM SB431542, 1 µM Dorsomorphin, 3 µM CHIR, 0.5 µM PMA. Two days later the medium was changed to NPC-medium, which is composed of N2B27 medium supplemented with 3 µM CHIR, 0.5 µM PMA and 150 µm ascorbic acid (AA; Sigma-Aldrich). On day 6, part of the medium was removed and the EBs were triturated by pipetting up and down. The EB pieces were moved to a new Matrigel coated well of a 6-well plate containing fresh NPC-medium with 10 µM ApoI. Between day 8 to 10, the cells were split 1:10 using Accutase (Sigma-Aldrich). Every 2 days the medium was changed. When the cells were pure NPCs, the cells were split once a week when a confluent NPC layer covered well bottom. To start a differentiation to midbrain dopaminergic neurons, $1.25x10^6$ NPCs were split in a Matrigel coated 6-well containing NPC-medium with 10 µM ApoI. The following day the medium was changed to Differentiation medium. Differentiation medium is composed of N2B27 medium containing 100 ng/ml Fibroblast growth factor 8 (FGF8, PeproTech), 1 µM PMA and 200 µM AA. Medium change continued to be done every 2 days. Day 6 after starting the differentiation, $3x10^6$ cells were split into a Matrigel-coated well of a 6-well plate containing fresh Differentiation medium with 10 µM Rock inhibitor. The next day the medium was changed to Maturation medium supplemented with 0.5 µM PMA. Maturation medium consists of N2B27

medium supplemented with 10 µg/ml brain derived neurotrophic factor (BDNF; PeproTech), 10 µg/ml Glial-derived Neurotrophic Factor (GDNF; PeproTech), 1 ng/ml Transforming growth factor-ß3 (TGF-ß3; PeproTech), 500 µM N^6,2′-O-Dibutyryladenosine 3′,5′-cyclic monophosphate sodium (db-cAMP; PanReac AppliChem) and 200 µM AA. The medium was then changed every 2 days with Maturation medium. On Day 13 of the differentiation, the final splitting of the neurons was done using Accutase. During this splitting, the neurons were split in the final Matrigel-coated experimental plate or on coverslips. After 21 days of differentiation, the cells were ready to be used for experiments. To evaluate the differentiation potential, the cells were stained for TH, marker of dopaminergic neurons and ß3Tubulin, a pan neuronal marker. Antibodies are listed in table 4-14. The nucleus was stained with 4',6-Diamidino-2-Phenylindole, Dihydrochloride (DAPI, Biolegend). Pictures were taken in blinded fashion by Claudio Giuliano. Total nuclei were counted, as well as TH and ß3Tubulin positive cells. The number of dopaminergic neurons as well as the ß3Tubulin cells was divided by the number of nuclei to obtain the percentage of all and TH positive neurons.

4.7 Western blot analysis

Cells were collected and washed 1x with PBS. The pellets were lysed, and protein concentration determined as described for co-immunoprecipitation. 20 µg protein or 20-30 µl eluate of the Flag precipitation were mixed with 6x Laemmli containing 12.5 % ß-Mercaptoethanol. Samples were loaded on self-casted Acrylamide gels, usually containing 7.5-15% Acrylamide (composition shown in table 4-12) or gradient 4-12% pre-cast gels (Invitrogen™). Gels were run at 80 V until the samples reached the stacking gel, and then they were run at 120 V until the dye front run out of the gel or until desired separation was achieved.

Separation gel	Volume (ml) for 7.5%	Volume (ml) for 10%	Volume (ml) for 12.5 %	Volume (ml) for 15%	Stacking Gel	Volume (ml)
Lower Buffer	2,75	2,75	2,75	2,75	**Upper Buffer**	0,69
Acrylamide 40%	2,07	2,75	3,44	4,1	**Acrylamide 40%**	0,31
Milli-Q H2O	6,06	5,38	4,69	4,1	**Milli-Q H_2O**	1,72
APS 10%	0,11	0,11	0,11	0,11	**APS 10%**	0,028
TEMED	0,011	0,011	0,011	0,011	**TEMED**	0,003

Table 4-12: Composition of Western blot gels.

Polyvinylidene fluoride (PVDF) membrane (Life Technologies) was activated by 5-minute incubation in Methanol (VWR). Proteins were transferred on PVDF membrane for 2 hours at 200 milliampere or 20 V overnight at 4°C, followed by 2 hours at 100 V. PVDF membranes were blocked in TBS 0.1% Tween containing 5% Milk (Nonfat dried milk powder, PanReac

AppliChem) or 5% bovine serum albumin (Serva). Primary antibodies (Table 4-13) were diluted in antibody solution containing 5% Roche Block solution (Roche) or 5% BSA in TBS-T supplemented with 0.04% sodium azide. Primary antibody incubation was done overnight at 4°C on a shaker. The following day, the primary antibody was removed, and the membranes were washed 3x for 5 mins at RT. Then the secondary antibody was diluted in the same antibody solution as the primary antibody and incubated for 1 hour at RT on a shaker. After removal of the secondary antibody, the membrane was washed again 3x for 5 mins. ECL solution (Millipore) or for weak signals, SignalFire™ Elite ECL Reagent (Cell signaling technology) was prepared. The membranes were put on plastic in the developing cassette and the respective ECL was added on the membrane. After removal of the excess ECL, the membrane was covered with plastic and the cassette closed. In the dark room, the Ultra Cruz Autoradiography film (Santa Cruz) was laid on the plastic covering the membrane and incubated for the appropriate time depending on the target. Then the film was put into the developer. The membrane was scanned and the densitometric analysis was carried out with Image J (Schneider *et al*, 2012). For calculating the ratio of the interaction, the value obtained for the protein of interest was divided by the respective Flag value. Then all ratios were normalized on WT.

Target	Host	WB	Brand	Cat number
ß-Actin	Mouse	1:10000	Sigma Aldrich	A5441-0.1
ATP5B	Mouse	1:1000	Santa Cruz	sc-135903
Calnexin (TO-5)	Mouse	1:200	Santa Cruz	sc-80645
DJ-1	Mouse	1:1000	Santa Cruz	sc-55572
DYKDDDDK Tag (Flag)	Rabbit	1:1000	Cell Signaling Technology	14793S
GBA1	Mouse	1:1000	Sigma-Aldrich	WM0002629M1
GRP78	Rabbit	1:8000	Proteintech	11587-1-AP
GRP94	Rabbit	1:1000	Proteintech	14700-1-AP
HSC70	Mouse	1:1000	Santa Cruz	sc-7298
HSP60*	Mouse	1:3000	Santa Cruz	sc-271215
HSPA8 (D12F2)	Rabbit	1:1000	Cell Signaling Technology	8444S
LONP1	Rabbit	1:2000	Proteintech	15440-1-AP
NDUFA10	Mouse	1:1000/1:4000	Santa Cruz	sc-376357
TBC1D15	Rabbit	1:2500	Novus Biologicals	NBP2-36552
TIM23	Rabbit	1:1000	Proteintech	11123-1-AP
TOM70	Rabbit	1:1000	Proteintech	14528
Vinculin	Mouse	1:1000	Santa Cruz	sc-73614

Table 4-13: Antibodies used for Western blot analysis

4.8 Immunofluorescent labelling

For pluripotency staining, pieces of iPSC colonies were plated on Matrigel-coated (Corning) coverslips (VWR). For other immunofluorescent labellings, 10000-20000 cells were plated on Matrigel coated coverslips. Before fixation, the cells were washed once with PBS. Fixation was done for 10 minutes in 4% PFA (Sigma-Aldrich) at RT. Then the cells were washed 2x with PBS. The coverslips were stored in PBS at 4°C until the staining was performed. For the staining, the coverslips were moved to a new well and incubated for 1 hour with 250 µl blocking solution, which consisted of PBS containing 10% normal goat serum (NGS; Biozol) and 0.1% Triton-X (Carl Roth) in case of intracellular immunofluorescent staining, at RT. For the staining of cell membrane proteins, the blocking was done in the same way only that the blocking solution did not contain Triton-X. Primary and secondary antibody solutions were prepared in blocking solution containing 5% NGS. Primary antibodies (Table 4-14) were diluted and 50 µl were pipetted on parafilm in a wet chamber, consisting of a tip box with water and paper in the lower chamber and parafilm on the tip stray. The coverslips were removed from the well containing the blocking solution and put upside down on the antibody solution. Primary antibody was incubated O/N at 4°C. The next day, the coverslips were moved back in a 24-well plate and washed 3x for 5 mins with PBS only for surface markers or PBS containing 0.1% Triton-X for internal markers.

Target	Host	ICC	Brand	Cat number
DYKDDDDK Tag (Flag)	Rabbit	1:1000	Cell Signaling Technology Inc.	14793S
GBA1	Mouse	1:1000	Abcam	Ab88300
GFP	Mouse	1:500	Sigma-Aldrich	G6539
LAMP1	Mouse	1:40	Developmental Studies Hybridoma Bank	H4A3
LAMP1	Rabbit	1:200	Cell Signaling Technology Inc.	9091
LONP1	Rabbit	1:100	Proteintech	15440-1-AP
OCT3/4 (3A2A20)	Mouse	1:1000	Biolegend	653702
ß3tubulin	Mouse	1:1000	Biolegend	801202
Tom20	Mouse	1:500	Santa Cruz	sc-11415
Tra1-60	Mouse	1:50	Millipore	MAB4360
Tra1-81	Mouse	1:50	Millipore	MAB4381
Tyrosine Hydroxylase	Rabbit	1:500	Pel-Freeze Biologicals	P40101-150
V5 Epitope	Rabbit	1:1000	Novus Biologicals	NB600-381

Table 4-14: Antibodies used for immunofluorescent staining

Alexa Fluor conjugated secondary antibodies (Invitrogen™) were diluted, 250 µl were added to each well and incubated for 1 hour at RT in the dark. Then the coverslips were washed once, followed by a 5 min incubation with DAPI (Biolegend). Before the mounting, the cells were washed twice with PBS. For mounting 10 µl Dako mounting medium (Agilent) was added

to a slide. Then the coverslip was removed from the well, the side of it was dried on a paper towel to remove excess liquid. The coverslip was mounted upside down on the glass slide. The slides were assessed with the Zeiss Axio Observer.Z1/7 with either the Plan-Apochromat 20x/0.8 M27 objective or the Plan-Apochromat 63x/1.40 Oil DIC M27 using the Zen blue software (Zeiss) to acquire pictures. Alternatively, the TCS SP8 confocal microscope (Leica Biosystems) was used with the 63x 1.4NA plan-apochromat oil objective. For the thesis, the signal of the pictures, as well of the negative control, was enhanced.

4.9 Proximity ligation assay

Cells were fixed for 10 minutes with 4% PFA and then permeabilized for 1 hour in PBS-T at RT. Proximity Ligation assay (Duolink® In Situ Red Starter Kit Mouse/Rabbit, Sigma-Aldrich) was performed according to the Manufacture's protocol. All of the following incubation steps are performed at 37°C in a pre-warmed humidity chamber. In brief, after permeabilization of the cells blocking was performed by adding one drop of Duolink® Blocking Solution per well. The slide was placed in a prewarmed humidity chamber (as used in the immunofluorescent staining protocol) and incubated for 1 hour at 37°C. In the meantime, the primary antibody solution was prepared in Duolink® Antibody Diluent. Primary antibodies are listed in table 4-15. 15 µl primary antibody solution was incubated O/N at 4°C in a humidity chamber.

Target	Host	PLA	Brand	Cat number
DYKDDDDK Tag (Flag)	Rabbit	1:1000	Cell Signaling Technology	14793S
LONP1	Rabbit	1:1000	Proteintech	15440-1-AP
V5 Epitope	Mouse	1:1000	Biolegend	680602

Table 4-15: Primary antibodies used for the proximity ligation assay

For the washing steps, the slide was incubated twice for 5 mins in washing buffer A at RT. The next day the antibody solutions were tapped off the slide, which then was washed twice for 5 min in washing buffer, shaking at RT. In the meantime, the Duolink® PLA probe was prepared by mixing the Plus and Minus strands in a 1:5 in Duolink® Antibody Diluent. After the second wash, the washing buffer was removed and 15 µl Duolink® PLA probe was added per well and incubated for 1 hour at 37°C. After the incubation with the PLA probe, the solution is removed from the slide followed by a washing step. In the meantime, the ligation buffer is prepared by mixing 15.2 µl Milli-Q H_2O, 3.8 µl 5x buffer with 1 µl Ligase. 20 µl were applied per well and the ligation reaction was left for 30 min. After removal of the ligase, the slide is washed again while the amplification solution is prepared by mixing the buffer at a ratio of 1:5 with Milli-Q H_2O and 0.25 µl Polymerase is added per 20 µl Amplification buffer. The amplification reaction was performed for 100 min in the dark. Then the slides were washed twice for 10 minutes with wash buffer B followed by a 1 min wash with 0.01 % wash buffer B. The excess buffer was removed and the coverslip was mounted with Duolink® In Situ Mounting Medium with DAPI and the edges of the coverslip fixed with nail polish. 15 minutes later, the slides were assessed

with the microscope. Pictures were acquired with an Axio Observer.Z1 (Zeiss) using a 63x 1.4NA plan-apochromat oil objective or 20x 0.8 NA plan-apochromat objective. For the thesis, the signal intensity was enhanced for all the pictures including the negative controls.

4.10 qRT PCR analysis

4.10.1 RNA isolation

The RNA place was cleaned from RNase, by spraying RNAseZAP™ (Sigma-Aldrich) and whipping the place with Milli-Q H2O after incubation. The RNA was extracted using the RNeasy Mini kit (Qiagen) according to the manufacturer's protocol on ice. The cell pellet was lysed by adding 350 µl RLT buffer. Then 350 µl 70% ethanol was added, mixed by pipetting up and down and transferred to a RNeasy mini column (Qiagen). The column was then spun for 15 sec at 8000 RCF, which was as well the condition used for the following centrifugations. After the centrifugation, the flow-through was discarded. Next, 700 µl buffer RW1 was added and followed by a centrifugation step. The next step, addition of 500 µl RPE followed by spinning of the column was repeated twice. The second centrifugation step was elongated to 2 mins. After discarding the flow-through, the empty column was spun at 13000 RPM. The column was transferred to a new tube and 30 µl RNase-free water was added on top of the membrane. After 1 min incubation, the tube with the column was centrifuged for 1 min at 8000 RCF. The flow-through was kept on ice and directly processed or stored at -80°C until further processing.

4.10.2 Reverse transcription an qRT PCR

For the cDNA synthesis, the reagents from the QuantiTect Reverse Transcription kit (Qiagen) were thawed at RT. Only the Quantiscript Reverse Transcriptase was thawed on ice. The protocol was performed as described by the manufacturer (Qiagen). To remove genomic DNA, 12 µl of isolated RNA was mixed with 2 µl 7x gDNA Wipeout Buffer. This mix was then incubated for 10 mins at 42°C. After the incubation, the tubes were straight away put on ice. In the meantime, the master mix for the cDNA synthesis was prepared. Per sample, it consisted of 4 µl 5x Quantiscript RT Buffer, 1 µl RT Primer Mix, and 1 µl Reverse Transcriptase. 6 µl of the master mix were added per sample after removal of genomic DNA. This mix was then incubated for 30 mins at 42°C, followed by a 3 mins incubation at 95°C to inactivate the enzyme. The generated cDNA was then quantified with the NanoDrop2000™ (Thermo Fisher Scientific). For the qPCR, part of the sample is diluted to 50 ng cDNA/µl and 2 µl were distributed per well of an MicroAmp™ Optical 384-Well Reaction Plate with Barcode (Applied Biosystems™). Furthermore, 5 µl QuantiTect SYBR Green (Qiagen) and 3 µl of a mix containing 5 µM FW and RV primer were added per well. After 1 min centrifugation at 1000 RPM at 4°C, the plate was introduced into the QuantStudio RealTime PCR system (Applied Biosystems) and the standard program was run.

4.11 shRNA mediated KD using Lentivirus in T-Rex HEK cells

4.11.1 Virus generation

The day before the transfection, to reach a confluency of about 80%, 6x10^6 HEK 293 cells were seeded per 10 cm dish in DMEM+/- medium. The following day (Day1), 600 µl OptiMEM (Gibco) was mixed with 4.05µg psPAX2 (Addgene), 0.450 µg pMD2.G (Addgene) and 4.5 µg of the respective shRNA plasmid. Later are listed in table 4-16. psPAX2, encoding lentiviral packaging proteins, and pMD2.G, encoding viral envelope proteins, were a gift from Didier Trono (Addgene plasmid # 12260 and Addgene plasmid # 12259). The sequences for TIM23 KD1 and TIM23 KD2 were previously published (Goemans *et al*, 2008). Information on shRNAs is shown in Table 4-16. After addition of the plasmids to the OptiMEM, 40 µl of TransIT-X2 (Mirus) was added. The mix was swirled and incubated for 30 mins at RT. Afterwards the transfection mix was added dropwise to one 10 cm dish per shRNA.

Target	Vector name	Sequence	Vector ID	Design/Vendor
TIM23	pLV[shRNA]-Puro-U6>Tim23 KD1	ATGACAGGCATGTTGTATA	VB210128-1106hrg	Goemans et al., 2008/ VectorBuilder
TIM23	pLV[shRNA]-Puro-U6>Tim23 KD2	CTCTGTCTCCTTATTTAAA	VB210129-1039mum	Goemans et al., 2008/ VectorBuilder
Scramble (No-target)	pLV[shRNA]-Puro-U6>Scramble_shRNA#1	CCTAAGGTTAAGTCGCCCTCG	VB010000-0005mme	VectorBuilder
HSPA8	MISSION® pLKO.1-puro HSPA8 shRNA KD1	GCAACTGTTGAAGATGAGAAA	TRCN0000017279	Sigma Mission library
HSPA8	MISSION® pLKO.1-puro HSPA8 shRNA KD2	CCAAGACTTCTTCAATGGAAA	TRCN0000017281	Sigma Mission library
Scramble (non-target)	MISSION® pLKO.1-puro non-Target shRNA Control plasmid DNA	/	SHC016	Sigma Mission library

Table 4-16: shRNAs used to generate knockdown for HSC70 and TIM23

The following day the medium was changed to DMEM+/+ medium. Virus containing medium was collected at 2 timepoints, day 4 and 5 after transfection, and replaced with fresh DMEM+/+. The collected medium was filtered through a 0.45 µm PVDF syringe filter (Millipore) and stored at 4°C until the upconcentration of the virus on day 5. To concentrate the virus, the filtered medium was added in a Vivaspin20 centrifugal concentrator (Sartorius) and centrifuged at 3000 RCF at 4°C until the virus was concentrated to a volume between 0.5-1 ml. The concentrated virus was distributed into small aliquots of 20 µl and stored at -80°C until the infection of the cells. To estimate the amount of virus in the concentrate, Lenti-X GoStix Plus (TaKaRa) were used to determine the concentration of the viral protein p24. The viral concentrate was diluted with medium and 20 µl were applied on the test sticks. Then 80 µl of

chase buffer was added and the reaction was incubated for 10 mins at RT. Next the app was used to determine the concentration of p24.

4.11.2 Viral infection of T-Rex HEK cells

For the individual assays, the virus concentration leading to KD was determined. The same viral concentration was applied for scramble as well as the shRNAs of the respective target. 5x10^5 T-Rex HEK cells for induction of either CT or p.L444P were plated per 6-well in DMEM+/-. The following day cells were infected with the quantity of virus corresponding to 40000 ng p24/ml for scramble and both HSPA8 shRNAs and 80000 ng p24/ml for scramble and corresponding TIM23 shRNAs. 24 hours after infection, the medium was changed with DMEM+/- containing puromycin (InvivoGen) to start the selection. On day 4, the cells were split from the 6-well to a 10 cm dish (Falcon). The next splitting was on day 8 during which 10x10^6 cells were split in a 15 cm dish (Thermo Fisher Scientific). The following day induction of the expression of CT or p.L444P GCase was started by a medium change to DMEM+/- containing 50 ng/ml doxycycline. 48 hours later the cells were collected, and a small amount was subjected to WB analysis to make sure that the KD worked, before using up to 10 mg of lysate for Flag IP.

4.12 GCase activity assays

4.12.1 Whole cell activity assay

The day before the GCase activity assay, $1x10^5$ cells were split into one well of a 48-well plate. Per condition triplicates were seeded for each measurement. To assess background signal, Conduritol B epoxide (CBE), which is an inhibitor of GCase, was added to McIlvaine buffer (pH 6.0) to reach a final concentration of 4 mM. Cells were washed once with 1x PBS. After removal of PBS, 500 µl of McIlvaine buffer with and without CBE was added to the cells and incubated for 30 minutes at RT. In the meantime, 4-methylumbelliferyl-β-D-glucopyranoside (MUB-Glc; Glycosynth) was dissolved in 0.2 M acetate buffer (pH 5.2). Part of the substrate solution was mixed with CBE to achieve a final concentration of 1 mM CBE in acetate buffer. McIlvaine buffer was removed from the cells, and 150 µl substrate solution with or without 1mM CBE was added to the cells. The plate was then incubated for 5 hours at 37°C. Next 750 µl of 0.2 M Glycine (pH 10.2) was added. The plate was measured in the SpectraMax M2e reader (Molecular devices; excitation:355 nm; emission 460 nm). For evaluation, the value obtained in the wells treated with CBE were subtracted from the wells without CBE to remove non-GCase background signal and the average of the technical replicates calculated.

4.12.2 Cell lysate-based GCase activity assay

Cells were lysed by sonication in H_2O containing 0.01% Triton-X 100 (Carl Roth), and the protein concentration was determined by BCA (thermos Fisher Scientific). MUB-Glc was dissolved in 200 mM sodium citrate phosphate buffer by heating to 60°C. 10-20 µg protein was

mixed with 0.81 mM CBE (Calbiochem) or H_2O and 2.5 mM MUB-Glc in the presence of taurocholic acid (Sigma). The reaction was incubated for 1 hour at 37°C shaking in the dark. Addition of 1.8 ml 0.2 M glycine buffer (pH10) stopped the reaction. 200 µl were transferred to a microplate for fluorescence-based assays (Thermo Fisher Scientific Inc.). Measurement was done in triplicate on the SpectraMax M2e reader (Molecular devices; excitation: 355 nm; emission: 460 nm). Evaluation was done as for the GCase activity assay in whole cells.

4.13 Mitochondrial respiration analysis using Seahorse XF96 analysis

Three days prior the seahorse analysis, 1x10^4 T-Rex HEK cells were plated per well of a XF96 cell culture microplate. Next day, the 48 hours doxycycline treatment (50ng/ml) was started. Following the treatment, the cells were ready for assessment of mitochondrial respiration. For midbrain dopaminergic neurons, the differentiation protocol described above was followed. During the final splitting, 1.5x10^5 cells were plated in each well of a XF96 cell culture microplate (Agilent). One to two weeks later the Seahorse analysis was conducted. The evening before the experiment, the plate of the XFe96 sensor cartridges (Agilent) was filled with 200 µl water to hydrate the sensors at 37°C O/N. Before the calibration, water was removed, and warm calibration buffer added and incubated for 1 hour at 37°C. The 10x concentrated toxins were prepared in parallel. The final toxin concentrations used in the assays are listed in table 4-17.

Toxin	T-Rex HEK cells	Neurons
Oligomycin (Sigma-Aldrich)	20 µM	1 µM
CCCP (Sigma-Aldrich)	1µM	5 µM
Antimycin (Sigma-Aldrich)	2 µM	1 µM
Rotenone (Sigma-Aldrich)	2 µM	1 µM

Table 4-17: Toxins and concentrations for T-Rex HEK cells and iPSC-derived dopaminergic neurons used for Seahorse experiments.

After 1 hour, the XFe96 sensor cartridges was taken out of the incubators, and the toxins were added in the respective wells. Next, the calibration of the Seahorse XFe96 Analyzer (Agilent) was started. Seahorse medium was prepared by mixing 48.5 ml Seahorse XF DMEM medium (Agilent) with 500 µl GlutaMAX, 500 µl Seahorse XF 100 mM pyruvate solution (Agilent) and 500 µl Seahorse XF1.0M glucose solution (Agilent). In the meantime, the medium of the cells was changed to Seahorse medium by exchanging twice 180 µl of medium with seahorse medium. Next, the plate containing the cells was introduced into the Seahorse XFe96 Analyzer (Agilent) and the run started. After the assay, the medium was removed and replaced with 10 µl lysis buffer. The plate was then frozen at -80°C until the next day. For the lysis, the plate was placed on the shaker for 1 hour at 4°C. Afterwards, the lysis buffer was pipetted up and down, and the wells of the same condition collected in one tube. After centrifugation at 10000

RCF for 15 mins, the supernatant was collected and subjected to BCA (Thermo Fisher Scientific) to determine the protein concentration. The analysis was conducted using the Wave 2.6 software (Agilent) and was normalized to the protein concentration of the different conditions. Assessment of the individual curves allowed identifying the outlier wells, which did not respond well to the toxins.

4.14 Split-GFP analysis of GCase mitochondrial localization

4.14.1 Design of the constructs

Mitochondrial matrix targeted split-GFP1-10 (MTS-GFP1-10) was designed as previously described (Calì *et al*, 2015) and obtained from VectorBuilder. The sequences of the constructs used are listed in Appendix 9.2. MTS-GFP1-10 was cloned into pcDNA^{TM}5/FRT/TO, and the stable T-Rex HEK cells generated as described above. For GCase split-GFP (GBA1-S11ß), a 27 bp linker followed by the GFP-S11ß sequence (Calì *et al.*, 2015), was added at the C-terminal of the *GBA1* cDNA sequence. As positive control (MTS-GBA1-S11ß), the matrix targeting sequence was inserted at the same location as the V5-Flag-tag in the *GBA1* sequence and the linker plus GFP-S11ß was added at the C-terminal. Plasmids containing the *GBA1-S11ß* or *MTS-GBA-S11ß* constructs were ordered from VectorBuilder. p.E326K or p.L444P mutation was inserted in the WT construct using side-directed mutagenesis (QuikChange XL II, Agilent). For MTS-GFP1-10 induction, 2x10^4 MTS-GFP1-10 T-Rex HEK cells were seeded on Matrigel-coated chambered cell culture slides (Ibidi) for live-cell imaging or on glass coverslips for immunofluorescent staining. For the immunofluorescent staining, the cells were treated with 200 ng/ml doxycycline for 48 hours. For live-cell imaging, *GBA1-S11ß* or *MTS-GBA-S11ß* constructs were transfected the next day using ViaFect (Promega). To do so, 1.5 µg of the plasmid was mixed with OptiMEM (Gibco) to obtain 100 µl solution. Then 3 µl ViaFect was added, and the mix was incubated for 20 min at RT. Then 40 µl were added dropwise per well. The next day, MTS-GFP1-10 was induced by treatment with 50 ng/µl doxycycline in DMEM+/- for about 24 hours.

4.14.2 Live cell imaging

For live cell imaging, cells were washed once with OptiMEM (Gibco) and then incubated for 20 mins with 100 nM MitoTracker red CM-H_2Xros (Invitrogen^{TM}) in OptiMEM. Cells were washed once with OptiMEM, and new OptiMEM was added for imaging. Images were generated with a 63x 1.4NA plan-apochromat oil objective of a TCS SP8 confocal microscope (Leica Biosystems). Signal of images was increased for the thesis. As control of signal increase, the negative control was always increased as the highest increase for another picture.

4.15 Blue Native Electrophoresis for CI integrity assessment

Cell pellets of NPCs and iPSC-derived neurons from GD-1 and PD-3, isogenic controls and *GBA1* KO were generated and shipped on dry ice to Cristina Ugalde's lab in Madrid. Here María Illescas conducted the following steps. The mitochondria were isolated from the pellets and prepared for the analysis by blue native gel electrophoresis according to a published protocol (Lobo-Jarne *et al*, 2020), which was slightly modified. The mitochondrial pellets were treated with digitonin to solubilize them. Pre-cast NativePAGE™ 3-12% Bis-Tris gels (Invitrogen™) were used to run 40 µg of mitochondrial proteins and then transferred onto a PVDF membrane. The bands for CI and CII were detected using antibodies from Abcam against NDUFA9 and SDHA, respectively.

4.16 Statistical analysis

For statistical analysis GraphPad Prism Version 9 software (GraphPad software) was used. For the analysis of the data, we performed the two-tailed Students' t-test and the ordinary one-way ANOVA test followed by Tukey's multiple comparison test. Statistical significance was set to a P-value <0.05. Data is shown as mean ± Standard error of the mean (S.E.M.). Each replicate is shown as a circle in the graph and the number of technical or biological replicates is indicated in the figure legend.

4.17 Illustrations

Illustrations were created using PowerPoint (Microsoft office).

5 Results

5.1 Generation and characterization of T-Rex HEK cell lines

To gain insight into the interactome of GCase and aberrant interactions that might be linked to *GBA1*-PD, we decided to assess the interactome of WT, the severe p.L444P and the mild, non-GD p.E326K mutant GCase using co-IP, followed by quantitative TMT LC-MS analysis. To do so a tagged, inducible overexpression model was chosen as this approach minimizes patient-related genetic background issues. Furthermore, overexpression allows immunoprecipitation of sufficient p.L444P mutant protein for proper analysis. The V5-Flag-tag was attached at the N-terminus behind the first three amino acids after the leader sequence to not interfere with the targeting of GCase. To ensure that the function of the protein is not disturbed by the presence of the tag, these three amino acids were repeated after the tag. In order to assess whether the tag affects the proper localization of GCase, the sequence of V5-Flag-tagged WT *GBA1* and WT *GBA1* without a tag, called V5-Flag-GCase and WT-GCase respectively in the figures, were cloned into the plasmid pcDNA^{TM}3.0. *GBA1* KO neural precursor cells (NPCs) were nucleofected with either of these constructs. Immunofluorescent staining confirmed a diffuse localization of tagged and untagged GCase within the cell and the co-localization of tagged and untagged GCase with the lysosomal marker LAMP1 (Figure 5-1 A). Furthermore, HEK cells transfected with these plasmids for 48 hours showed a comparable increase in GCase activity compared to untransfected (UT) cells (Figure 5-1 B). These results confirm that GCase localization as well as activity is not affected by the chosen tagging strategy.

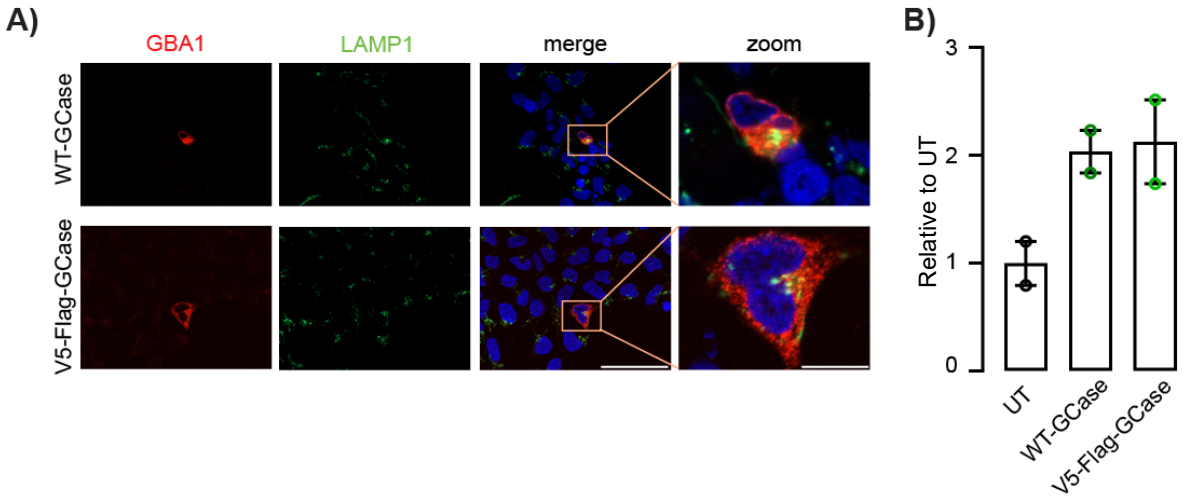

Figure 5-1: Evaluation of V5-Flag-tag model. A) *GBA1* KO neural precursor cells were nucleofected with a plasmid coding for either WT or V5-Flag-tagged WT GCase. Staining with anti-*GBA1* and anti-LAMP1 antibodies allowed assessment of localization (n=1). B) GCase activity measurement in untransfected (UT) and WT-GCase or V5-Flag-tagged WT GCase overexpressing HEK293 cells. (mean ± SEM is shown, n=2 biological replicates)

Next to generate the inducible cell lines, the sequence of tagged WT *GBA1* was cloned from the pcDNA^{TM}3.0 plasmid into the pcDNA^{TM}5/FRT/TO plasmid. As negative control for the co-

IP experiments, we generated T-Rex HEK cells with inducible overexpression of the V5-Flag-tag only. This sequence was cloned into pcDNA^{TM}5/FRT/TO too. Generation of the inducible T-Rex HEK cells was achieved by transfection of the cells with the plasmid of interest and the POG44 plasmid, which codes for the FLP recombinase. This allowed insertion of the plasmid at the FRT site in the T-Rex HEK cell genome. Based on literature, the induction was evaluated after 48 hours of treatment with 0, 50, 100, 200 and 400 ng/ml doxycycline. Since there was no apparent difference between the different concentrations (Figure 5-2 A), we chose to treat the cells with the lowest concentration of 50 ng/ml doxycycline for 48 hours to reduce potential side-effects. As no band was detectable using WB, after induction of V5-Flag-tag control (not shown), qPCR was performed to validate the expression (Figure 5-2 B).

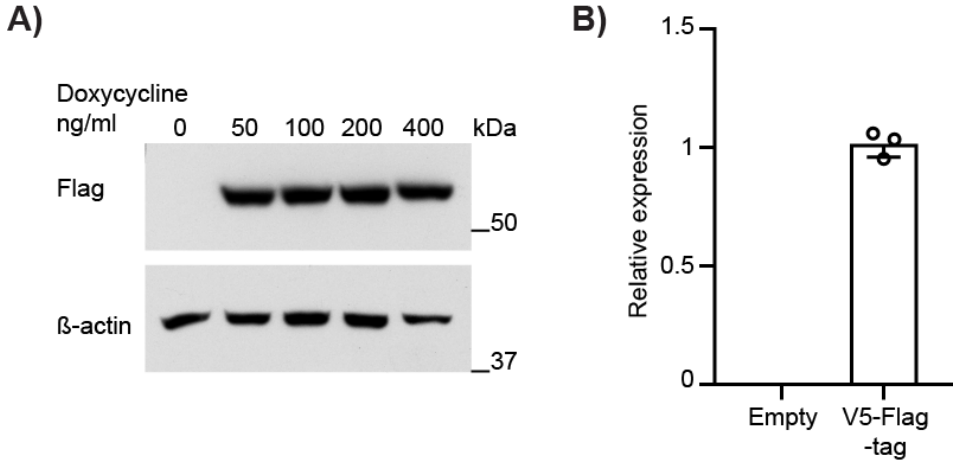

Figure 5-2 Doxycycline dose titration and V5-Flag-tag mRNA expression. A) Western blot of V5-Flag-tagged WT GCase expression in T-Rex HEK cells treated with 0, 50 ng/ml, 100 ng/ml, 200 ng/ml, and 400 ng/ml doxycycline for 48 hours (n=1) B) Quantification of V5-Flag-tag control mRNA expression determined by quantitative real-time PCR (n=3 technical replicates, mean ± SD is shown).

To generate the p.E326K and p.L444P mutant plasmids, site-directed mutagenesis was used to mutate the respective nucleotides on the WT plasmid. Figure 5-3 A shows correct mutation of the G to an A nucleotide originally at position 1093 in the *GBA1* gene for the p.E326K mutation, and mutation of the nucleotide T at position 1448 to a C to obtain the p.L444P mutation, respectively. The mutant GCase overexpression T-Rex HEK cell lines were generated in parallel to the WT GCase and control lines. After selection with Hygromycin B gold, clones were picked and expanded. Induction of expression upon treatment with 50 ng/ml doxycycline for 48 hours was analyzed by indirect immunofluorescence and WB (Figure 5-3 B and C respectively). As seen in patients, mutant GCase is unstable, leading to decreased immunofluorescent signal. WB quantification demonstrated a decreased GCase protein level between WT and mutant GCase (Figure 5-3 C). On average, tagged p.E326K GCase levels were lowered by 27% compared to tagged WT. p.L444P GCase protein level was only about 40% of WT levels. p.E326K GCase protein levels were 1.8-fold increased compared to p.L444P GCase. Furthermore, overexpression of WT GCase led to an average 11.8-fold increase of GCase activity compared to V5-Flag-tag expressing cells (Figure 5-3 D). GCase

activity of tagged p.E326K and p.L444P mutant resulted in a 3.6-fold and 1.7-fold increase in GCase activity respectively compared to the V5-Flag-tag control (Figure 5-3 D).

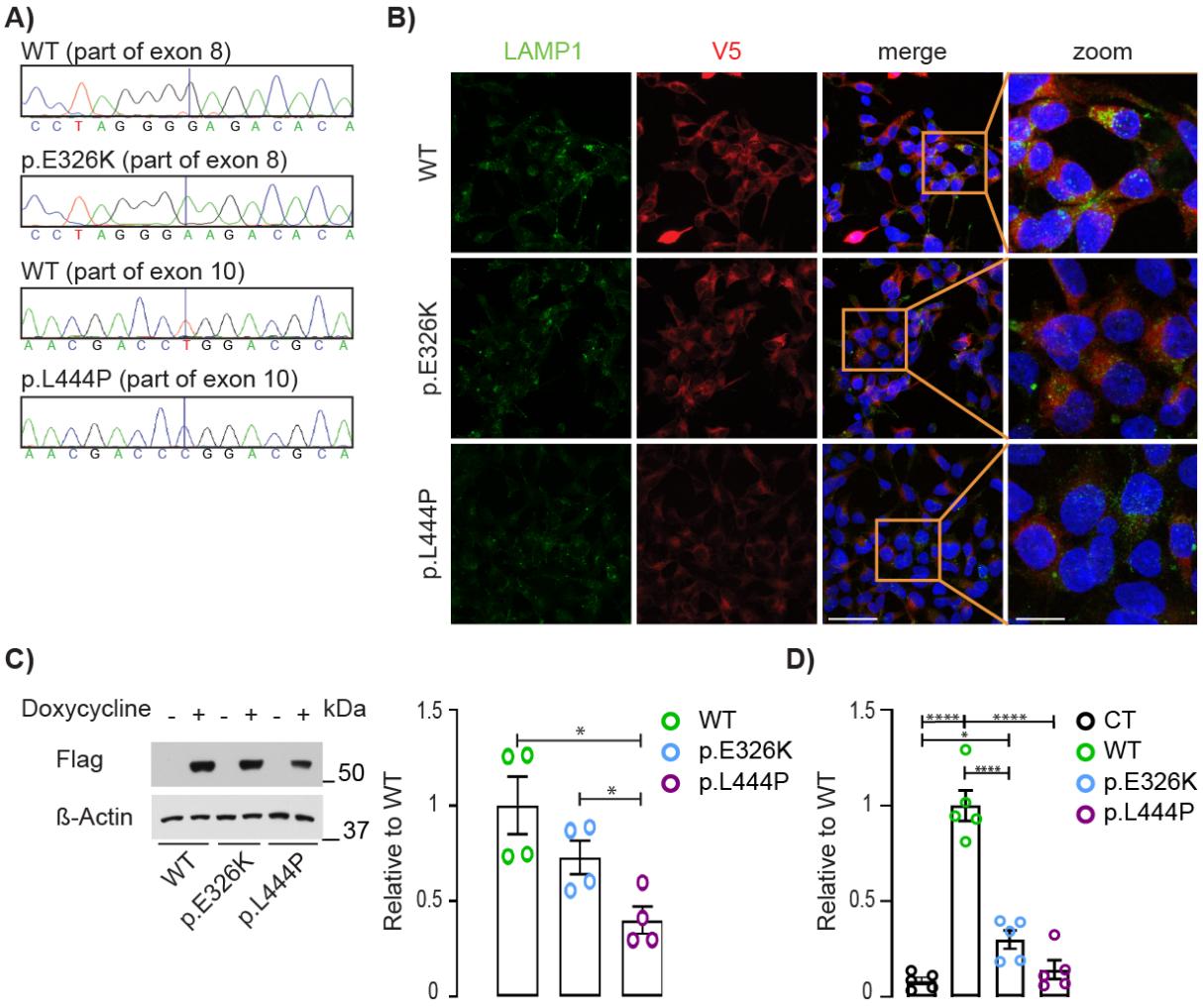

Figure 5-3 Characterization of the V5-Flag-tagged glucocerebrosidase (GCase) overexpression T-Rex HEK cell model. A) Sanger sequencing of tagged p.E326K- and p.L444P-*GBA1* plasmids used for generating the T-Rex HEK cell lines showing correct mutagenesis of the WT plasmid. B) Immunofluorescent labelling for the lysosomal marker LAMP1 (green) and V5 (GCase, red) of T-Rex HEK cells overexpressing tagged WT-, p.E326K- or p.L444P-GCase. (Scale bar is 50 µm and 10 µm in the zoomed pictures.) C) Representative Western blot for Flag (GCase) of uninduced and induced T-Rex HEK cells and quantification (Mean ± SEM is shown, unpaired students T-test was performed, * <0.05, n=4 biological replicates). Representative Western blot is shown in the publication by Baden, Pérez et al. (Baden et al., 2023). D) Glucocerebrosidase activity assay of V5-Flag-tag control (CT) and V5-Flag-tagged WT, p.E326K and p.L444P mutant GCase (n=5 biological replicates; Mean ± SEM is shown, one-way ANOVA was performed, *<0.05, ****<0.0001).

5.2 Analysis of the T-Rex HEK cell proteome after overexpression of WT and mutant GCase

To analyze the impact of WT and mutant GCase overexpression on the proteome, expression of tag-CT, WT and mutant tagged GCase was induced for 48 hours with 50 ng/ml doxycycline. After harvesting the cells, the pellets were snap frozen. Cells were lysed and 40 µg treated with Benzonase to remove nucleic acids. The proteins were labelled for TMT LC-MS and measured. The resulting data was analyzed by Limma analysis. Files containing the hits and candidates comparing mutant and WT GCase to tag-CT were generated. Using STRING Version 11.0 (Szklarczyk *et al.*, 2019; von Mering *et al*, 2005), an enrichment analysis was performed. Upon overexpression of tagged WT GCase most proteins upregulated are related to protein folding and unfolded protein response (Figure 5-4 A). Interestingly, in the p.E326K mutant, in addition to folding related proteins, proteins related to mitochondrial function (i.e., respiratory electron transport chain) are increased (Figure 5-4 B). In the tagged p.L444P mutant the enrichment in mitochondrial protein clusters related to function, i.e., mitochondrial and ATP coupled electron transport as well as mitochondrial organization, is even more pronounced (Figure 5-4 C). 4 proteins were picked to validate the proteome data (Figure 5-4 D). Three of these proteins were related to the ER, BiP, Calnexin and HSP90B1. The other protein is part of mitochondrial complex I, NDUFB8. As indicated by the proteomic data, an increase in these proteins is observed in the p.L444P mutant overexpressing T-Rex HEK cells. Even though the proteomic data does not indicate an increase in NDUFB8 when comparing WT or p.E326K to CT, the WB shows an increase in protein level. This could be due to a not significant increase, as there is as well no significant difference between WT or p.E326K compared to p.L444P mutant.

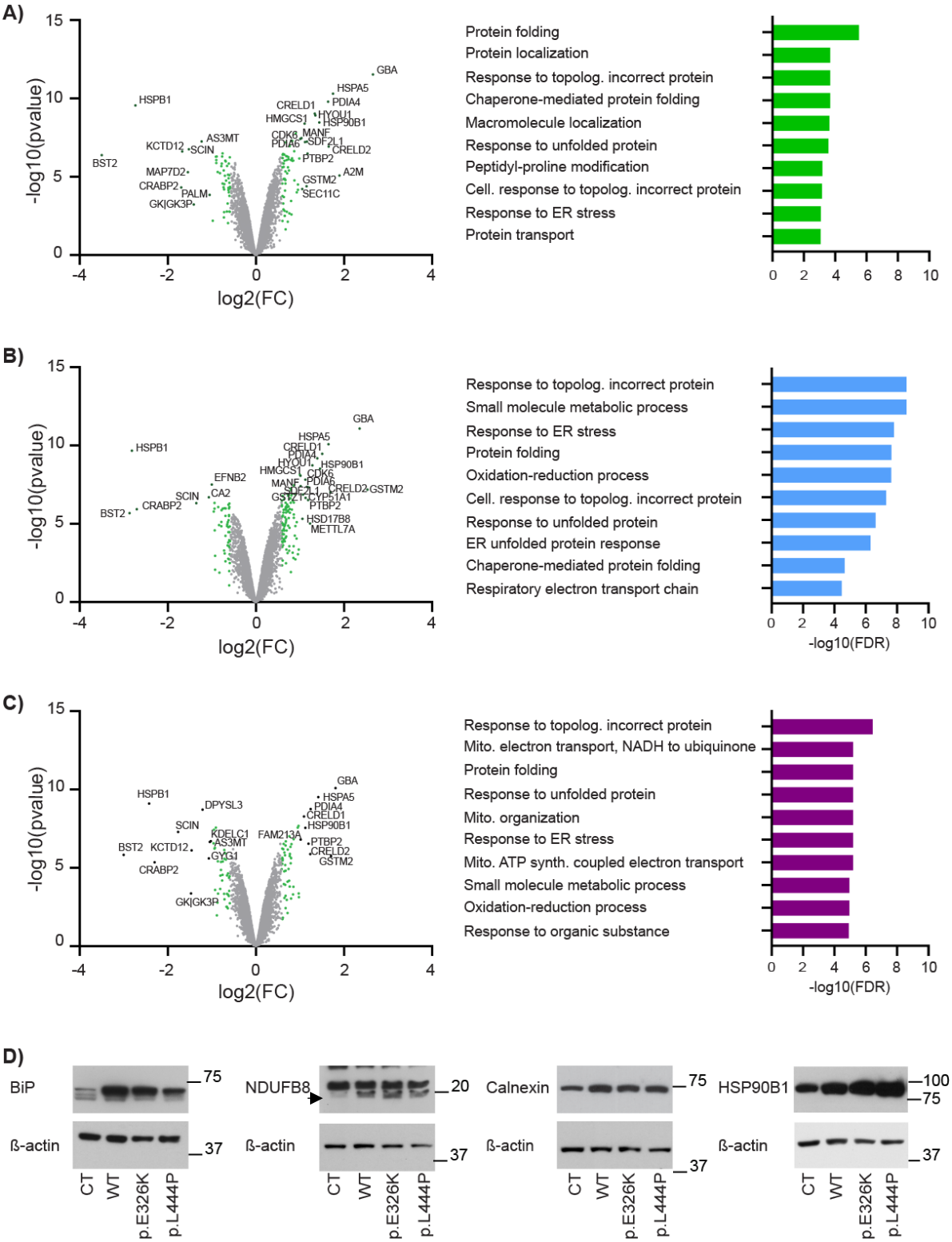

Figure 5-4 Overexpression of mutant GCase leads to upregulation of mitochondrial proteins. A-C) Proteome of overexpressed tagged WT (A), p.E326K (B) and p.L444P GCase (C) were compared to the control proteome (CT, V5-Flag-tag overexpression). Volcano plots and STRING analysis of the top enriched biological processes (BP) of proteins that show significant changed protein levels (Volcano plot: fold change ≥ 2, false discovery rate 5%; BP: fold change ≥ 1.5, false discovery rate 5%) are shown. Volcano plots from A-C are included in the publication by Baden, Pérez et al. (Baden et al., 2023). D) Representative WB to validate increased expression of BiP, Calnexin, HSP90B1 and NDUF8B (n=2-3 biological replicates).

5.3 Analysis of the GCase interactomes

To analyze the GCase WT and mutant interactome, as for the proteome of the whole lysate, the cells were induced for 2 days with 50 ng/ml doxycycline. 10 mg of protein was used to perform the co-IP. Next, the samples were TMT labelled and analyzed by LC-MS.

5.3.1 Analysis of the WT GCase interactome

Figure 5-5 A shows the first 100 hits of the WT interactome. As marked by the different colors, WT GCase interacts with proteins from many different compartments. On one hand, ER proteins, which is to be expected as GCase is synthesized and folded in the ER. On the other hand, as expected lysosomal proteins interact with GCase. Interestingly, 19% of the Top 100 hit GCase interactors are mitochondrial proteins and 4% of the proteins are defined as ER and mitochondrial by the GO terms. When comparing the endogenous WT interactome published by Tan et al. (2014) to our interactome, we found that 12.8% of our interactors were shared as shown by the Venn diagram in figure 5-5 B. In order to corroborate our overexpression T-Rex HEK cell model for LC-MS analysis, we decided to confirm interactors from different cellular compartments by WB (Figure 5-5. C). As ER related markers we checked BiP, Calnexin and HSP90B1. Next, we analyzed LIMP2, which is a known interactor involved in the transport of GCase to the lysosome, and the cytosolic proteins HSC70 and DJ-1. As a bridge between lysosomes and mitochondrial proteins, we validated TBC1D15, which is linked to mitochondrial lysosomal contacts (Wong *et al*, 2018). TOM70, TIM23, ATP5B, HSP60 and LONP1 were chosen to underpin the interaction with different mitochondrial proteins.

For the analysis of the enrichment of biological processes, hits, which were defined as having an FC of at least 2 and an FDR of maximum 5%, as well as candidates, FC of at least 1.5 and FDR of maximum 20%, were considered. Furthermore, the log(FC) was used as rank and the FDR of the String V11.0 analysis was set to 5%. As shown in figure 5-5 D the most enriched clusters engage in protein processing in the ER. However, to our surprise one cluster of biological processes was related to mitochondrial protein import into the matrix. Based on the unexpectedly high number of mitochondrial proteins in the Top 100 proteins, the WT hits and candidates were analyzed for mitochondrial proteins using MitoCarta3.0 list (Calvo *et al.*, 2016; Rath *et al.*, 2021). The comparison ended up with a list of 278 proteins shared between our interactome and the mitochondrial protein list from MitoCarta3.0, which means that the list with hits and candidates, which contains 2095 proteins in total, contains 13.3% of mitochondrial proteins. This list was then analyzed for the enriched mitochondrial biological processes. This time the log(FC) could not be used as rank, as too few proteins were contained in the list. Mitochondrial proteins from different processes are interacting with GCase, including mitochondrial organization, mitochondrial transport as well as interestingly oxidation and reduction processes and cellular respiration (Figure 5-5 E). This is interesting in the light of

mitochondrial respiratory defects in GCase mutant PD patient iPSC-derived neurons (Schöndorf *et al.*, 2018).

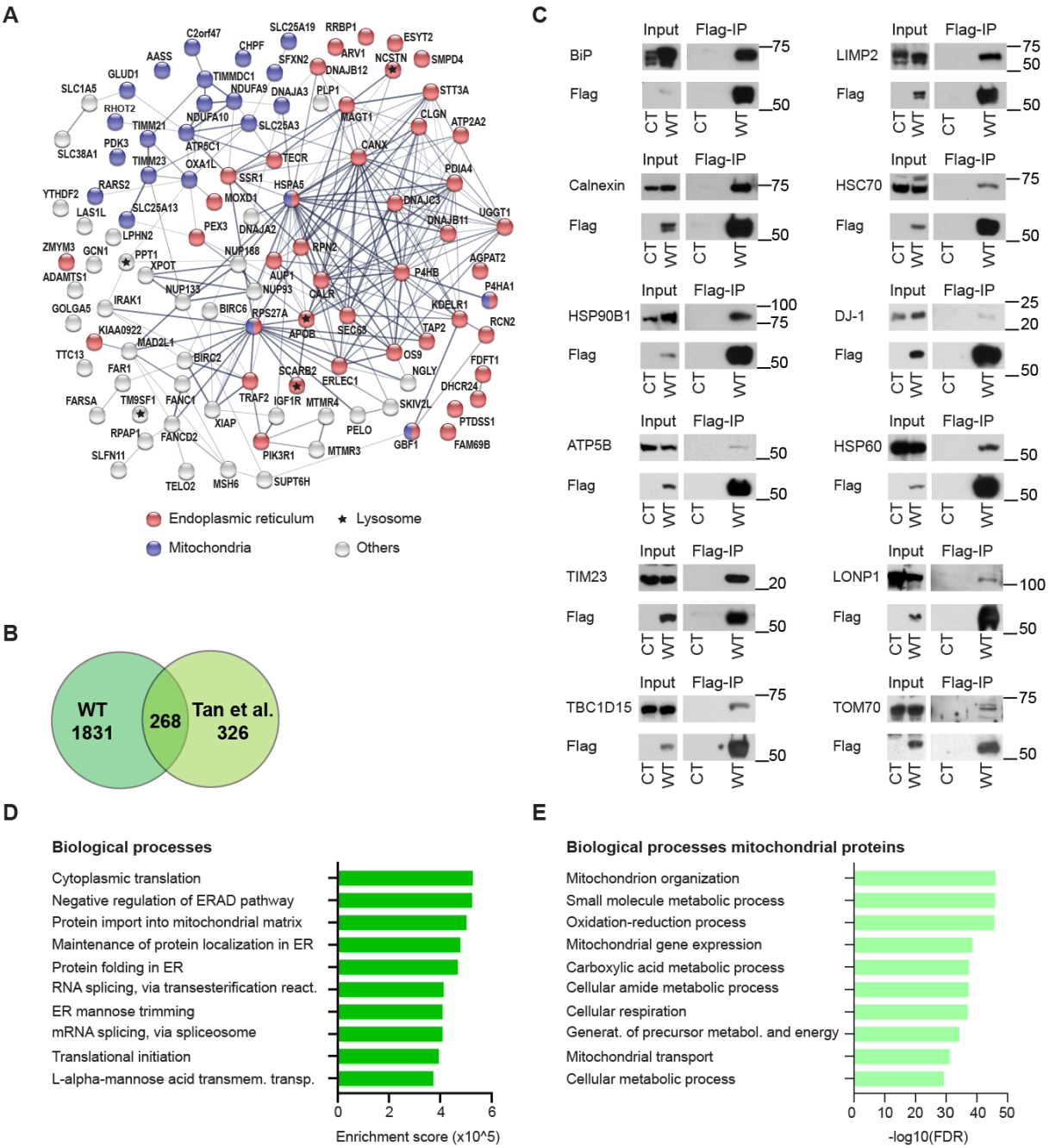

Figure 5-5 TMT proteomic profiling reveals GCase mitochondrial interactors: A) STRING representation of the Top 100 WT GCase interactors prominently showing components of the mitochondrial (blue), ER (red), and lysosome (star). B) Venn diagram representing the overlap between our overexpression interactome and the endogenous HeLa interactome from Tan et al. (2014) C) Co-IP of the GCase interactors of the ER (BiP and Calnexin), cytosol (LIMP2, TBC1D15, DJ-1, HSC70, and HSP90B1) and mitochondria (ATP5B, TIM23, TOM70, HSP60 and LONP1). Western blots are used in the publication by Baden, Pérez et al. (Baden et al., 2023). D) Top biological processes (BP) enriched in the WT-GCase interactome. E) Top enriched BP in GCase mitochondrial interactors.

5.3.2 Investigation of differences between the WT and mutant GCase interactome

Next, we compared the interactomes of WT, p.E326K and p.L444P mutant GCase. To this end, overexpression of V5-Flag-tagged WT and mutant GCase as well as the V5-Flag-tag CT was induced, and the biological replicates (n=2-3) were processed in parallel. After Limma analysis of the data, volcano plots were generated to highlight the hit proteins, fold change at least 2 times and FDR less than 5%, between WT and mutant and comparing both mutants to one another (Figure 5-6). Interestingly, interaction with LIMP2 (encoded by *SCARB2*), which is the scavenger receptor important for the trafficking of GCase to the lysosome, is decreased in the mutants.

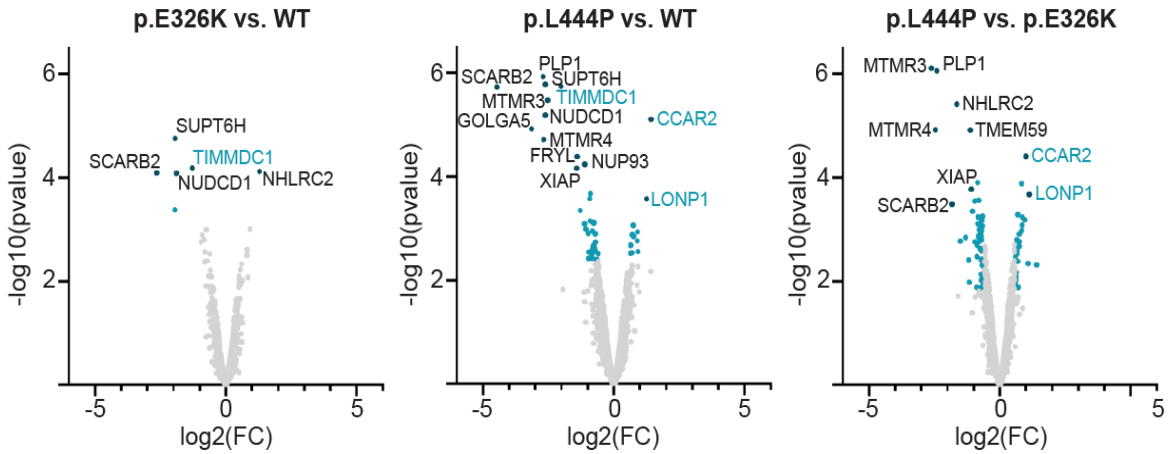

Figure 5-6 Volcano plots demonstrate variance in the interaction of mutant GCase with mitochondrial proteins. Interactors that differ by 2-fold change (FC) and have a false discovery rate (FDR) of ≤5% are labelled. Proteins labelled in blue are associated with mitochondria. Volcano plots are presented in the publication by Baden, Pérez et al. (Baden et al., 2023).

In the light of mitochondrial dysfunction being associated with *GBA1* mutations and PD, it is of note that few mitochondrial proteins were interacting to a different degree with mutant GCase compared to WT (highlighted in blue in Figure 5-6). Comparing the interactome of tagged p.E326K mutant to WT GCase, 1 out of 5 hit proteins was mitochondrial. Comparing tagged p.L444P mutant to WT GCase, 3 out of 13 hit proteins were mitochondrial related. In the comparison of both mutants, mitochondrial proteins represented 2 out of 9 hit proteins. These surprising results taken together with the fact that overexpression of tagged p.E326K mutant GCase and to a higher degree with tagged p.L444P mutant GCase leads to an increase of mitochondrial proteins, made us wonder whether there is a more direct link between GCase and mitochondrial function. Therefore, the next step was to analyze if GCase potentially traffics to mitochondria and if it is imported into mitochondria.

5.4 Mitochondrial targeting and import of GCase

5.4.1 Internal matrix targeting sequence-like sequence of GCase

Most proteins that are targeted to the mitochondrial matrix have a matrix targeting sequence (MTS). Therefore, since among the Top10 enriched biological processes of the WT interactors, proteins of mitochondrial import were represented (Figure 5-5), we analyzed if GCase has a N-terminal MTS. To do so we used TargetP2.0, which is a program developed to detect these N-terminal MTS sequences (Almagro Armenteros *et al*, 2019). No classical MTS was detected for GCase (Figure 5-7 A). Since it has been shown that several mitochondrial matrix proteins have internal matrix targeting sequence-like sequences (iMTS-ls), we assessed whether GCase at least has an iMTS-ls. Recently a protocol has been published to detect iMTS-ls using TargetP2.0 (Boos *et al*, 2018). To do so the sequences resulting from sequential removal of the first amino acid are analyzed by TargetP2.0. Three iMTS-ls are detected (Figure 5-7 A). To verify that the V5-Flag-tag did not lead to an artificial MTS, as it is straight after the leader sequence, we as well analyzed the sequences used for the overexpression. The V5-Flag-tag does not lead to an artificial MTS (figure 5-7 B) However, in the leader sequence of GCase, the TargetP2.0 score is reduced. This should not affect the targeting of GCase to mitochondria, as after synthesis in the ER, the leader sequence is cleaved off (Tsuji *et al.*, 1986). Tagged p.E326K mutant GCase has only one additional point caused by the mutation that is over the threshold (Figure 5-7 C). Tagged p.L444P mutant GCase does not have any additional points over the iMTS-ls threshold (Figure 5-7 D).

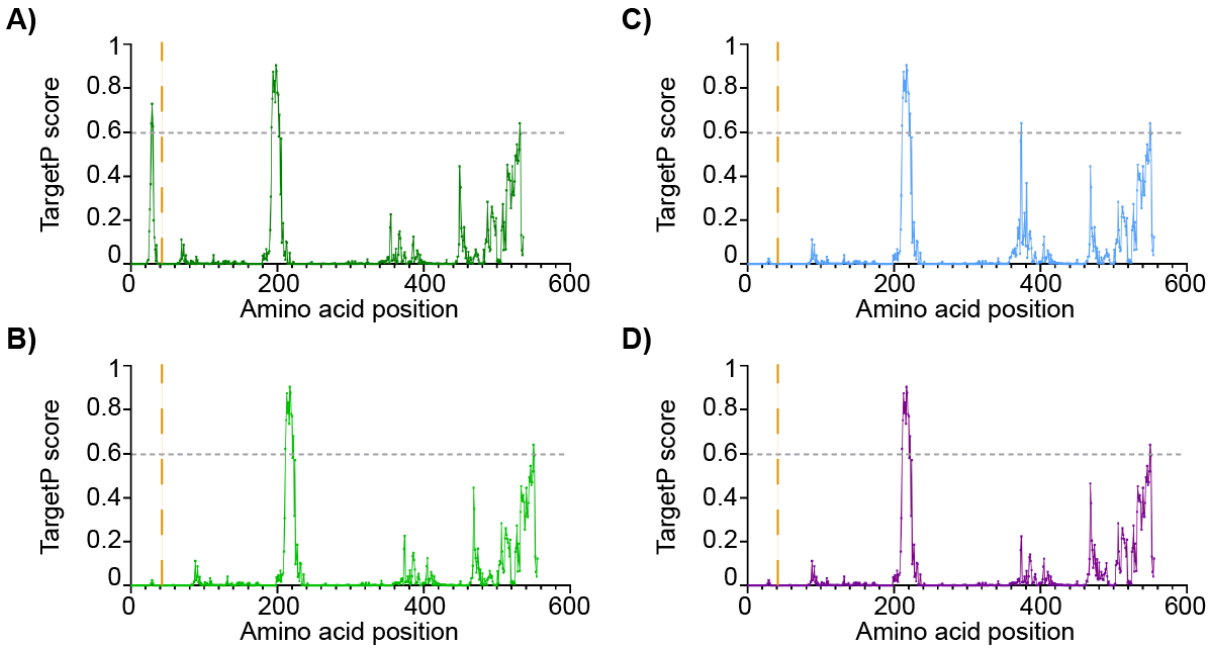

Figure 5-7 TargetP score indicates that *GBA1* has internal matrix targeting sequence- like sequences (iMTS-ls) but no N-terminal MTS. TargetP2.0 was used to calculate the MTS score to detect iMTS-ls in A) WT GCase, B) V5-Flag-tagged WT GCase, C) V5-Flag-tagged p.E326K and D) V5-Flag-tagged p.L444P mutant GCase. The grey line indicates the threshold for MTS and iMTS-ls sequences. The orange line indicates the first amino acid after the leader sequence cleavage site.

5.5 GCase is localized in mitochondria

To confirm the mitochondrial targeting of GCase, we decided to use a split-GFP reporter to demonstrate the presence of GCase in the mitochondrial matrix. The construct designs were done according to the publication by Calì et al. (2015) and are listed in the Appendix 9.2. Figure 5-8 A-C explains the experimental setup of the split GFP experiments.

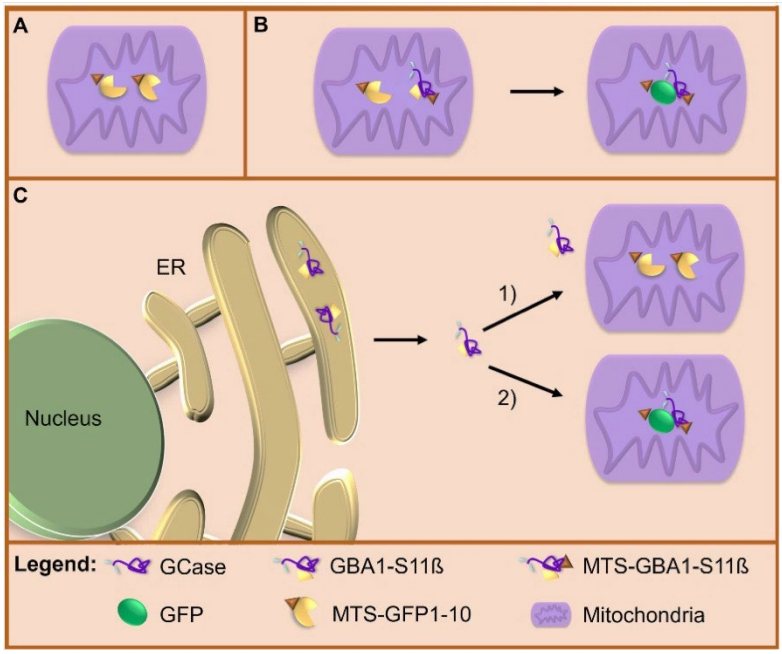

Figure 5-8 Illustration of split GFP experimental design. A) Upon doxycycline treatment, mitochondrial matrix targeted MTS-GFP1-10 is expressed. B) If the GFP-S11ß sheet is present, in the compartment, in which the MTS-GFP1-10 is located, in our case mitochondrial matrix, they bind and emission of GFP signal occurs. This is the case in the positive control, the mitochondrial matrix targeted MTS-GBA1-S11ß. C) Potential outcome of overexpression of GBA1-S11ß: 1) If GCase does not traffic into the mitochondrial matrix, no GFP signal will be detected. 2) In case, GCase traffics into mitochondria, GFP signal will be observed.

For this experiment, T-Rex HEK cells with inducible expression of matrix targeted GFP1-10 (MTS-GFP1-10), which is missing the GFP-S11ß sheet, were generated to avoid co-transfection. After selection different clones were picked. Expression of MTS-GFP1-10 was induced for 48 hours and the cells were stained for GFP and LONP1. Co-localization, as observed by orange signal in the merge, confirms correct localization of MTS-GFP1-10 in the mitochondrial matrix (Figure 5-9).

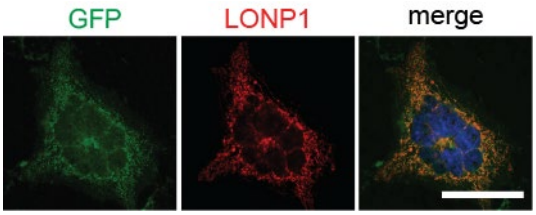

Figure 5-9 MTS-GFP1-10 is targeted to the mitochondrial matrix. Overexpression of MTS-GFP1-10 was induced by treating the T-Rex HEK cells with 50 ng/ml doxycycline for 48 hours. To confirm matrix localization of MTS-GFP1-10 staining for LONP1 (red) and GFP (green) was performed. Scale bar is 20 µm. Immunofluorescence pictures are part of the publication by Baden, Pérez et al. (Baden et al., 2023).

In addition, a construct for transient overexpression of WT GBA1-S11ß as well as mitochondrial targeted GBA1-S11ß (MTS-GBA1-S11ß) were designed. The S11ß strand of GFP missing from MTS-GFP1-10 is added after a linker to the C-terminus of the *GBA1* sequence. MTS-GBA1-S11ß was used as positive control in the experiments. As depicted in Figure 5-8 C2, when MTS-GFP1-10 combines with GBA1-S11ß, GFP signal is emitted. Therefore, if GCase traffics to the same mitochondrial compartments as MTS-GFP1-10,

mitochondria will appear green. If this is not the case, no GFP signal will be visible (Figure 5-8 C1).

Figure 5-10 illustrates the outcome of the different experimental setups. In 5-10 A, mitochondria were stained with MitoTracker red (red) to show colocalization with GFP signal. In Figure 5-10 B, no MitoTracker red was used to prevent bleed through. Induction of MTS-GFP1-10 does not lead to green fluorescence, as seen in the negative control. However, when transfecting these cells 48 hours before imaging with the MTS-GBA1-S11ß construct, which is leading to the overexpression of mitochondrial targeted WT GBA1-S11ß in these cells, GFP signal can be detected and the signal co-localized with the mitochondrial marker. Similar image is obtained when transfecting the T-Rex HEK cells with WT GBA1-S11ß. In addition to WT GBA-S11ß, SDM was performed to introduce the p.E326K mutation as well as the p.L444P mutation in the construct. Overexpression of mutant GBA-S11ß constructs confirms mitochondrial localization of mutant GCase. On the other hand, the iMTS-ls of WT GBA-S11ß (WT ΔiMTS-ls) was removed to evaluate if the iMTS-ls has an impact on GCase localization. Removal of the iMTS-ls prevents GFP signal, meaning GCase does not traffic to mitochondria anymore (Figure 5-10 B).

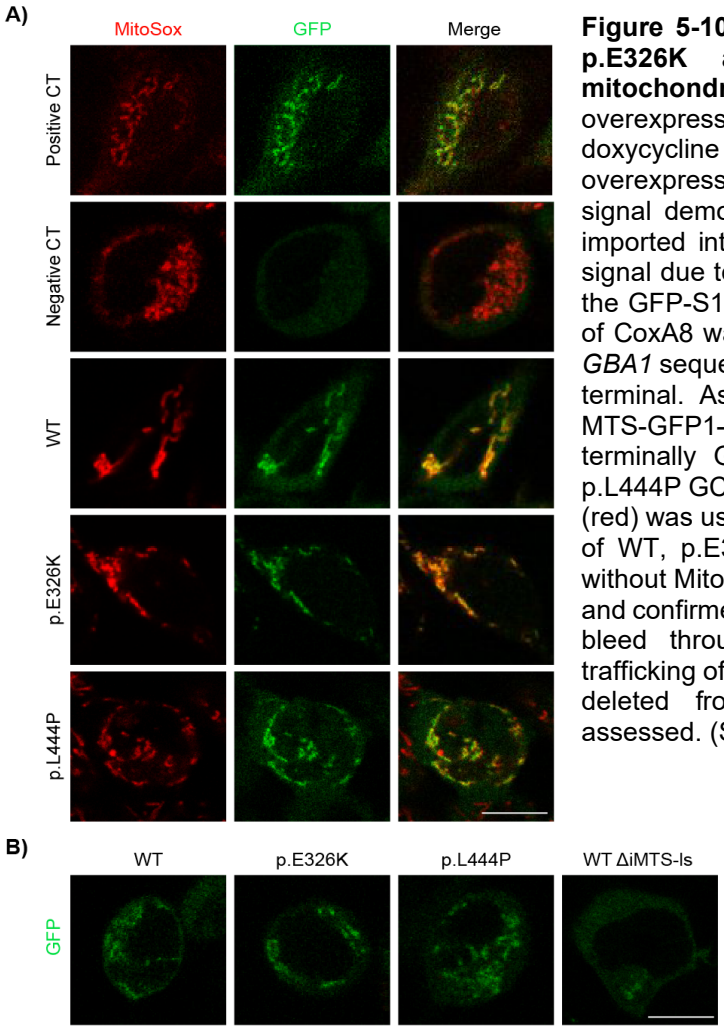

Figure 5-10 Split-GFP reporter shows that WT, p.E326K and p.L444P GCase traffic to mitochondria. A) MTS-GFP1-10 was overexpressed by treatment with 50 ng/ml doxycycline for 24 hours and 48 hours overexpression of the construct of interest, GFP signal demonstrates that the protein of interest is imported into mitochondria and is leading to GFP signal due to the association of MTS-GFP1-10 with the GFP-S11ß strand. As positive control, the MTS of CoxA8 was inserted at the N-terminal of the WT *GBA1* sequence and the GFP-S11ß strand at the C-terminal. As negative control, only expression of MTS-GFP1-10 was induced. Overexpression of C-terminally GFP-S11ß tagged WT, p.E326K- and p.L444P GCase resulted in GFP signal. MitoTracker (red) was used as mitochondrial marker. B) Imaging of WT, p.E326K and p.L444P mutant GBA-S11ß without MitoTracker as signal was easier detectable and confirmed that the GFP signal did not result from bleed through. In this condition, mitochondrial trafficking of WT ΔiMTS-ls, in which the iMTS-ls was deleted from *GBA1* sequence, was as well assessed. (Scale bar is 10 µm)

5.6 Import pathway of GCase

5.6.1 WT and mutant GCase interact with proteins of mitochondrial import

To better understand how GCase is imported into mitochondria, we assessed the interaction with proteins known to be involved in the mitochondrial import pathway. Recently it has been published that misfolded proteins can be imported through a HSC70-, TOM70- and TIM23-depent pathway (Li *et al*, 2019; Ruan *et al*, 2017). Therefore, we assessed these proteins as well. However, these proteins are not only involved in the import of misfolded proteins. It was previously shown that HSP90, HSC70 and TOM70 are as well involved in the import of mitochondrial proteins like the carrier protein ANT, that lack the MTS (Bhangoo *et al*, 2007). TOM70 is as well involved in the import of mitochondrial proteins with an iMTS-ls (Backes *et al*, 2018). In addition, TIM23 is involved in targeting of mitochondrial matrix proteins (Schulz *et al*, 2015; Wiedemann & Pfanner, 2017). As shown in Figure 5-11, WT and both mutant GCase interact with HSC70 (A), TOM70 (B) and TIM23 (C).

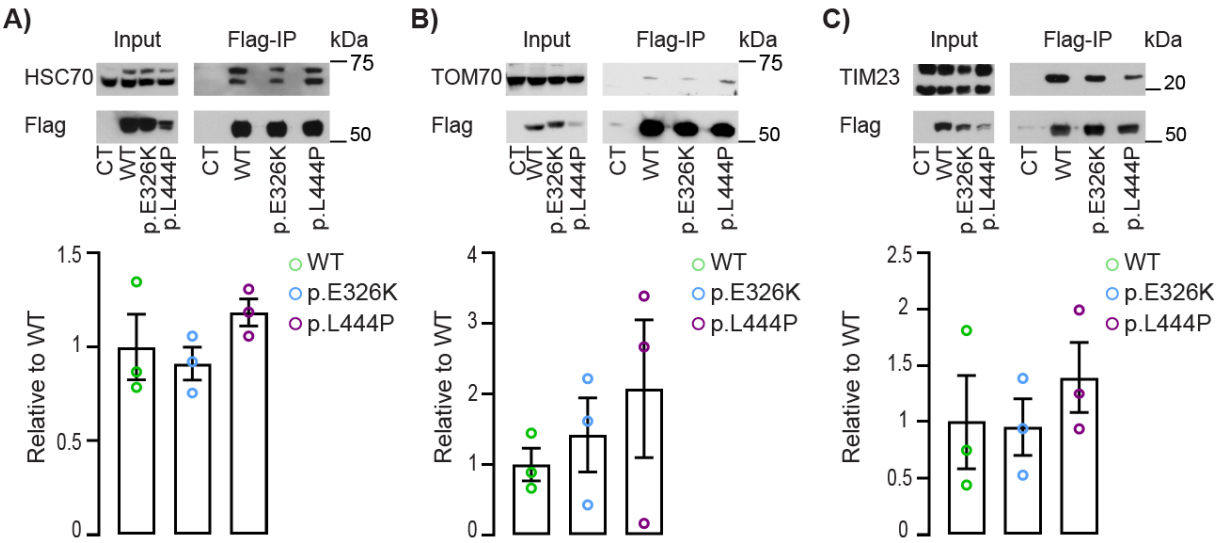

Figure 5-11 WT and mutant GCase interact with proteins involved in the mitochondrial import. A-C) Representative Western blot and densitometric quantification normalized to WT are shown for HSC70 (A), TOM70 (B) and TIM23 (C). (n=3 biological replicates, mean ±SEM is shown, one-way ANOVA with Tukey's multiple comparison was used). Representative Western blots from A-C are shown in the publication from Baden, Pérez et al. (Baden et al., 2023).

5.6.2 HSP60 and LONP1 are interactors of WT and mutant GCase

Next, we confirmed the interaction with proteins with which tagged p.L444P mutant GCase interacted more than tagged WT GCase. We decided to investigate these proteins as the increased interaction was surprising due to the decrease of tagged p.L444P mutant GCase protein level compared to tagged WT protein. As it has been shown that misfolded cytosolic proteins can get imported into mitochondria and be degraded by LONP1 (Li *et al.*, 2019), a mitochondrial protease, or the yeast homologue PIM1 (Ruan *et al.*, 2017), our interest was caught by the increased interaction of p.L444P mutant GCase with LONP1. Interestingly, it was shown that WT as well as mutant TDP-43 interact with LONP1 (Wang *et al*, 2019a).

Western blot analysis of the eluate confirmed a higher interaction of p.L444P mutant GCase and LONP1 compared to WT and p.E326K mutant GCase (Figure 5-12 A). MS data show that HSP60, a mitochondrial chaperone, was close to be a candidate protein but did not reach significance most likely due to an outlier. In addition, HSP60 had already been discovered in a previous interactome study of GCase (Tan *et al.*, 2014). Therefore, we checked the interaction on WB. Densitometric analysis confirmed that WT GCase interacted significantly less with HSP60 than p.L444P mutant GCase (Figure 5-12 B). To ensure that the interaction is not caused by overexpression, we gene-corrected an p.L444P homozygous iPSC line (GD-2 and isogenic control GC-2) and differentiated them into NPCs (described in chapter 5.7). Co-IP was performed on lysates of GC-2 and GD-2. The p.L444P homozygous mutant and isogenic control were selected to get a clearcut picture, as in the heterozygous we would still pull-down as well WT GCase. As negative control WT lysate was incubated with IgG control antibody. As shown in Figure 5-12, interaction of endogenous mutant and WT GCase with LONP1 (C) and HSP60 (D) was confirmed on WB.

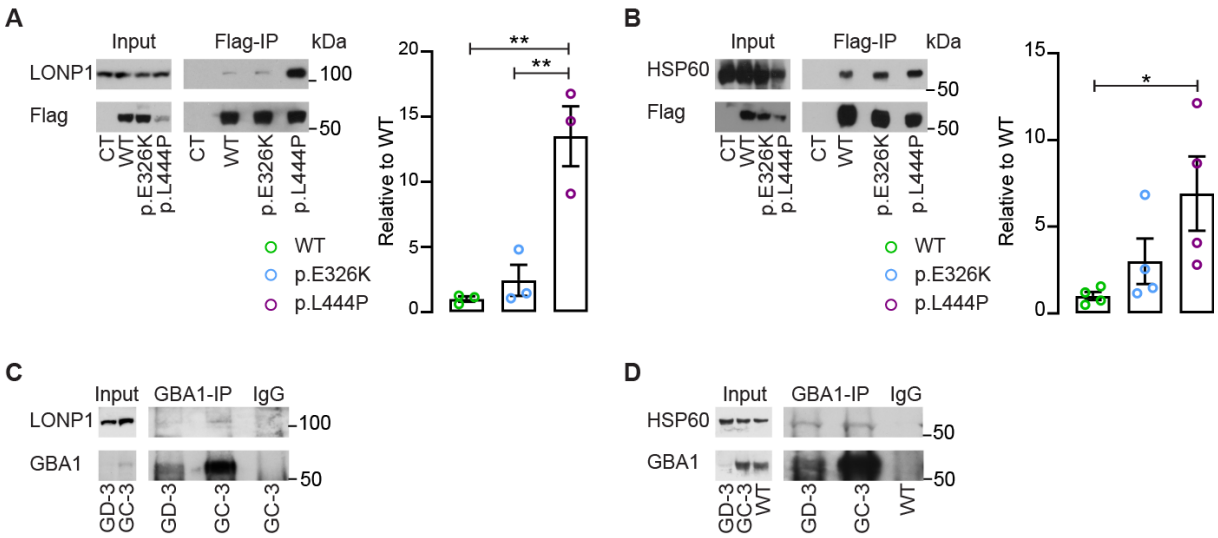

Figure 5-12 Interaction of tagged p.L444P mutant GCase with LONP1 and HSP60 is increased compared to tagged WT GCase. A-B) Representative western blot picture and quantification of interaction relative to WT with LONP1 (A) and HSP60 (B). The representative Western blots are published in the publication of Baden, Pérez et al. (Baden et al, 2023). To quantify the interaction between GCase and LONP1 or HSP60, Flag and signal of interest was densitometrical quantified. The amount of HSP60 and LONP1 was divided by Flag and then normalized on WT. (n=3-4 biological replicates, mean ± SEM are shown, one-way ANOVA with Tukey's multiple comparison was used; *<0.05, **<0.01). C-D) Eluates of GCase immunoprecipitation were probed against LONP1 (C) or HSP60 (D) to confirm the interaction with endogenous p.L444P mutant and WT GCase.

As IP is performed on lysate, proteins from other compartments could interact artificially. Validating interaction with LONP1 by proximity ligation assay allows to confirm that the interaction is not due to the nature of the IP. PLA was performed using antibodies against V5, which is part of the tag attached to p.L444P mutant GCase, and LONP1. Positive signal in Figure 5-13 shows that GCase interacts with LONP1 in V5-Flag-tag p.L444P GCase overexpressing T-Rex HEK cells.

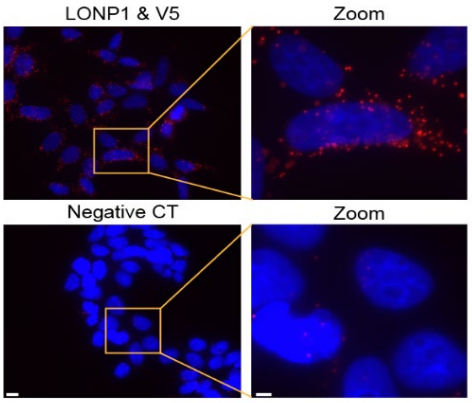

Figure 5-13 Interaction between V5-Flag-tagged p.L444P mutant GCase and LONP1 was demonstrated by proximity ligation assay (PLA). In exogenous overexpressing p.L444P mutant GCase T-Rex HEK cells, PLA results in positive signal (red dots), demonstrating that GCase is close enough to LONP1 to interact. Only few dots are observed in the negative control. (Scale bar is 10 µm respective 50 µm in the zoomed picture.)

To make sure that the PLA signal is not unspecific, several controls were included (Figure 5-14). As negative control, we performed the PLA on uninduced cells, without any primary antibody meaning secondary antibodies only, and with only one of both primary antibodies. There was barely any unspecific signal in the negative controls (Figure 5-14). As positive control we used anti-V5 and anti-Flag antibodies, which are both part of the tag, leading to completely red cells. As described above, PLA using the anti-V5 and anti-LONP1 antibody on p.L444P mutant T-Rex HEK cells resulted in many red puncta, showing that LONP1 is interacting with GCase in cells (Figure 5-13 and 5-14).

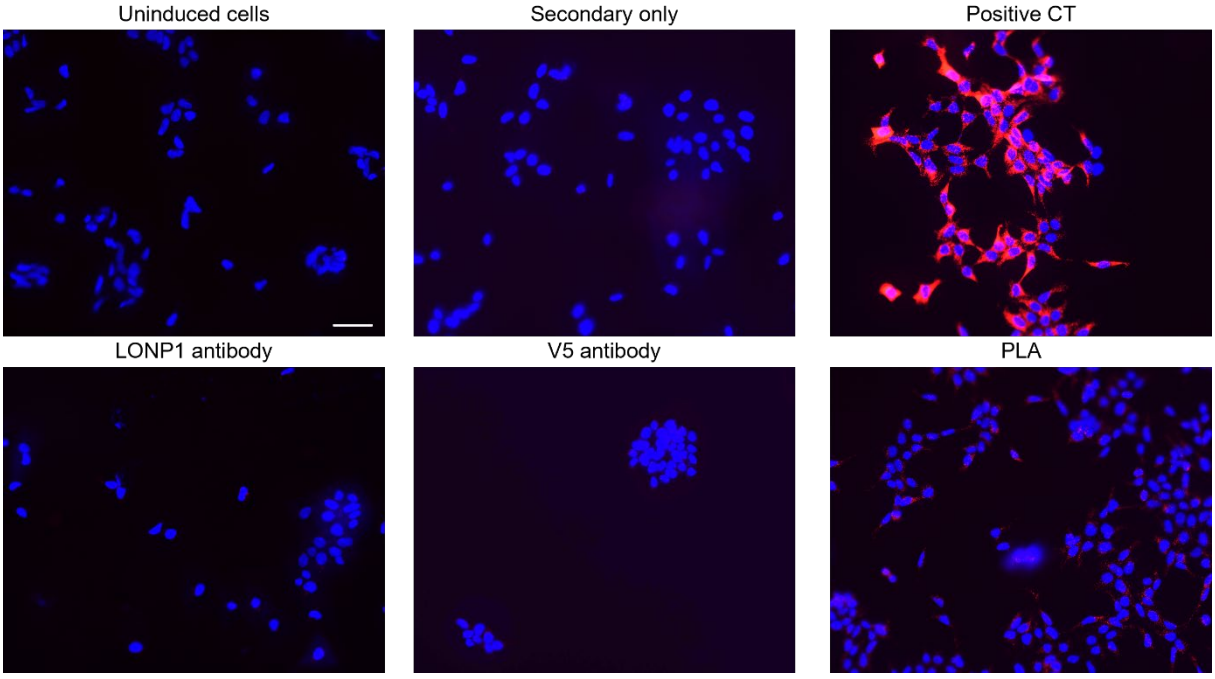

Figure 5-14: PLA demonstrates interaction between V5-Flag-tagged p.L444P mutant GCase and LONP1. Negative controls include uninduced cells, secondary only, anti-LONP1 antibody and anti-V5 antibody. Primary antibodies of positive control are anti-V5 and anti-Flag, both binding to tagged p.L444P GCase. For the experimental condition (PLA), anti-LONP1 and anti-V5 antibody was used. (Scale bar 20 µm)

5.6.3 Confirmation of the import pathway by KD of HSC70 and TIM23

To further validate the proteins involved in the mitochondrial import of GCase, we used shRNAs to knockdown (KD) HSC70 and TIM23. Two shRNA specific for each protein of interest were selected. As control a non-target scramble was selected. For efficient transfection, we generated Lentivirus for each shRNA and the scrambles. p.L444P mutant T-Rex HEK cells were infected with the Lentivirus for one shRNA or scramble. HSC70 KD led to an average reduction of the protein level by 76% (Figure 5-15 A). On average 34% of TIM23 protein levels were left after TIM23 KD (Figure 5-15 C). While expanding the cells for IP, they were grown in medium containing Neomycin to select infected cells. 48 hours before harvesting the cells p.L444P mutant GCase expression was induced by treatment with 50 ng/ml doxycycline. Flag IP was performed on the lysates. The eluates were examined by WB to assess whether the interaction between GCase and the validated mitochondrial interactor LONP1, was decreased upon KD of proteins linked to the import.

The interaction between LONP1 and p.L444P mutant GCase seem reduced upon KD of HSC70 (Figure 5-15 B). In the HSC70 KD1, interaction was decreased by approximately 52% and in the HSC70 KD2, an average decrease of 61% is detected. A decreased interaction between p.L444P GCase and LONP1 is as well observed after TIM23 KD (Figure 5-15 D). In TIM23 KD1, the interaction was on average decreased by 66%. The average decrease in the interaction between GCase and LONP1 in TIM23 KD2 was 44%. Unfortunately, the high variability prevented the reduction from reaching significance. However, the results support the HSC70- and TIM23-dependent mitochondrial import of GCase. Furthermore, they as well further confirm interaction of p.L444P GCase with LONP1 inside mitochondria.

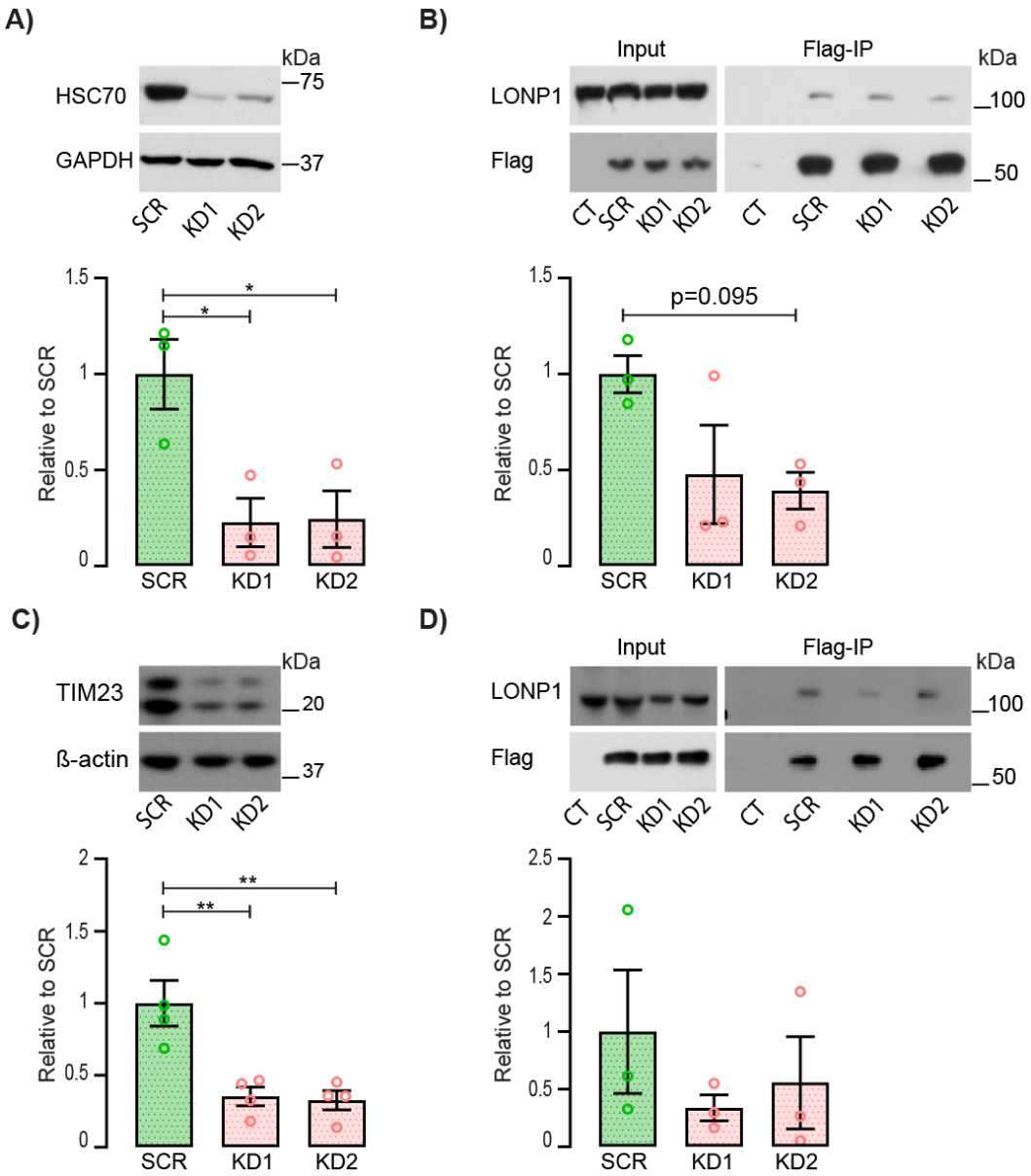

Figure 5-15: GCase is imported into mitochondria by a HSC70 and TIM23 dependent mechanism. A) Representative western blot (WB) and evaluation of HSC70 knockdown (KD) efficiency of 2 shRNAs (KD1 and KD2) expressed as normalized on scramble. B) Representative WB of input and co-immunoprecipitation of Flag in HSC70 KD cells (KD) overexpressing tagged p.L444P mutant GCase. C) Representative blot and evaluation showing TIM23 KD after shRNA expression. D) Interaction between LONP1 and tagged p.L444P mutant GCase on representative blot and quantification relative to scramble. (n=3 biological replicates, mean ±SEM are illustrated, ordinary one-way ANOVA was performed). Representative Western blots were included in the publication by Baden, Pérez et al. (2023).

5.7 Generation of patient-derived induced pluripotent stem cell (iPSC) models

5.7.1 Generation of human GBA1 mutant iPSC lines

Three new iPSC lines from *GBA1*-PD patients' fibroblasts were generated by reprogramming. The first patient was p.L444P heterozygous and had early onset PD, and the two other patients were p.E326K heterozygous *GBA1* mutant and just did not have early onset PD, for which the threshold lays at below 50 years (Neumann *et al.*, 2009). The information on the patients of the newly generated clones including nomenclature for the thesis are listed in table 5-1.

Subjects	Gender	Age	Age of onset	GBA genetic variants	iPSC clones (synonym used)
150021	M	60	49	p.L444P/WT	21#1 21#3 (PD-1)
150046	M	62	52	p.E326K/WT	46 #1 46 #2 (PD-2)
150047	M	60	50	p.E326K/WT	47 #3 47 #4 (PD-3)

Table 5-1: Parkinson's disease patient and clone information of newly generated iPSC lines.

To confirm pluripotency of the new iPSC lines, cells were stained for the pluripotency markers Oct 4, Tra1-60 and Tra1-81. The newly generated clones of the iPSC lines are positive for the nuclear marker Oct 4, and cell membrane proteins Tra1-60 and Tra1-81 (Figure 5-16 A-B; Figure 5-17 A-D). Integration free reprogramming was checked by PCR. The primers used for the PCR target the plasmid regions encoding the pluripotency genes Klf4, L-Myc, Sox2, and Oct4. The positive control allowed to verify that the PCR worked and to observe the correct height of the band. The absence of bands was confirmed on the agarose gel, proofing that the plasmids were not integrated into the DNA of the newly generated lines (Figure 5-16 C and Figure 5-17 E). In addition, to exclude occurrence of chromosomal aberrations during reprogramming the karyotype was analyzed by SNP array at the Life & Brain GmBH. Lines with chromosomal defects were not used in the follow up experiments.

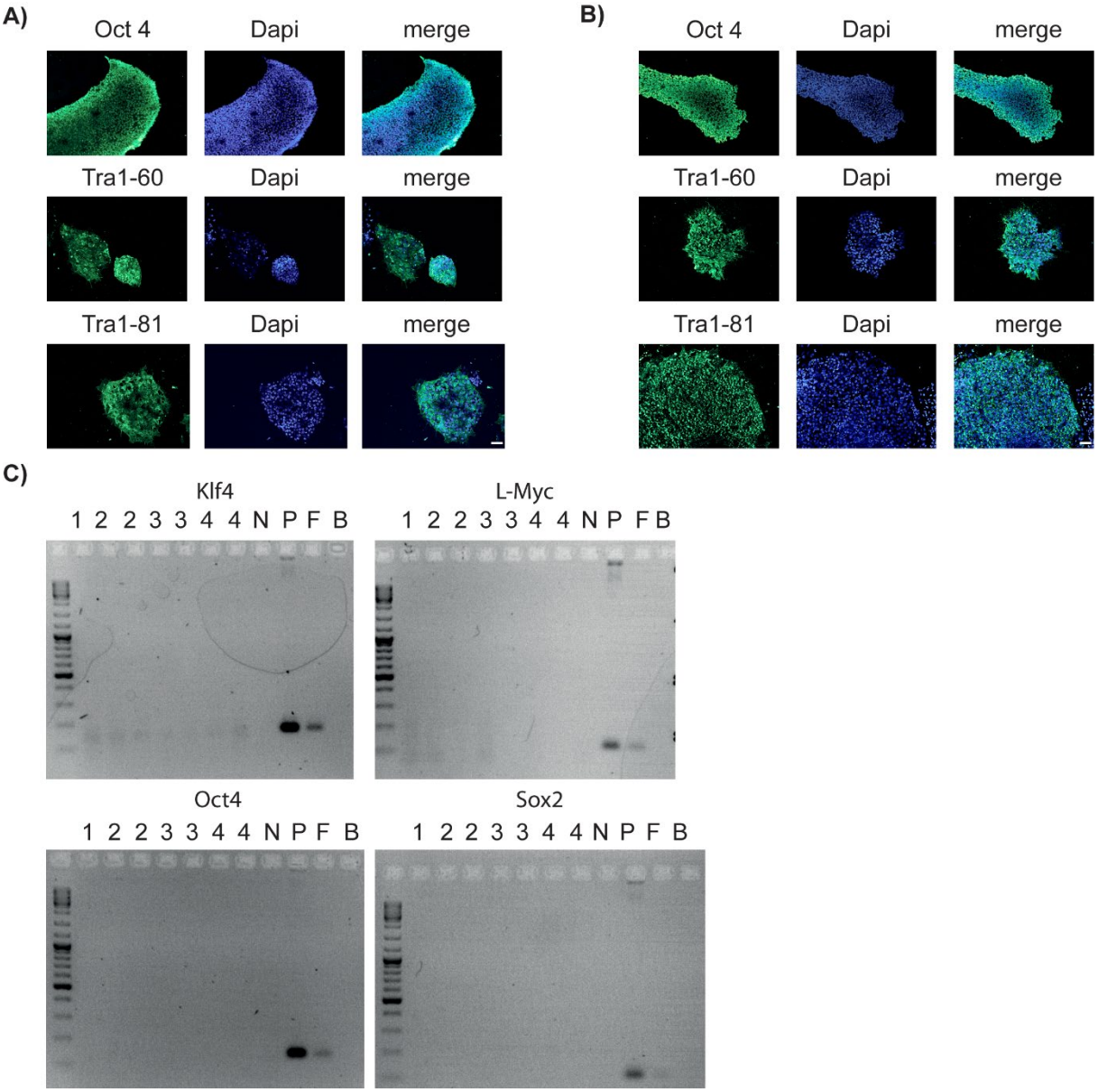

Figure 5-16 Characterization of the p.L444P heterozygous *GBA1* mutant induced pluripotent stem cells (iPSC). Clone #1 (A) and #3 (B) of Parkinson's disease patient 150021 were stained for the pluripotency markers Oct 4, Tra1-60 and Tra1-81 and the nuclear marker Dapi (scale bar is 100 µm). C) Polymerase chain reaction on the iPSC from patient 150021 clones #1 and #3 validated integration-free reprogramming. #2 and #4 are additional clones not used in the thesis. (N: negative control; P: positive control, F: transfected fibroblasts positive control; B: blank)

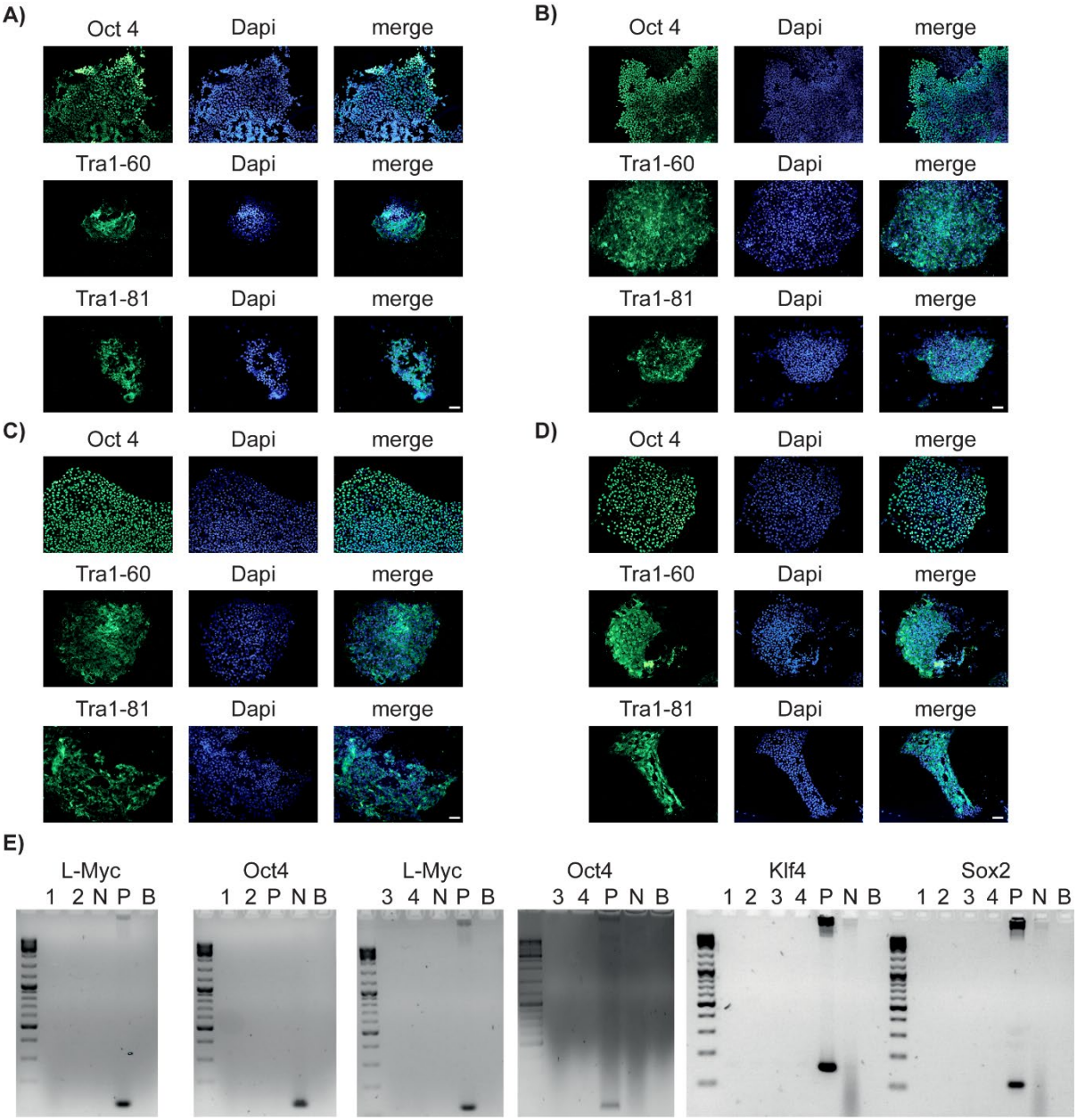

Figure 5-17 Characterization of the p.E326K heterozygous *GBA1* mutant induced pluripotent stem cells (iPSC). Clone #1 (A) and #2 (B) of Parkinson's disease (PD) patient 150046 as well as clone #3 and #4 of PD patient 150047 were stained for the pluripotency markers Oct 4, Tra1-60 and Tra1-81. The nucleus was stained with Dapi (scale bar is 100µm). E) Polymerase chain reaction on the iPSC from patient 150046, clones #1 and #2, as well as on the clones #3 and #4 from PD patient 150047 validated integration-free reprogramming. (N: negative control; P: positive control, B: blank)

5.7.2 Gene-correction of the p.L444P mutation

The method published by Schöndorf et al. (2014) using zinc finger nucleases (ZFNs) in combination with a homologous construct was exploited to gene-correct the p.L444P GCase mutation in the newly generated p.L444P heterozygous iPSC line from patient 150021 clone #3, called hereafter PD-1. Furthermore, the p.L444P homozygous GD iPSC line that was previously published (Schöndorf *et al.*, 2014), called GD-2 was gene-corrected in the same way. A double-strand break was induced by cleavage with the 2 ZFNs binding on the opposing DNA strands. The homozygous construct served as a template for homology-directed repair and in this way lead to gene-correction. The neomycin resistance cassette that is integrated into the intronic region between exon 9 and 10, allowed selection of clones in which recombination between the homologous construct and the DNA occurred. Sanger sequencing was used to validate the gene correction. Mixed clones were further subcloned to get clean clones arising from one cell. As shown in Figure 5-18 A, the homozygous mutation of the Gaucher patient as well as the mutation of the p.L444P heterozygous clone was gene-corrected by replacement of the C by a T. The gene-corrected line of PD-1 will be called GC-1 and of GD-2 will be called GC-2 in the following text. Interestingly, one clone of the PD-1 appeared to be homozygous for the p.L444P mutation after gene-correction. Sanger sequencing displayed that 2 additional point mutations p.A456P, G to C, and p.A460V, G to C, were introduced upon gene editing (Figure 5-18 B and C). These additional mutations lead to an artificial homozygous RecNcil mutation, which is a severe *GBA1* mutation resulting from recombination with the *GBA1* pseudogene (*GBAP*) (Latham *et al*, 1990). The artificial homozygous RecNcil line will be called GD-1. Gene editing was as well confirmed at the mRNA level by sequencing. To confirm gene-correction as well at protein level, lysates from the iPSC-derived neurons of the isogenic couples were subjected to WB analysis. An increase in protein level was observed in GCs compared to mutants (Figure 5-18 E). As expected, increased protein level was more obvious between GC and homozygous mutants than between heterozygous mutant and the GC. In addition, GCase activity assay was performed to verify that gene-correction restored GCase activity in the mutants too. For the GCase activity assay lysate from NPCs of the isogenic couples was incubated at a near lysosomal, pH5.4, with MUB-Glc, which serves as substrate for GCase. Cleavage of MUB-Glc leads to fluorescent signal that can be measured with the SpectraMax reader. The higher the fluorescent intensity the more MUB-Glc was cleaved and the higher the GCase activity. PD-1 displayed a 18.5% decrease in activity when compared to the isogenic control (Figure 5-18 D). Comparing the GC-1 to the homozygous RecNcil mutant we observed an increase by 95.8% in the GC (Figure 5-18 D). The GC-2 had an 8-fold increase in GCase activity compared to GD-2 (Figure 5-18

D). The rise in protein level as well as GCase activity when comparing mutant to GC validates gene-correction of the iPSC lines.

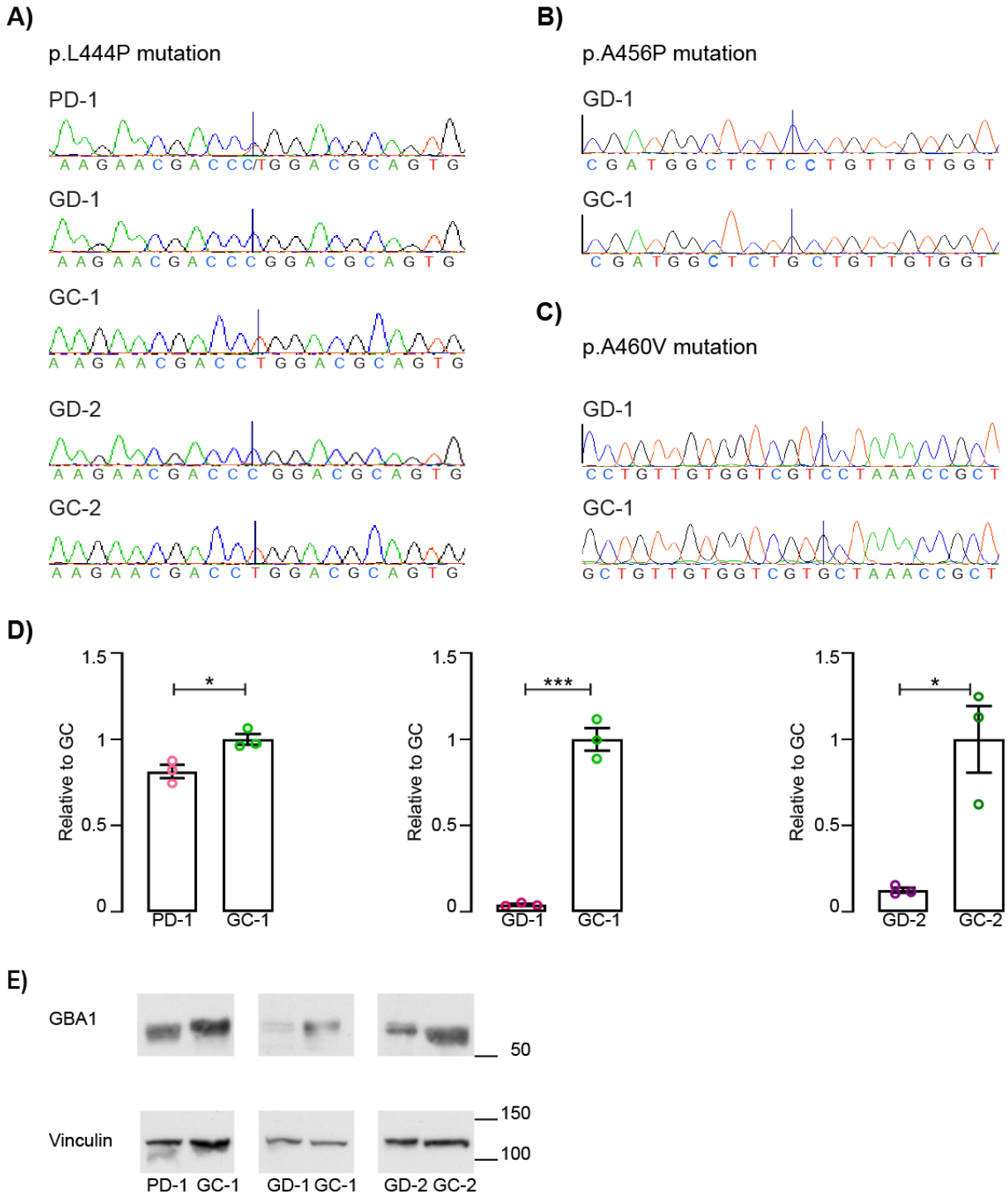

Figure 5-18 Validation of the p.L444P gene-correction and artificial RecNcil mutation. A) The p.L444P mutant allele with the C nucleotide was corrected showing now a T nucleotide at the location of the line. B) The p.A456P mutation and C) the p.A460C mutation were artificially inserted on both alleles shown by the C nucleotide instead of G at the position of the line. D) GCase activity assay comparing PD-1, GD-1 and GD-2 activity to isogenic control was performed on iPSC-derived neural precursor cells. Data are shown as mean ±SEM. Unpaired students T-test was performed; n=3 independent experiments (*p ≤ 0.5, ***p ≤ 0.0001) E) Western blot analysis of GCase protein levels and Vinculin as loading control in iPSC-derived midbrain neurons showing increased GCase protein levels after gene-correction. Sequencing results (A) and the representative Western blots are included in the publication by Baden, Pérez et al. (Baden et al., 2023).

After gene-editing of PD-1 and GD-2, the generated isogenic couples were differentiated into midbrain neurons. Staining for ß3Tubulin, a pan-neuronal marker, and Tyrosine hydroxylase (TH, dopaminergic neuron marker) in all lines confirmed successful differentiation into midbrain neurons (Figure 5-19 A). The percentage of ß3Tubulin and TH positive cells was calculated based on the nuclei (DAPI) count (Figure 5-19 B and C). As shown, no significant difference in differentiation to neurons (approximately 81-85%) or dopaminergic neurons (around 27-29%) was detected.

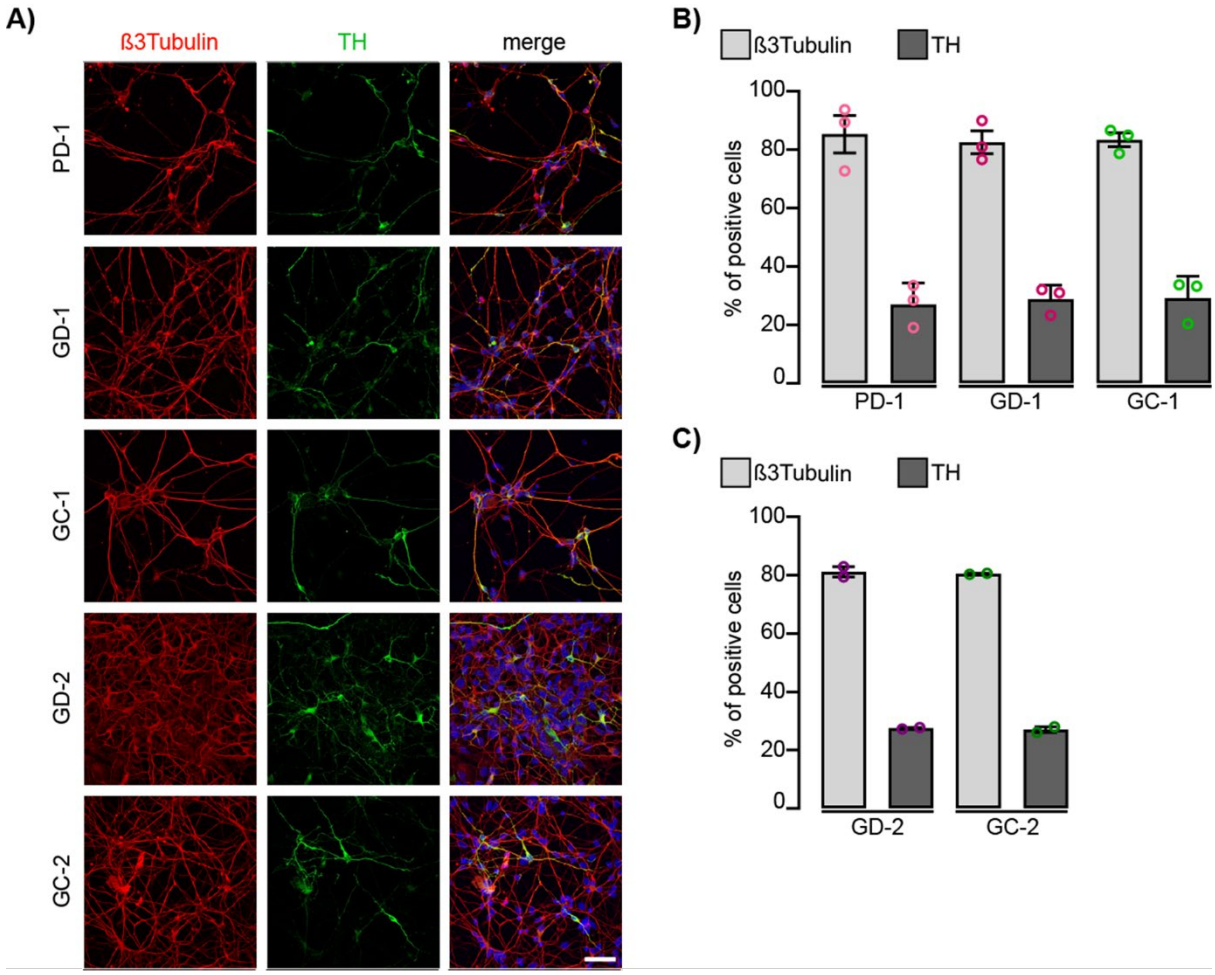

Figure 5-19 Differentiation potential of isogenic couples is comparable. A) Representative pictures of midbrain neurons stained with the pan-neuronal marker ß3tubulin and the dopaminergic neuron marker, tyrosine hydroxylase (TH). (Scale bar is 50 µm). Merged picture of PD-1 and GD-1 is part of the publication by Baden, Pérez et al. (Baden et al., 2023). B-C) Quantification of ß3Tubulin and TH positive cells. (n=2-3 independent differentiations)

5.7.3 Gene-correction of the p.E326K mutation

Figure 5-20 illustrates the chosen strategy for the gene-correction of the heterozygous p.E326K mutation. The sequence of intron 7 to intron 9 of *GBA1* containing the mutation in exon 8 was analyzed with http://www.genome-engineering.org/ (Ran et al., 2013) for potential guides. The PAM of one guide was only a few nucleotides away from the mutation and the guide sequence spanned the point mutation. This guide was chosen and the ssODN designed. For the design of the ssODN, a sequence that has left and right of the point mutation 55 bases of a homology region was chosen. A silent mutation was introduced in the PAM to avoid repeated cleavage of the sequence after gene-correction. Having a guide with the mutation in the sequence that gets recognized, increased the specificity for the mutant allele.

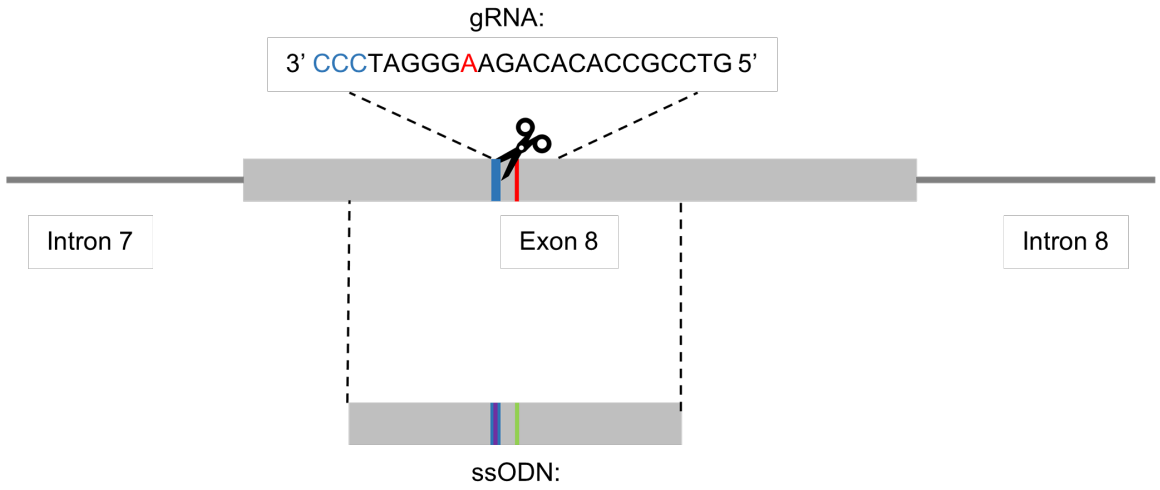

Figure 5-20 CRISPR-Cas9 strategy for gene-correcting the *GBA1* p.E326K mutation: The guide sequence (gRNA) includes the p.E326K mutation (red) and the protospacer adjacent motive (PAM, blue) is 5 nucleotides upstream of the mutation. The Cas9 cleaves the mutant allele 3 bases upstream of the PAM. The single stranded oligodinucleotide (ssODN) contains the corrected nucleotide G (green) the PAM (blue), which contains a silent mutation (violet).

For the gene-correction an Atto550-fluorescent tracrRNA was combined with the crRNA to generate the guides. These were incubated with the Cas9 protein to obtain the ribonucleoprotein (RNP) complex. iPSCs from PD-3, one of the p.E326K heterozygous *GBA1* mutant lines, were nucleofected with latter and were FACS sorted for Atto550 positive cells. In Figure 5-21 A, the gating for the live cells in the Atto550 negative sample is presented. Two Atto550 positive populations were separated from the Atto550 negative cells (Figure 5-21 B). One was Atto550 high and the other Atto550 medium. These 2 populations were sorted into separate tubes.

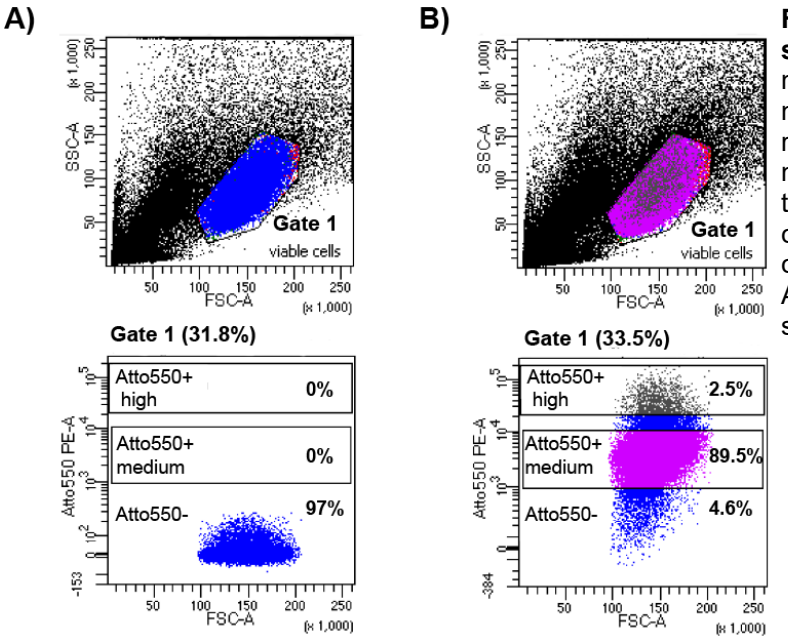

Figure 5-21 Gating strategy for FACS sorting Atto550+ cells. A) First the negative control consisting of cells nucleofected without the ribonucleoprotein (RNP) complex was measured by FACS to set the laser and to gate for the viable cells. B) Gating of cells nucleofected with the RNP complex. The medium and high signal Atto550+ cells were sorted into separate tubes for replating.

Sorted cells were replated and the clones picked as soon as the size of the colonies was sufficient. Gene-correction was confirmed by Sanger sequencing of the DNA and mRNA showing the exchange of the A with a G (Figure 5-22 A). In the following text, the isogenic control will be called GC-3. Interestingly, the silent mutation was not present in the gene-corrected clones. GCase activity was increased after gene-correction as well when compared to the other p.E326K mutant line, PD2 (Figure 5-22 B). Western blot analysis of GCase revealed an increase in protein level in the GC-3 compared to the mutant PD-3 (Figure 5-22 C). These results confirmed proper gene-correction of the p.E326K mutation with this CRISPR-Cas9 based strategy and restoration of GCase levels and activity in the GC line.

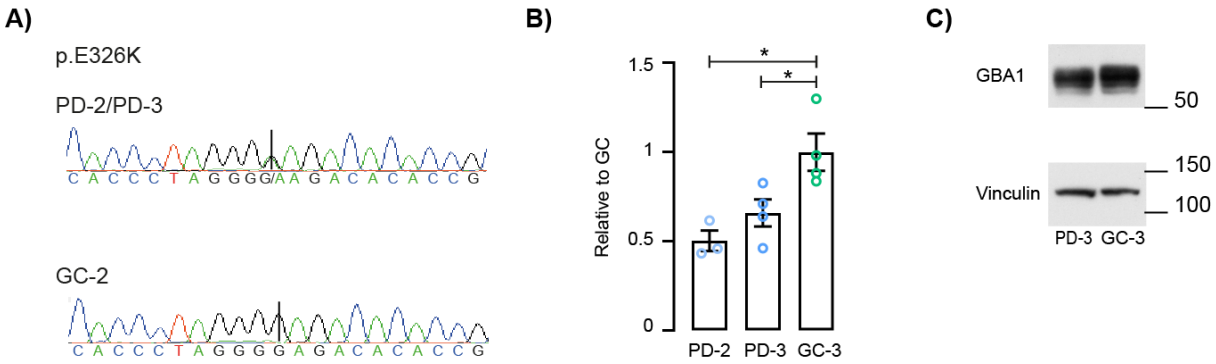

Figure 5-22 Confirmation of p.E326K gene-correction (GC). A) Sanger sequencing confirmed GC by replacement of the A by a G at the line. B) Gene-correction rescued GCase activity of iPSC-derived neural precursor cells in the isogenic control (GC-3) compared to the heterozygous p.E326K GCase mutant (PD-3) and another heterozygous PD patient (PD-2) (n=3-4,mean±SEM are shown, for statistical analysis the student's T-test was performed). C) Representative Western blot of iPSC-derived midbrain dopaminergic neurons lysate for GCase and Vinculin. The sequencing result (A) and the Western blot picture (C) are part of the publication by Baden, Pérez et al. (2023).

In addition, the 5 most likely off-target effects predicted by two CRISPR tools, CCTOP (https://cctop.cos.uni-heidelberg.de:8043/; (Stemmer *et al.*, 2015)) and CRISPOR (V.4.98; http://crispor.tefor.net/crispor.py; (Concordet & Haeussler, 2018) were analyzed by Sanger

sequencing. The lists of off-targets generated is displayed in the Appendix. (Appendix 9-3: Off-Target effects predicted by CCTOP; Appendix 9.4: Off-target effects predicted by CRISPOR. The 5 highest ranked exonic off-targets are marked in yellow.) As shown in Figure 5-23, the sequences around the potential off-target site have the correct sequence. Sequencing of RP11-576I22.2 showed a heterozygous point mutation, which is as well observed in the patient line. Therefore, it is not caused by the gene-editing.

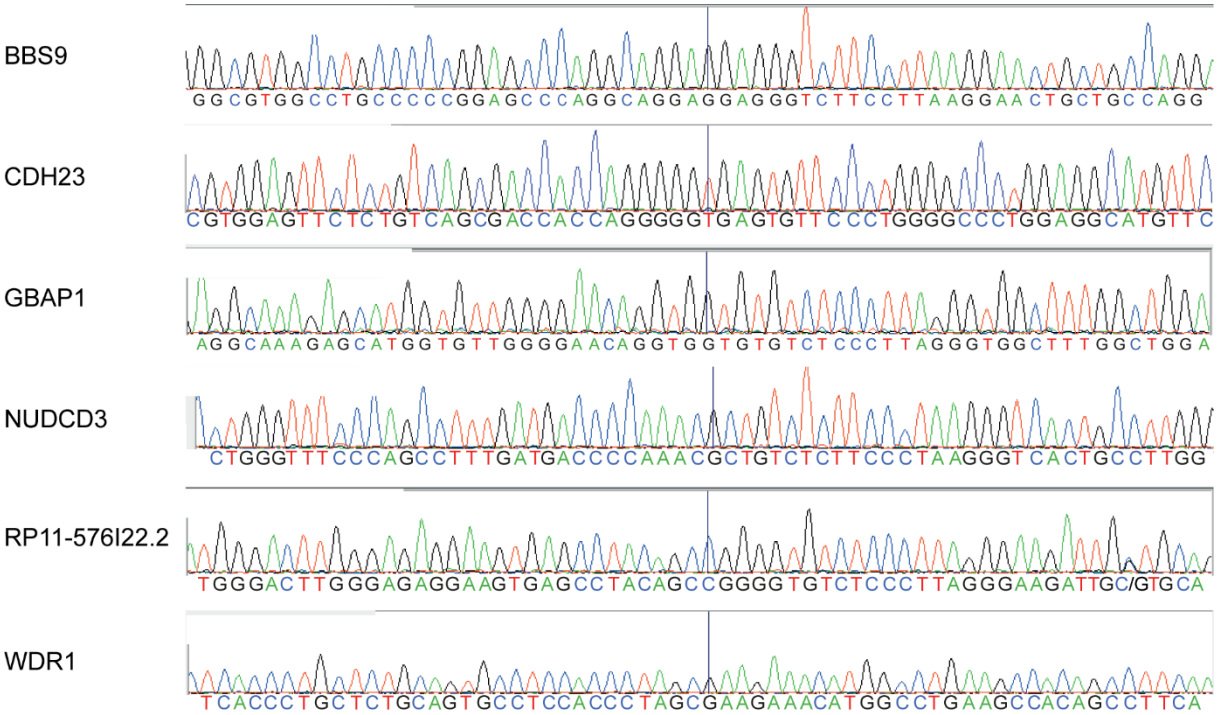

Figure 5-23: Sequencing did not show off-target effects caused by p.E326K gene-correction. The sequences of the first five possible exonic off-target effects detected with CCTOP and CRISPOR (V.4.98) are shown.

As it was done for the p.L444P isogenic couples, the newly generated p.E326K lines were differentiated into midbrain dopaminergic neurons and stained for ß3tubullin and TH (Figure 5-24 A). The differentiation potential of PD-2, and the isogenic couple PD-3 and GC-3 was determined (Figure 5-24 B). No significant difference was observed in the percentage of neurons (around 81-84%) or dopaminergic cells (around 27-30%).

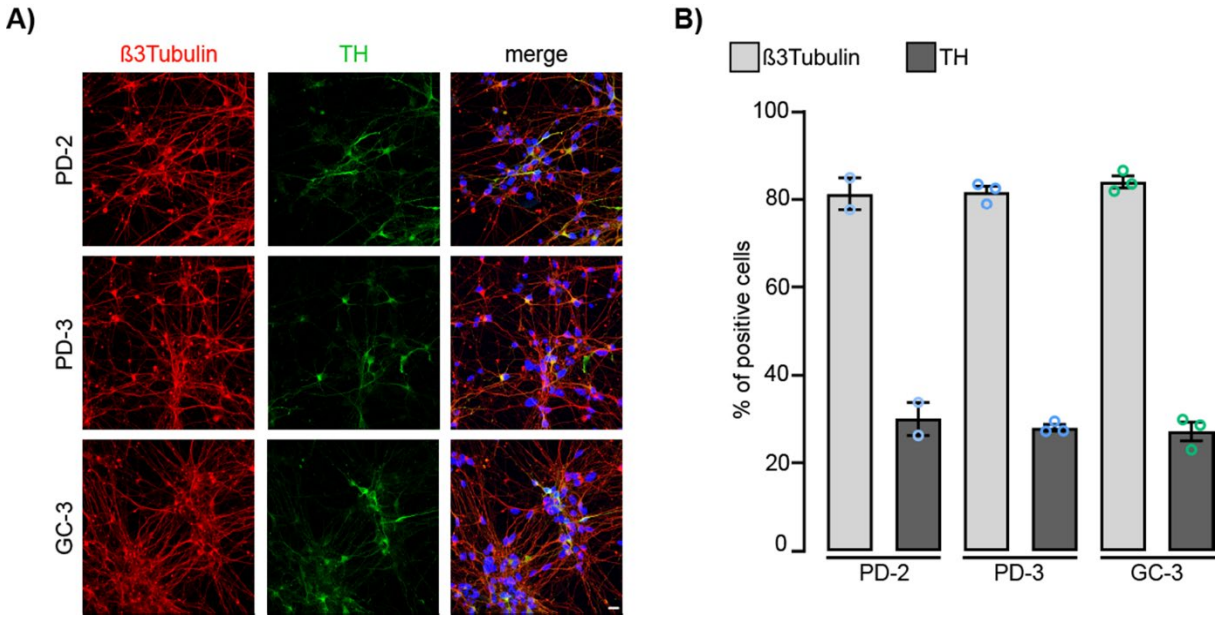

Figure 5-24: Differentiation potential of PD-2 and the PD-3/GC-3 isogenic couple is not different. A) Representative picture of midbrain neuronal differentiation of PD-2, PD-3, and GC-3 stained for the pan-neuronal marker ß3Tubulin (red) and the dopaminergic neuronal marker Tyrosine Hydroxylase (TH, green). Nuclei are counterstained with DAPI (blue). B) Percentage of neurons and dopamine neurons was calculated based on the number of nuclei. (n=2-3 independent differentiations, scale bar is 10 µm)

5.7.4 Summary of patient derived iPSC lines used in this thesis

Table 5-2 summarizes the clones and lines that were generated as well as the genotype and the name used in the thesis.

Subject	Gender	Age	Age of onset	Diagnosis	iPSC clones	GBA genetic variants	Synonym in Thesis
150021	M	60	49	PD	21#3	p.L444P/WT	PD-1
					21#3.8.11 GC *	WT/WT	GC-1
					21#3.5 *	RecNcil/RecNcil	GD-1
150046	M	62	52	PD	46 #2	p.E326K/WT	PD-2
150047	M	60	50	PD	47 #4	p.E326K/WT	PD-3
					47 #4.2 *	WT/WT	GC-3
49/10 (Schöndorf et al., 2014)	F	2	2	GD type 3	49/10	p.L444P/p.L444P	GD-2
					49/10 #5.6 *	WT/WT	GC-2

Table 5-2: Cell lines and patient information of cell lines generated and used in this thesis. * are the gene-edited lines.

5.8 Effect of WT and mutant GCase on mitochondrial function

5.8.1 Mitochondrial function is impacted in GCase mutant iPSC-derived midbrain neurons

GBA1 mutations have been associated with mitochondrial dysfunction. Mice lacking GCase displayed mitochondrial respiratory shortage, lower membrane potential, defects in mitophagy and fragmentation of mitochondria in astrocytes and neurons (Osellame *et al.*, 2013). The same was observed in *GBA1* KO iPSC mDa neurons (Schöndorf *et al.*, 2018). Furthermore, iPSC-derived midbrain neurons of heterozygous p.N370S, p.L444P and RecNcil mutant *GBA1* PD patients showed similar mitochondrial defects (Schöndorf *et al.*, 2018). To characterize the new iPSC lines and assess whether they show the same defects as it had been previously reported, we used the seahorse XF96 to evaluate mitochondrial respiration in the newly generated lines compared to their isogenic control (Figure 5-25 A-H).

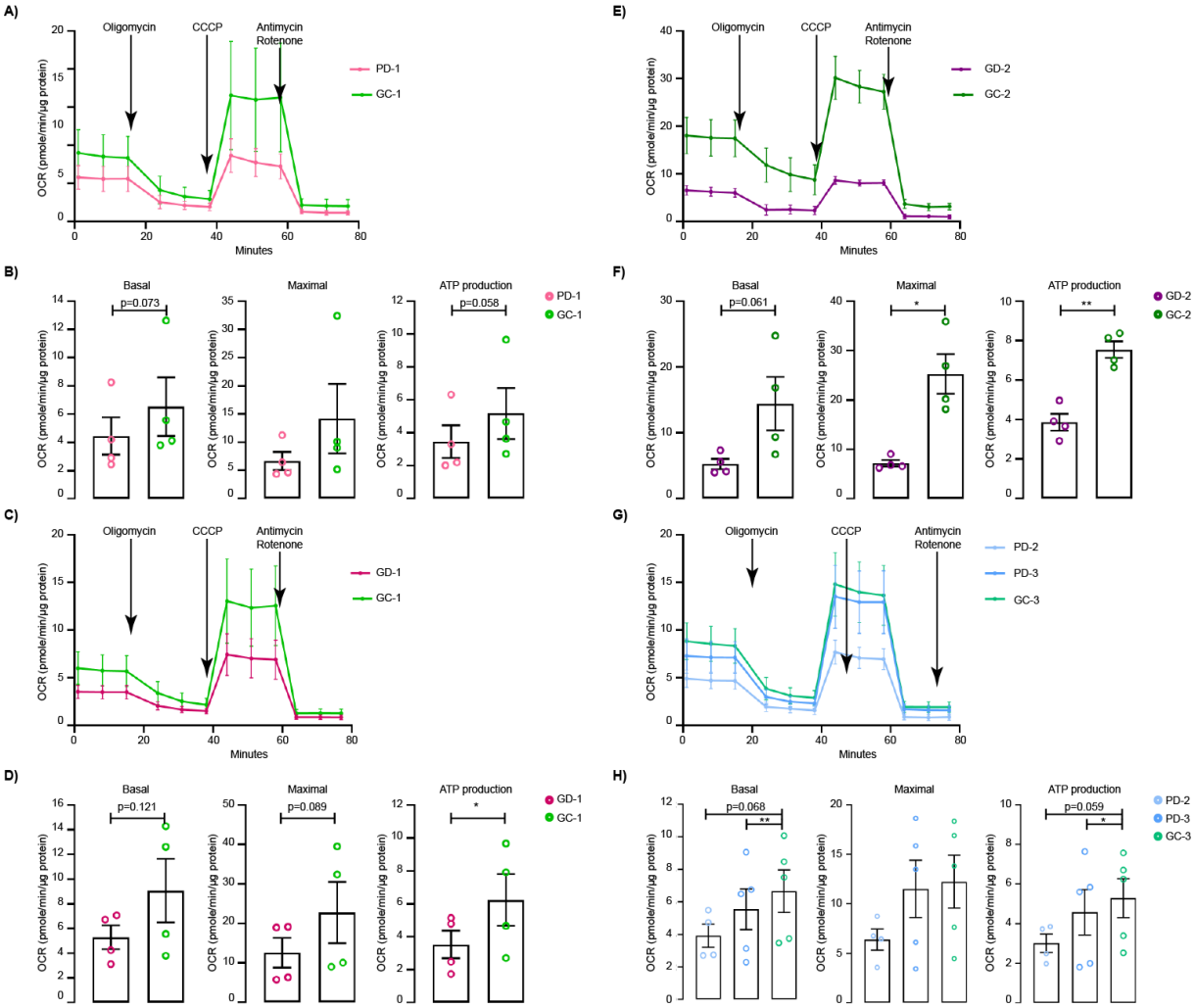

Figure 5-25: Mitochondrial respiration is affected by *GBA1* mutations in induced pluripotent stem cell (iPSC)-derived midbrain neurons. Oxygen consumption rate (OCR) was measured for (A) PD-1, (C) GD1, (E) GD-2 and (G) PD-2 and PD-3 compared to the respective control. Basal, Maximal and ATP-linked OCR were evaluated for (B) PD-1, (D) GD-1, (F) GD-2 and (H) PD-2 and PD-3 compared to the controls. (n=4-5 biological replicated, mean ±SEM is shown, paired students' t-test was performed. * p<0.05; ** p<0.01)

In the new lines, mitochondrial basal respiration and ATP-linked OCR are decreased in the mutants compared to the respective control (Figure 5-25 B, D, F, H). Even though due to the high variability significance for basal respiration was only reached in PD-3 compared to GC-3 (Figure 5-25 H). For ATP-linked OCR only the p.E326K isogenic couple (Figure 5-25 H) and the two homozygous isogenic couples reached significant differences (Figure 5-25 D, F). Furthermore, maximal respiration was as well decreased in the homozygous couples, even though only reaching significance when comparing GD-2 to GC-2 (Figure 5-25 E).

5.8.2 *Mitochondrial function is improved in HEK cells overexpressing WT and mutant GCase*

Based on the results in neurons, we were curious to find out whether mitochondrial function is affected by tagged WT and mutant GCase overexpression in T-Rex HEK cells with a WT *GBA1* background. Overtime, first basal oxygen consumption rate (OCR) was measured, then OCR after injection of oligomycin, CCCP and the Antimycin-Rotenone mix using Seahorse XF96-well (Figure 5-26 A).

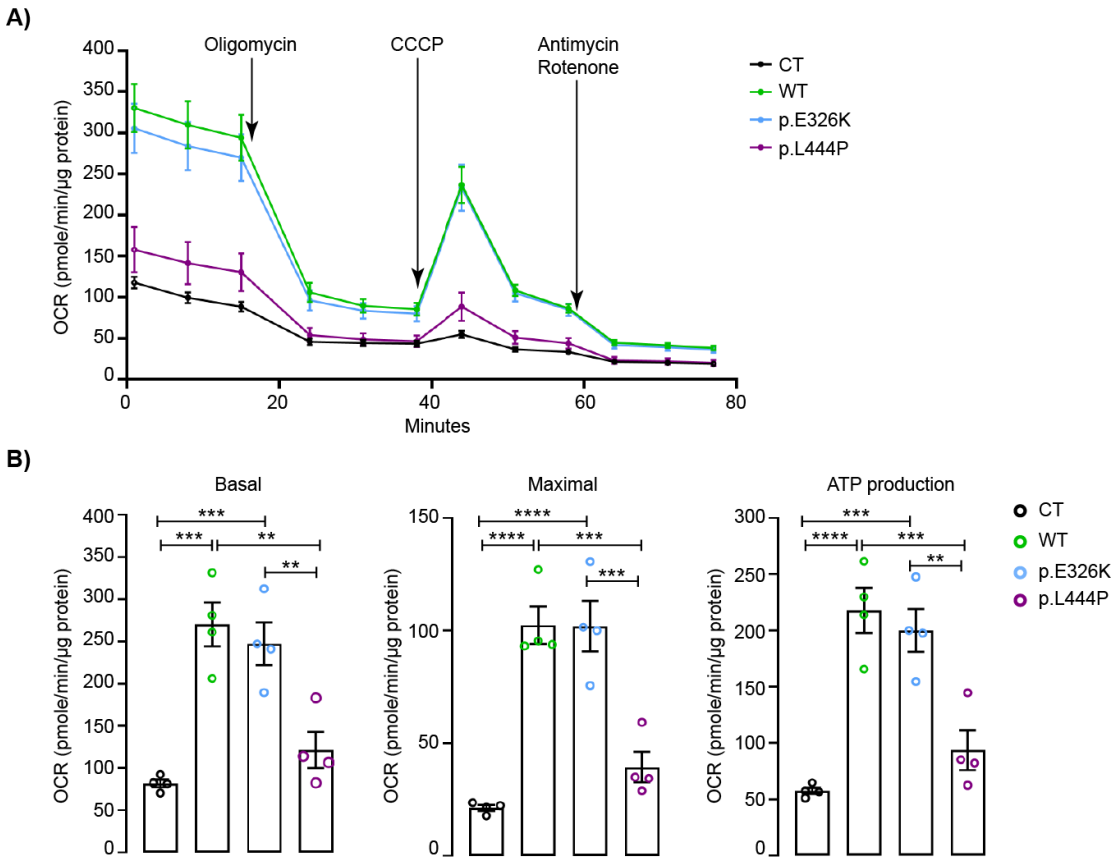

Figure 5-26 Overexpression of tagged WT and p.E326K mutant GCase improve mitochondrial respiration. A) Timecourse of oxygen consumption rate measurement in T-Rex HEK overexpressing tag control, tagged WT, p.E326K and p.L444P mutant GCase before and after injection of toxins. Injection of Oligomycin, CCCP, Antimycin and Rotenone are marked by arrows. Evaluation of basal (B), maximal (C) and ATP linked (D) OCR. (n=4 biological replicates. Ordinary one-way Anova was performed. ** p<0.01, *** p<0.001, **** p<0.0001; n=4 biological replicates, Ordinary one-way Anova was used.)

Basal, Maximal and ATP-Linked respiration was decreased comparing tagged WT and p.E326K mutant to tag control or tagged p.L444P mutant (Figure 5-26 B). No significant difference was observed between WT and p.E326K as well as between p.L444P mutant and CT. Although mitochondrial respiration seemed slightly increased in the p.L444P mutant.

Since the MS data had shown a decreased interaction between TIMMDC1 and mutant GCase, we decided to evaluate next whether we could confirm this observation to evaluate if there might be a direct link between GCase and mitochondrial dysfunction, as TIMMDC1 is involved in CI assembly, which is important for respiration (Guarani *et al*, 2014; Wang *et al*, 2021).

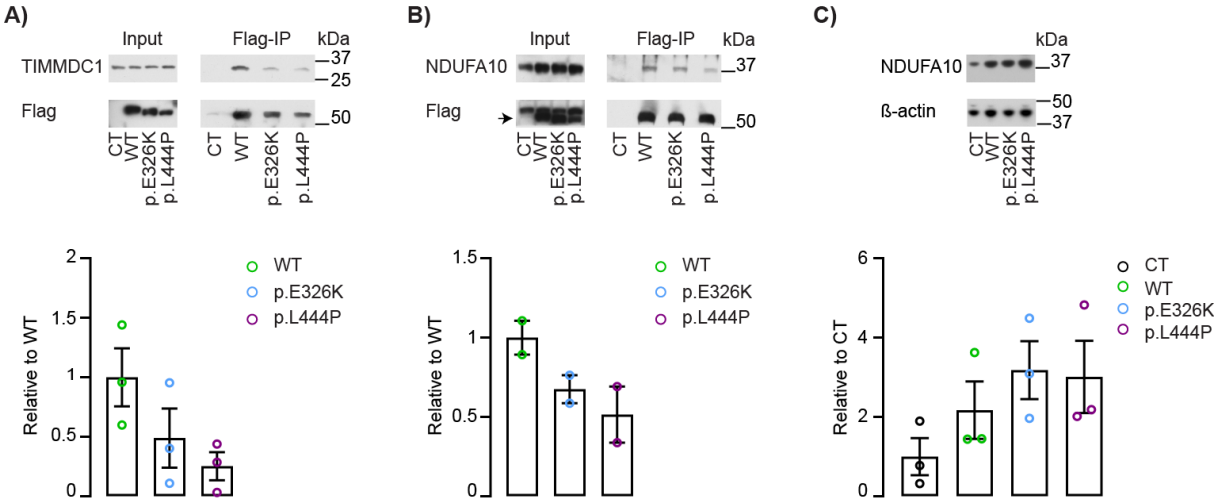

Figure 5-27: Interaction with TIMMDC1 and NDUFA10 seems to be reduced in tagged p.E326K and p.L444P mutant. Representative blot showing the input and the IP result including evaluation of the interaction for tagged WT, p.E326K and p.L444P mutant GCase for (A) TIMMDC1 and (B) NDUFA10. Representative Western blots are published by Baden, Pérez et al. (Baden et al., 2023). C) Representative blot for NDUFA10 and ß-actin as well as quantification of NDUFA10 protein levels relative to CT. (n=2-3 biological replicates, ordinary one-way ANOVA was performed.)

Western blot analysis of the eluates from the co-IP shows a trend towards less interaction between mutant GCase and TIMMDC1 (Figure 5-27 A). TIMMDC1 participates in CI assembly. The interaction was decreased on average by 51% in the p.E326K mutant and by on average 75% in the p.L444P mutant compared to WT GCase. A similar trend was observed for the interaction between mutant GCase and NDUFA10 (Figure 5-27 B). Tagged WT GCase interaction with NDUFA10 was increased by 1.5-fold compared to p.E326K and by 1.9-fold compared to p.L444P mutant GCase. Furthermore, we observed a trend towards increased NDUFA10 levels in tagged WT and tagged mutants overexpressing cells (Figure 5-27 C). As these results point towards defects in CI assembly or integrity, we did a preliminary experiment to assess CI supercomplex formation in iPSC-derived NPCs and midbrain neurons of GCase mutant and KO cells in collaboration with Cristina Ugalde's group. NDUFA9 was used as a marker for the CI in the CI-$CIII_2$ supercomplex and SDHA is the loading control. The preliminary blot shows a decrease in the presence of CI in the supercomplex especially in GD2 and KO NPCs (Figure 5-28 A) and neurons (Figure 5-28 B).

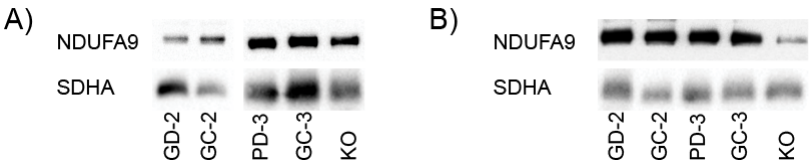

Figure 5-28 CI supercomplex integrity seems to be affected in GCase mutant and KO. Lysates of NPCs (A) and midbrain neurons (B) were analyzed for NDUFA9 as marked for complex I in the CI-$CIII_2$ supercomplex, and the loading control SDHA (complex II). (n=1)

Taken together these results points towards problems with CI integrity in GCase mutant cells.

6 Discussion

The goal of this study was to get a better understanding of the pathological mechanisms linked to *GBA1* mutations, which are the most frequent genetic risk factor for PD. To this end, we generated inducible T-Rex HEK cells overexpressing V5-Flag-tag control, WT, p.E326K or p.L444P mutant GCase upon treatment with doxycycline. Utilizing co-immunoprecipitation followed by TMT-labelling and LC-MS analysis on the cell lysates, we investigated the interactome of WT and mutant GCase. Surprisingly, our MS data uncovered that some of the GCase interactors belong to different mitochondrial compartments (outer and inner mitochondrial membrane, intermembrane space and matrix). First, we show that WT and mutant GCase are imported into mitochondria via a HSC70, translocase of outer mitochondrial membrane (TOM)-, and translocase of inner mitochondrial membrane (TIM)-dependent mechanism. Next, we investigated how mutant GCase interaction with mitochondrial proteins could lead to pathology. On one hand, we show increased interaction with the mitochondrial unfolded protein response (mtUPR) proteins LONP1 and HSP60 with p.L444P mutant GCase. On the other hand, we showed that interaction with TIMMDC1 and NDUFA10 is decreased, potentially leading to reduced CI integrity. Interestingly, mitochondrial respiration was increased in WT and p.E326K mutant GCase overexpressing T-Rex HEK cells compared to control and p.L444P mutant GCase. Additional iPSC lines were generated and gene-corrected to validate the interaction with LONP1 and HSP60 in neural precursor cells (NPC). In addition, we assessed mitochondrial respiration in isogenic iPSC-derived neurons, which tended to be decreased in the mutants. Furthermore, a preliminary assessment in iPSC-derived NPC and midbrain neurons points towards a potential impact of mutant GCase on CI assembly into supercomplex.

6.1 Newly generated GBA1- PD iPSC lines and isogenic controls

In the past, one of the drawbacks in elucidating pathological mechanisms underlying neurodegenerative diseases was the lack of relevant models. Most postmortem brain tissues only allow analysis of the progression or even end-stage of the disease. It was a huge advance, when in 2006 a method for reprogramming mouse fibroblasts into iPSCs was published (Takahashi & Yamanaka, 2006). It was shown that retroviral expression of the transcription factors Oct3/4, Sox2, c-Myc and Kfl-4 were sufficient for the generation of iPSCs (Takahashi & Yamanaka, 2006). One year later it was shown that this method works as well for human fibroblasts (Takahashi *et al*, 2007). Reprogramming became even more attractive when an improved protocol showed that expression of Lin28 and L-MYC in addition to the factors Sox2, Kfl4, and Oct3/4 was an efficient and mostly integration-free way to generate iPSC (Okita et al., 2011).

One of the big advantages of iPSC is that they allow to generate tissue specific cells of interest. For the analysis of neurodegenerative disorders, different types of neurons can be differentiated from iPSCs including midbrain dopaminergic neurons, which are relevant for PD (Ishikawa et al, 2021; Reinhardt et al., 2013). Other brain cell types relevant for neurodegeneration like astrocytes (Janssen *et al*, 2019; Soubannier *et al*, 2020) and microglia (Abud *et al*, 2017; Muffat *et al*, 2016) can also be obtained by iPSC differentiation. As co-cultures or even tricultures became available, it is even possible to elucidate the mutual effect of different cell types (de Rus Jacquet, 2019; Muffat *et al.*, 2016; Ryan *et al*, 2020). Nowadays iPSCs offer the opportunity to generate organoids, which model the complexity of different brain regions to a greater extent than 2D cell cultures (Jo *et al*, 2016; Lancaster *et al*, 2017). iPSC-based disease modeling has been further improved when gene-correction strategies became more easily available and efficient (Ran et al., 2013). Therefore, one does not have to use healthy patients as sole controls anymore. In this way, the contribution of mutations to pathology can be investigated in a disease relevant genetic patient background. Gene-correction allows the co-culture of mutant and WT protein expressing cells to assess whether there would be a spread of the pathology or a protective mechanism even between different cell types.

Different groups have already shown that iPSC-derived neurons from GD and *GBA1*-PD patients cover many relevant aspects of PD. One of the major pathological phenotypes is α-synuclein aggregation. iPSC-derived midbrain neurons from GD or *GBA1*-PD patients have been shown to accumulate α-synuclein (Aflaki et al., 2016; Mazzulli et al., 2011; Schöndorf et al., 2014; Woodard et al., 2014). As in PD, a mislocalization of α-synuclein from the synapsis to cell body was as well observed in GD midbrain neurons (Aflaki *et al.*, 2016; Mazzulli *et al.*, 2016b) and *GBA1*-PD neurons (Woodard *et al.*, 2014). GCase substrate accumulation potentially contributes to the pathology by increasing α-synuclein aggregation (Kim et al., 2018b; Paul et al., 2021; Zunke et al., 2018). Therefore it is of note that GlcCer and GlcSph accumulation was as well detected in GD neurons (Aflaki *et al.*, 2016; Schöndorf *et al.*, 2014) and even in *GBA1*-PD iPSC-derived midbrain neurons (Fernandes et al., 2016; Kim et al., 2018a; Schöndorf et al., 2014). Furthermore, reduced autophagic flux and lysosomal dysfunction have been observed in *GBA1*-PD (Fernandes et al., 2016; Schöndorf et al., 2014; Schöndorf et al., 2018) and GD midbrain neurons (Awad *et al.*, 2015; Mazzulli *et al.*, 2011; Schöndorf *et al.*, 2014), leading to lower levels of degradation of long lived proteins (Mazzulli *et al.*, 2011). Another important phenotype with regard to PD is mitochondrial dysfunction. This is as well recapitulated in *GBA1*-PD iPSC-derived neurons (Schöndorf *et al.*, 2018).

In a previously published study, the heterozygous p.E326K mutant had a residual lysosomal GCase activity of 1.6 fold compared to isogenic control (Ysselstein *et al*, 2019). This is a similar leftover activity as we observed comparing GC versus p.E326K mutant NPC. The RecNcil

mutant had 4.3% of WT activity. The gene-correction of p.L444P was associated with a significant rescue of GCase activity. As previously shown, the differentiation efficiency was comparable among mutants and gene-corrected lines (Schöndorf *et al.*, 2014). Unfortunately, the neuronal cultures contained only approximately 25% of TH positive neurons. Therefore, potential differences might be covered by other neuronal cell types or other cells, as about 20% of the cells were not neuronal. To get a better understanding of midbrain dopaminergic specific phenotypic pathologies, it would have been better to FACS sort the cells either by adding a fluorescent tag to TH or by introduction of a fluorescent reporter of TH expression. This would maybe even give the opportunity to compare them with other neuron types.

6.2 Difference in interactome of WT and mutant GCase

6.2.1 Assessment of the overexpression model

GBA1 mutations are the most frequent genetic risk factor for PD (Sidransky *et al.*, 2009). Several mechanistic insights could already be gained. However, the complete picture is still missing. To elucidate new pathological mechanisms, we investigated the interactomes of WT and p.E326K as well as p.L444P mutant GCase. p.L444P mutant GCase is rapidly degraded via ERAD, hampering further proteomic studies. For this reason, we employed an overexpression model that would allow us to obtain sufficient protein quantities for downstream analysis. We used a tagged approach as the antibodies are specific and allow a reduced background. In addition, using a model with a tag allowed us to compare the WT and mutant interactome of GCase, even though in our cellular model we still had expression of WT GCase from the T-Rex HEK cells. To validate that the tag does not influence the trafficking of GCase to the lysosome, we used iPSC-derived *GBA1* KO NPCs and transfected them with WT *GBA1* or the tagged *GBA1* construct. As expected, co-localization has been observed between tagged GCase and the lysosomal marker LAMP1. WT and tagged WT GCase staining shows a diffuse cellular localization. This was previously seen when overexpressing C-terminal mCherry tagged GCase in Hela cells (Morabito *et al*, 2017). Furthermore, in transient, selected HEK cells overexpressing either WT or V5-Flag-tagged GCase, we showed that the tag does not influence GCase activity. In both cases the GCase activity was increased by approximately 2-fold compared to untransfected cells. In the study employing HeLa cells for the analysis of overexpressed C-terminal tagged GCase, the increase in GCase activity seems to be higher than in our experiments (about 7-fold increased based on the figure). This is most likely due to the fact that in the paper they used cell lysate for the activity whereas we performed the assay in live cells. On the other hand, transfection efficiency might lead to the discrepancy. In the experiments, using the inducible T-Rex HEK cells and performing the assay as well on lysate, we have a higher increase in GCase activity (on average 14-fold), which most likely is due to the fact that all cells overexpress GCase. Overexpression of p.E326K mutant GCase in HeLa cells leads to a reduction of 46% of the GCase activity compared to WT overexpression (Malini

et al., 2014). In the more severe mutant p.L444P GCase activity was even reduced by 87% (Malini *et al.*, 2014). This was comparable to what we observed in our model with p.L444P mutant having about 14% of WT activity left. However, overexpression of p.E326K mutant decreased the activity only by about 30% of the increase seen in WT. Compared to V5-Flag-tag overexpression control, there was no significant difference with p.L444P overexpression. This had been previously observed in another overexpression HEK cell model (Polissidis *et al.*, 2022). About 80% of the WT GCase protein level is left in p.E326K homozygous mutant GCase fibroblasts (McNeill *et al*, 2014). This value is similar to what we observed when transiently overexpressing the p.E326K mutant GCase variant with a tag in our inducible T-Rex HEK cell model.

6.2.2 WT GCase interactome

To validate the interactome, we first assessed known GCase interactors, including BiP (Schmitz *et al.*, 2005; Tan *et al.*, 2014), Calnexin (Ron & Horowitz, 2005; Tan *et al.*, 2014), LIMP2 (Reczek *et al.*, 2007), HSP90B1 (Tan *et al.*, 2014), and HSC70 (Kuo *et al.*, 2022). For BiP, interaction was only observed with WT and not with the p.L444P mutant (Schmitz *et al.*, 2005). However, the co-IP was done in patient fibroblasts were p.L444P mutant GCase protein levels are much more reduced and might not be sufficient to be detected on the blot. Furthermore, the blot does not look as expected as p.L444P GCase levels in 50 µg lysates are like WT levels and no loading control is included as well as the BiP blot is missing to show that the IP worked in all groups. Therefore, a discrepancy between our results and the previous publication cannot be concluded. Overexpression might lead to retention of WT GCase in the ER (Ron & Horowitz, 2005). This was concluded as overexpressed Myc-tagged WT GCase was partially sensitive to EndoH treatment, which was not observed in the endogenous WT cells (Ron & Horowitz, 2005). However, this might be due to the experimental setup, as it was previously shown that WT GCase is as well sensitive to EndoH treatment (Bergmann & Grabowski, 1989). However, the overexpression of GCase might lead to a higher ER fraction, which then is easier detected in co-IPs and EndoH treatment experiments. The higher ER fraction might as well lead to the increase in ER folding related proteins. It was proposed that due to overexpression, there is a lack of possible binding partners which support the proper trafficking of the overexpressed protein resulting in ERAD of the overexpressed protein (Ron & Horowitz, 2005). Furthermore, the list of proteins leading to interaction of WT with proteins related to unfolding proteins, i.e., Calnexin, are as well involved in normal protein folding of N-glycosylated proteins (Kozlov & Gehring, 2020).

Up to date, only one study has assessed the interactome of endogenous WT GCase in HeLa cells (Tan *et al.*, 2014). Interestingly, 45.3% of proteins listed in the interactome of Tan et al. (2014) are as well present in our WT overexpression interactome. The discrepancy can have several explanations. First, we use an overexpression model whereas Tan et al. (2014) used

endogenous HeLa cell GCase. The overexpression model most likely allowed us to obtain higher quantities of GCase and in this way, might allow us to detect low abundance interactors. Due to the low protein level of mutant GCase, overexpression was in our case necessary to get sufficient mutant GCase for analysis. Second the co-IP and MS analysis were different between both studies. For the endogenous interactomic study a DSP cross-linker in intact cells was used (Tan *et al.*, 2014). This does not only allow to stabilize weak and transient interactions of GCase, but it also will stabilize proteins that are part of a complex between lysines within 12 Å radius (Smith *et al*, 2011). Therefore, the number of proteins that do not interact directly with GCase but with an GCase interactor might be increased as well. Furthermore, direct labelling by SILAC was used for the analysis of the endogenous GCase and we had used TMT-labelling post isolation of GCase and its interactors by co-IP.
Interestingly, the list of WT endogenous interactors published by Tan et al. (2014) contained 7.8% of mitochondrial proteins when compared to MitoCarta3.0 (Rath *et al.*, 2021). As in our interactome, they belong to different clusters of mitochondrial proteins, including mtUPR (i.e., HSPD1, HSPA9, TRAP1), carrier proteins (i.e., SLC25A13), and proteins related to oxidative respiration (ATP5A, ATP5B, ATP5C1, SDHA). The proteins listed here are shared with our interactome and demonstrate that interaction with mitochondrial proteins cannot be explained by the tag or the overexpression model.

6.2.3 Difference between the p.E326K and p.L444P GCase mutant

In the current study, the severe GD causing p.L444P and the milder, not GD causing p.E326K GCase mutation were included. Comparison of both interactomes could lead to a better understanding which pathological mechanism might be disease driving in *GBA1*-related PD, as p.E326K is not causing GD but is still increasing the risk for PD (Duran *et al.*, 2013; Malini *et al.*, 2014; Park *et al.*, 2002). Our results show that there is a significantly higher interaction between proteins of the mitochondrial unfolded protein response (mtUPR), HSP60 and LONP1 with the p.L444P mutant compared to p.E326K mutant GCase. Therefore, the effect on mtUPR might not be the main mechanism in *GBA1*-PD. Furthermore, the interaction between TIMMDC1 and NDUFA10 with p.E326K and p.L444P mutant GCase is decreased to a similar degree. This goes along with a decrease in CI activity which seems comparable between both mutants (Baden *et al*, 2022). This could suggest that in *GBA1*-related PD, the defects in CI assembly and activity associated with mutant GCase are a major pathological consequence. This as well fits the recently published data, where mitochondrial dysfunction due to KO of a catalytic subunit of CI leads to defects in dopamine signaling first in axons then progressing to the soma accompanied by increasing motor dysfunction (González-Rodríguez *et al*, 2021).

6.3 Import of GCase into mitochondria

The WT GCase interactome contained 13.3% of mitochondrial proteins according to MitoCarta3.0 annotation. Since it is unexpected that the lysosomal protein GCase interacts with mitochondrial proteins, we first assessed the presence of GCase in mitochondria. Usually, mitochondrial matrix proteins have a mitochondrial matrix targeting sequence (MTS). Analysis of the *GBA1* sequence did not uncover an N-terminal MTS. Furthermore, to proof the validity of our model, we showed that the V5-Flag-tag of GCase does not lead to an MTS, which could have explained the mitochondrial targeting in our overexpression model. However, we uncovered internal MTS-like sequences (iMTS-ls). Using the split-GFP approach (Cabantous *et al*, 2005; Calì *et al.*, 2015), location of WT and mutant GCase in the mitochondrial matrix was confirmed. Using the mitochondrial protein ATP1, it has been previously shown that mutation of the iMTS-ls leads to disruption of the mitochondrial import (Backes *et al.*, 2018). According to this result, removal of the iMTS-ls from the *GBA1* sequence prevented mitochondrial import of GCase. This was not due to protein instability as shown by ongoing experiments in the laboratory.

For the import of mitochondrial proteins with an iMTS-ls, TOM70 is an essential component of the mitochondrial import machinery (Backes *et al.*, 2018) and cytosolic HSC70 is associated in the mitochondrial import through TOM70 (Young *et al*, 2003). Interaction of GCase with HSC70 and TOM70 suggests that these two proteins are important for the initiation of mitochondrial import of GCase. KD of HSC70 and TOM70 was shown to decrease import of unfolded cytosolic proteins into mitochondria (Li *et al.*, 2019), thereby it should be reducing the interaction with LONP1. In our model, upon HSC70 KD we observed a decrease in the interaction between GCase and LONP1, although not significant. This further supports the dependents on HSC70 for the mitochondrial import of GCase. After the protein passed the TOM-complex, the proteins get imported through the TIM-complex into the mitochondrial matrix (Harbauer *et al*, 2014; Schulz *et al.*, 2015; Wiedemann & Pfanner, 2017). In yeast *tim23* KD prevents the import and degradation of aggregation-prone cytosolic proteins (Ruan *et al.*, 2017), which should as well decrease the interaction with the mitochondrial protease. Here, we show that GCase interacts with TIM23 for mitochondrial import and that TIM23 KD reduces the interaction between LONP1 and GCase. To summarize, the import of GCase depends on the interaction with HSC70 and the initiation of the import through the TOM complex, followed by the import into the mitochondrial matrix by the TIM complex. However, as GCase is lacking a classical MTS, the exact import mechanism of GCase into mitochondria needs further investigation.

6.4 Mutant GCase leads to mitochondrial dysfunction

Until now, mitochondrial dysfunction was considered rather a side-effect of sphingolipid accumulation. As described above, GCase deficiency results in the elevation of its substrates.

In brain tissue from GD type 2 and type 3 patients, the accumulation of GlcCer and GlcSph was observed (Nilsson & Svennerholm, 1982; Orvisky *et al.*, 2002; Tayebi *et al.*, 2003). Latter was as well slightly increased in GD type 1 brain (Tayebi *et al.*, 2003). Recently, it was observed that total and C18 GlcCer were elevated in the middle temporal gyrus in *GBA1*-PD patients (Blumenreich *et al.*, 2022). In fibroblasts from p.L444P *GBA1*-PD patients total sphingolipid levels were elevated whereas total phospholipids were reduced (Galvagnion *et al.*, 2022). In p.N370S heterozygous *GBA1*-PD iPSC neurons, the levels of GlcCer species were perturbed, having higher levels of C16 and C24 and lower levels of C20 GlcCer (Fernandes *et al.*, 2016). Furthermore in *GBA1*-PD iPSC-derived midbrain neurons the mitochondrial fraction had enriched levels of C16 ceramide*,* whereas in KO midbrain neurons all GlcCer species and GlcSph were enriched (Schöndorf *et al.*, 2018). Interestingly in serum levels of *GBA1*-PD patients several lipid levels were altered (Guedes *et al*, 2017). Among these, ceramide and sphingomyelin (SM) belong to the enriched lipid species whereas phosphatidylethanolamine (PE) and phosphatidic acid (PA) are part of the lipid species with reduced levels (Guedes *et al.*, 2017). In a mouse model of non-alcoholic fatty liver disease, lipid alterations including ceramide, SM, PA and PE species, were observed and linked to increased ROS levels (Durand *et al*, 2021). Furthermore, it was discovered that a high fat diet leads to hepatic lipid alterations, which were associated with a decrease in respiratory complex proteins in the mitochondrial membrane (Kahle *et al*, 2015).

The interaction of mitochondrial proteins with WT and mutant GCase to varying degrees made us wonder if there is a direct link between GCase and mitochondrial function. Interaction of GCase with proteins from different complexes including CI and the CI supercomplex assembly factor TIMMDC1 supports this idea. One of the characteristics of PD, is mitochondrial dysfunction. Improved mitochondrial respiration observed in p.E326K mutant and WT tagged GCase overexpressing cells, was lost upon p.L444P mutant overexpression. A similar effect was seen on CI activity when overexpressing WT GCase (Baden *et al.*, 2022). Our lab has shown that iPSC-derived midbrain dopaminergic neurons from *GBA1-PD* patients, including p.E326K and p.L444P heterozygous mutants, have a reduced mitochondrial respiration and CI activity when compared to the isogenic control (Baden *et al.*, 2022; Schöndorf *et al.*, 2018). A loss-of-function mechanism could explain the reduced respiration and CI activity in mutants. This idea is supported by the decreased interaction of mutant GCase with CI subunit NDUFA10 as well as TIMMDC1. Latter is involved in CI assembly (Guarani *et al.*, 2014) by adding CI subunits to a respirasome subcomplex, which is formed by CI, CIII and CIV subunits (Fang *et al*, 2021). In the study of Guarani et al. (2014)(Guarani *et al.*, 2014), GCase was already found to be an interactor of exogenously expressed tagged TIMMDC1. If GCase would stabilize TIMMDC1 and prevents its degradation, as it was shown for C9ORF72 (Wang *et al.*, 2021) or if it has another function in CI integrity needs to be further elucidated in the future. Preliminary

data on CI integrity in supercomplex in p.E326K heterozygous, p.L444P homozygous and *GBA1* KO iPSC-derived NPCs and midbrain neurons gives a first hint towards this idea that GCase is involved in CI assembly or integrity, as there seems to be a slight decrease in mature CI containing supercomplex (Baden *et al.*, 2022). Defects in CI assembly had been previously linked to a decrease in mature CI (Guarani *et al.*, 2014; Wang *et al.*, 2021). Moreover, defects in CI assembly are accompanied with an accumulation of CI smaller building blocks (Wang *et al.*, 2021). In iPSC from *GBA1* mutant PD patients, a non-significant increase in CI subunits was observed when compared to the isogenic control (Schöndorf *et al.*, 2018). Our MS data show that overexpression of mutant GCase goes along with an increase in mitochondrial proteins, including subunits of CI. In GCase mutants more subunits are increased compared to control than in WT. No difference between tagged WT GCase compared with mutant GCase or the control was seen in the MS data. However, by WB we could only determine a general increase associated with overexpression of WT or mutant GCase compared to control. This could be due to a decrease in sensitivity of the WB, as the MS data did not indicate a significant difference between WT and any other group, which could point towards a slight but not significant increase in WT. Increase of CI subunits in WT, could be linked to the increased activity that we have observed when compared to control cells. Furthermore, it had been previously shown that partial rescue of mitochondrial function can be achieved by Nicotinamide riboside treatment (Schöndorf *et al.*, 2018). However, GCase activity as well as mitochondrial respiration did not improve (Schöndorf *et al.*, 2018). This data supports the idea that there might be a more direct link between GCase and mitochondrial dysfunction.

Mitochondrial dysfunction could as well be partially caused by a gain-of-function of mutant GCase. Our interactome contained proteins of the mtUPR, like the mitochondrial protease LONP1, which has been shown to degrade unstable and misfolded cytosolic proteins (Li *et al.*, 2019; Sánchez-Lanzas & Castaño, 2021). Furthermore, it was shown that WT and mutant TDP-43, which is associated with neurodegeneration, interact with LONP1 (Wang *et al.*, 2019a). Mitochondrial phenotype in TDP-43 mutant, swollen with disrupted cristae (Wang *et al.*, 2019a), is comparable to what was observed for mutant GCase (Schöndorf *et al.*, 2018). KD of LONP1 reduced cell survival when WT or mutant TDP-43 was overexpressed (Wang *et al.*, 2019a). Previously, literature already showed as well a link between mtUPR and PD. Increased LONP1 expression has been observed in a PD mouse model as well as PD patient brain, along with reduced LONP1 activity (Bulteau *et al*, 2017). Other PD models support the involvement of the mtUPR in PD. Mutation of the PD associated genes *pdr1*, homologue of the human *Parkin* gene, and *pink-1* lead to an increase in the mtUPR, which was shown to be neuroprotective (Cooper *et al*, 2017). Furthermore, CLPP is decreased in PD patients' brain and iPSC-derived neurons from p.A53T mutant PD patients (Hu *et al*, 2019). Interestingly, inhibition of LONP1 and HtrA2 lead to an increased α-synuclein aggregation, further supporting

a link between mtUPR and PD (Lautenschläger *et al*, 2020). In our overexpression model, we show increased interaction between p.L444P mutant GCase and HSP60, a chaperone of the mtUPR, as well as with LONP1. There might be a slight trend towards an increased interaction between LONP1 and the p.E326K mutant GCase. Both interactions were confirmed in p.L444P homozygous mutant iPSC-derived NPCs. p.L444P homozygous mutant is still a relevant model for PD. First, homozygous p.L444P *GBA1* mutations are frequently linked to neuropathic GD (Tayebi *et al.*, 2001; Tayebi *et al.*, 1998). Second, Lewy bodies and accumulation of α-synuclein had been seen in GD patients with parkinsonism (Goker-Alpan *et al*, 2010; Tayebi *et al.*, 2003). Furthermore, GD cellular and animal models recapitulate α-synuclein accumulation and mitochondrial dysfunction (Cleeter *et al.*, 2013; Osellame *et al.*, 2013; Peng *et al*, 2021). Last, this GD disease iPSC line was previously employed together with a p.L444P heterozygous PD patient and its isogenic control (Schöndorf *et al.*, 2014). The observed defects in calcium homeostasis and autophagic-lysosomal pathway, as well as accumulation of α-synuclein protein levels, were comparable between the GD and PD line (Schöndorf *et al.*, 2014). Western blot analysis also showed increased interaction. Using expansion microscopy, increased co-localization between p.L444P mutant GCase and LONP1 was confirmed in iPSC-derived neurons as well as midbrain organoids (Baden *et al.*, 2022). Recently it has been reported that LONP1 does not only have protease activity, but that it is as well involved in the folding of mitochondrial proteins (Shin *et al*, 2021). Upon CDDO treatment or LONP1 KD, several proteins including subunits of CI were found to aggregate in mitochondria (Shin *et al.*, 2021). As p.L444P mutant GCase interacts to a higher degree with LONP1, this might prevent LONP1 from its function in protein biogenesis. In this way, LONP1 clients might start accumulating as seen in our proteome analysis and cause CI dysfunction. This could explain why inhibition of LONP1 by CDDO treatment only reduced CI activity in isogenic controls and not in GCase mutant neurons (Baden *et al.*, 2022). Furthermore, this gain-of-function of mutant GCase by preventing LONP1 from its activity in protein folding could as well explain that there was only a trend towards decreased CI activity in *GBA1* KO iPSC-derived midbrain neurons (Schöndorf *et al.*, 2018).

Having defects in mitochondrial CI and general respiration, neurons which are highly dependent on ATP, need to compensate for the decreased ATP production by mitochondria. A possible compensatory mechanism is to rely more on glycolysis for ATP production (Wang *et al.*, 2021). An increase in protein expression of the glycolytic pathway points towards this mechanism in dopaminergic neurons of RecNcil homozygous mutant organoids compared to the isogenic control (Baden *et al.*, 2022). The switch towards increased glycolysis was seen as well in a novel PD mouse model, in which one catalytic subunit of CI was knocked out in dopaminergic neurons (González-Rodríguez *et al.*, 2021). In this model, mitochondrial deficiency led to disturbances of dopaminergic signaling, which started in the striatal axons

(González-Rodríguez *et al.*, 2021). As signaling issues proceed to the soma, motor symptoms start to arise (González-Rodríguez *et al.*, 2021). Upon loss of TH signal in the substantia nigra, gross motor function is affected as seen in PD (González-Rodríguez *et al.*, 2021). This study highlights the importance of mitochondria as potential disease driver of PD. Therefore, based on the presented data, improving GCase activity in mitochondria could be a potential target in *GBA1*-related PD but as well other PD forms in which GCase activity is decreased (Burbulla *et al.*, 2019; Burbulla *et al.*, 2017; Rocha *et al.*, 2015a; Ysselstein *et al.*, 2019). Increasing GCase activity in LRRK2 mutant lines lead to a decrease in PD pathological markers in iPSC-derived neurons (Ysselstein *et al.*, 2019). In addition, treatment to stimulate GCase activity might as well prevent the vicious cycle between GCase deficiency and α-synuclein accumulation. Thereby as well preventing the negative effect of α-synuclein on mitochondria. It has been previously observed that α-synuclein co-localizes with mitochondrial markers in primary cortical neurons and brain slices from 9H/PS-NA mice (Xu *et al*, 2014). PD models, including a p.L444P heterozygous mouse model, and patient brain samples have also shown the import of α-synuclein into mitochondria (Devi *et al*, 2008; Wang *et al*, 2019b). Accumulation of α-synuclein was shown to lead to mitochondrial defects (Devi *et al.*, 2008; Wang *et al.*, 2019b; Yun *et al.*, 2018). To treat consequences of decreased GCase activity in different forms of PD, stabilizers, and activators of GCase activity like S-181 might be of interest. This compound was shown to cross the BBB in D409V heterozygous mutant mice resulting in increased GCase activity (Burbulla *et al.*, 2019). Elevation of GCase activity by S-181 was as well as observed in iPSC-derived neurons from LRRK2 and Parkin mutants and sporadic PD patients (Burbulla *et al.*, 2019). Upon treatment with S-181, iPSC-derived dopaminergic neurons of LRRK2 mutant cells as well as idiopathic PD accumulate less α-synuclein and less oxidized dopamine (Burbulla *et al.*, 2019). Reduced oxidized dopamine might be an indicator for reduced mitochondrial stress, as mitochondrial antioxidants were shown to decrease the occurrence of oxidized dopamine as well (Burbulla *et al.*, 2017). This might occur due to improved mitochondrial respiration. Therefore, it would be interesting to investigate whether S-181 as well improved mitochondrial GCase function. If so, S-181 could have the potential to be used to treat pathology resulting from GCase activity deficits in different PD patient groups.

To conclude, we identified that GCase traffics to mitochondria through a HSC70-, TOM70- and TIM23-dependent mechanism. Furthermore, we show that WT GCase potentially supports CI assembly by stabilizing TIMMDC1. In this case, mutant GCase loss-of-function leads to a decrease in this interaction, thereby potentially leading to CI integrity issues. In the severe p.L444P mutant, an additional gain-of-function mechanism was uncovered. p.L444P mutant GCase promotes the interaction with LONP1 and it might prevent LONP1 to assist folding of CI proteins. Figure 6-1 summarizes the proposed mechanism.

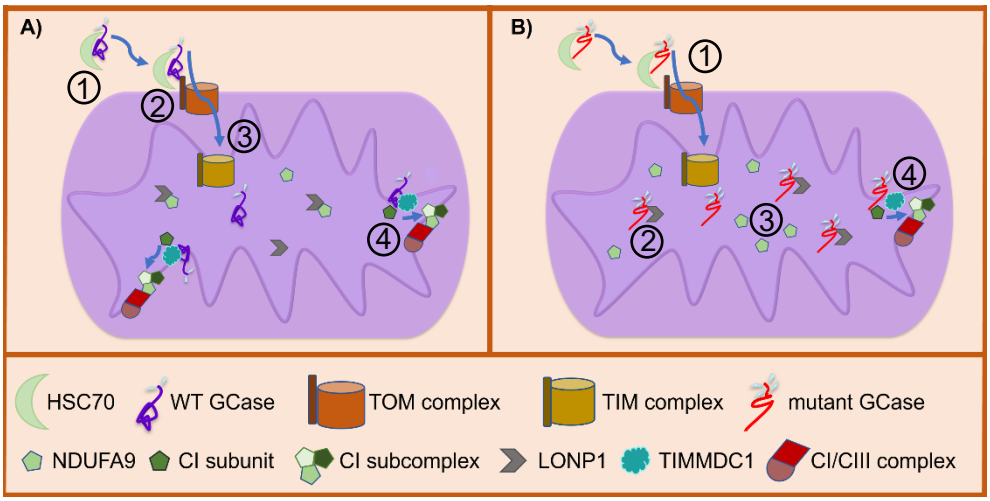

Figure 6-1: Illustration of proposed role of WT and mutant GCase in mitochondria function and dysfunction. A) (1) WT binds HSC70 in the cytosol. (2) HSC70 targets WT GCase to TOM70. (3) GCase is transported by TOM and TIM complex into the mitochondrial matrix. (4) GCase interacts with TIMMDC1 to support CI subcomplex assembly allowing proper mitochondrial respiration. B) (1) Like, WT GCase, mutant GCase is trafficked in a HSC70-, TOM and TIM complex-dependent way. (2) In the mitochondrial matrix, misfolded mutant GCase associates with LONP1. (3) Thereby mutant GCase prevents LONP1 from folding CI subunits like NDUFA9, which start to accumulate in the matrix. (4) Less mutant GCase associates with TIMMDC1 leading to reduced CI integrity, resulting in reduced mitochondrial respiration.

7 Outlook

In this study, we present data providing a direct link between GCase and mitochondrial function. We show that GCase is imported into the mitochondrial matrix in a HSC70-TOM-TIM-dependent manner, and it supports the stability or assembly of mitochondrial CI. However, PD-linked *GBA1* mutations lead to a decreased interaction with TIMMDC and CI protein with defects in CI integrity in supercomplex. Interestingly, the severe mutant p.L444P GCase interacts more with LONP1, preventing LONP1 from its protease and chaperoning activity, likely leading to worsened mitochondrial dysfunction. Even though these data make GCase an interesting target for *GBA1*-related PD, it might as well be interesting in general for PD patients. As described above, GCase activity is as well decreased in sporadic PD and it was reported that the reduced GCase activity correlated with accumulation of GCase substrate, GlcSph (Rocha *et al.*, 2015a). Both decreased GCase activity and increase GLS levels lead to increased α-synuclein levels. However, additional questions need to be addressed.

One crucial point to address is the mitochondrial GCase import and if the import of mutant GCase is perturbed as it looks like interaction with import proteins is slightly increased in p.L444P mutant GCase. This might as well help to find ways to target GCase to mitochondria and potentially improve mitochondrial function in PD. In case, the import of mutant GCase is disturbed, it would be interesting to assess, whether this has an effect on import of other mitochondrial proteins. Since it was shown that α-synuclein impacts mitochondrial import (Di Maio *et al*, 2016), it would be interesting to investigate if mitochondrial GCase levels are decreasing with increasing α-synuclein pathology. In how far the increased interaction of mutant GCase with LONP1 is part of the previously described mechanism of supporting the overloaded proteosome needs to be investigated as well.

Even though our data indicate a defect in CI integrity in *GBA1* mutant and KO neurons, additional experiments must validate this observation. In addition, it needs to be investigated how GCase functions with regard to CI stability. It would be interesting to find out whether increasing mitochondrial GCase could rescue CI dysfunction in *GBA1*-related PD. Our data showing improved mitochondrial respiration after GCase overexpression point towards this possibility. A first step would be to assess the effect of mitochondrial targeted WT GCase on the mitochondrial function and compare this to what happens when mutant GCase is targeted to the mitochondria. This could then be compared to overexpression of WT and mutant GCase or a mutant variant that does not have the iMTS-ls anymore. Although one has to keep in mind, that deletion of the iMTS-ls will as well impact GCase structure and activity. As CI dysfunction may be one of the most important events in the development of PD (González-Rodríguez *et al.*, 2021) and GCase activity is decreased in several forms of familial as well as sporadic PD (Burbulla *et al.*, 2019; Rocha *et al.*, 2015a; Ysselstein *et al.*, 2019), it would be interesting to see whether increasing mitochondrial GCase can as well rescue genetic and idiopathic PD.

On the other hand, improving GCase activity will as well lead to a decrease in α-synuclein pathology, thereby improving GCase activity and trafficking to the different compartments. This in turn might improve both α-synuclein and mitochondrial pathology. If this treatment would need to be based on AAV-dependent overexpression of GCase or if a stabilizer like S-181 could be sufficient still needs to be investigated.

A slight increase in the CI protein NDUFA10 has been observed, unfortunately not reaching significance on the blot, though several CI proteins were increased in the more sensitive LC/MS analysis. It would be interesting to see whether the increase is due to an upregulation of the expression or if it is an accumulation at the protein level.

In the light of this new potential role of GCase in mitochondrial function, it would be interesting to monitor the GCase activity over time and assess whether in sporadic PD GCase activity is decreased before diagnosis. This might give a hint whether decreased GCase activity is a driver of PD or a result of other pathological mechanisms, like α-synuclein aggregation.

8 References

Abud EM, Ramirez RN, Martinez ES, Healy LM, Nguyen CHH, Newman SA, Yeromin AV, Scarfone VM, Marsh SE, Fimbres C *et al* (2017) iPSC-Derived Human Microglia-like Cells to Study Neurological Diseases. *Neuron* 94: 278-293.e279

Aflaki E, Borger DK, Moaven N, Stubblefield BK, Rogers SA, Patnaik S, Schoenen FJ, Westbroek W, Zheng W, Sullivan P *et al* (2016) A New Glucocerebrosidase Chaperone Reduces α-Synuclein and Glycolipid Levels in iPSC-Derived Dopaminergic Neurons from Patients with Gaucher Disease and Parkinsonism. *The Journal of Neuroscience* 36: 7441-7452

Aflaki E, Stubblefield BK, Maniwang E, Lopez G, Moaven N, Goldin E, Marugan J, Patnaik S, Dutra A, Southall N *et al* (2014) Macrophage models of Gaucher disease for evaluating disease pathogenesis and candidate drugs. *Sci Transl Med* 6: 240ra273

Alarcón F, Maldonado JC, Cañizares M, Molina J, Noyce AJ, Lees AJ (2020) Motor Dysfunction as a Prodrome of Parkinson's Disease. *J Parkinsons Dis* 10: 1067-1073

Alcalay RN, Levy OA, Waters CC, Fahn S, Ford B, Kuo SH, Mazzoni P, Pauciulo MW, Nichols WC, Gan-Or Z *et al* (2015) Glucocerebrosidase activity in Parkinson's disease with and without GBA mutations. *Brain* 138: 2648-2658

Almagro Armenteros JJ, Salvatore M, Emanuelsson O, Winther O, von Heijne G, Elofsson A, Nielsen H (2019) Detecting sequence signals in targeting peptides using deep learning. *Life science alliance* 2: e201900429

Atrian S, López-Viñas E, Gómez-Puertas P, Chabás A, Vilageliu L, Grinberg D (2008) An evolutionary and structure-based docking model for glucocerebrosidase-saposin C and glucocerebrosidase-substrate interactions - relevance for Gaucher disease. *Proteins* 70: 882-891

Awad O, Sarkar C, Panicker LM, Miller D, Zeng X, Sgambato JA, Lipinski MM, Feldman RA (2015) Altered TFEB-mediated lysosomal biogenesis in Gaucher disease iPSC-derived neuronal cells. *Hum Mol Genet* 24: 5775-5788

Backes S, Hess S, Boos F, Woellhaf MW, Gödel S, Jung M, Mühlhaus T, Herrmann JM (2018) Tom70 enhances mitochondrial preprotein import efficiency by binding to internal targeting sequences. *Journal of Cell Biology* 217: 1369-1382

Baden P, Perez M-J, Kalb S, Raji H, Illescase M, Giuliano C, Bertoli F, Oldrati M, Calogero A, Cappelletti G *et al* (2022) Glucocerebrosidase, a Parkinson´s disease-associated protein, is imported into mitochondria and regulates complex I assembly and function. doi.org/10.21203/rs.3.rs-1521848/v1 [PREPRINT]

Baden P, Perez MJ, Raji H, Bertoli F, Kalb S, Illescas M, Spanos F, Giuliano C, Calogero AM, Oldrati M *et al* (2023) Glucocerebrosidase is imported into mitochondria and preserves complex I integrity and energy metabolism. *Nat Commun* 14: 1930

Bembi B, Zambito Marsala S, Sidransky E, Ciana G, Carrozzi M, Zorzon M, Martini C, Gioulis M, Pittis MG, Capus L (2003) Gaucher's disease with Parkinson's disease: clinical and pathological aspects. *Neurology* 61: 99-101

Bendikov-Bar I, Ron I, Filocamo M, Horowitz M (2011) Characterization of the ERAD process of the L444P mutant glucocerebrosidase variant. *Blood Cells Mol Dis* 46: 4-10

Berg-Fussman A, Grace ME, Ioannou Y, Grabowski GA (1993) Human acid beta-glucosidase. N-glycosylation site occupancy and the effect of glycosylation on enzymatic activity. *J Biol Chem* 268: 14861-14866

Berge-Seidl V, Pihlstrøm L, Maple-Grødem J, Forsgren L, Linder J, Larsen JP, Tysnes OB, Toft M (2017) The GBA variant E326K is associated with Parkinson's disease and explains a genome-wide association signal. *Neurosci Lett* 658: 48-52

Bergmann JE, Grabowski GA (1989) Posttranslational processing of human lysosomal acid beta-glucosidase: a continuum of defects in Gaucher disease type 1 and type 2 fibroblasts. *Am J Hum Genet* 44: 741-750

Bhangoo MK, Tzankov S, Fan AC, Dejgaard K, Thomas DY, Young JC (2007) Multiple 40-kDa heat-shock protein chaperones function in Tom70-dependent mitochondrial import. *Mol Biol Cell* 18: 3414-3428

Blumenreich S, Nehushtan T, Barav OB, Saville JT, Dingjan T, Hardy J, Fuller M, Futerman AH (2022) Elevation of gangliosides in four brain regions from Parkinson's disease patients with a GBA mutation. *NPJ Parkinsons Dis* 8: 99

Bonifati V, Rizzu P, van Baren MJ, Schaap O, Breedveld GJ, Krieger E, Dekker MC, Squitieri F, Ibanez P, Joosse M *et al* (2003) Mutations in the DJ-1 gene associated with autosomal recessive early-onset parkinsonism. *Science* 299: 256-259

Boos F, Mühlhaus T, Herrmann J, 2018. Detection of Internal Matrix Targeting Signal-like Sequences (iMTS-Ls) in Mitochondrial Precursor Proteins Using the TargetP Prediction Tool.

Brekk OR, Korecka JA, Crapart CC, Huebecker M, MacBain ZK, Rosenthal SA, Sena-Esteves M, Priestman DA, Platt FM, Isacson O *et al* (2020) Upregulating β-hexosaminidase activity in rodents prevents α-synuclein lipid associations and protects dopaminergic neurons from α-synuclein-mediated neurotoxicity. *Acta Neuropathol Commun* 8: 127

Brockmann K, Srulijes K, Hauser A-K, Schulte C, Csoti I, Gasser T, Berg D (2011) GBA-associated PD presents with nonmotor characteristics. *Neurology* 77: 276-280

Brockmann K, Srulijes K, Pflederer S, Hauser AK, Schulte C, Maetzler W, Gasser T, Berg D (2015) GBA-associated Parkinson's disease: reduced survival and more rapid progression in a prospective longitudinal study. *Mov Disord* 30: 407-411

Bulteau AL, Mena NP, Auchère F, Lee I, Prigent A, Lobsiger CS, Camadro JM, Hirsch EC (2017) Dysfunction of mitochondrial Lon protease and identification of oxidized protein in mouse brain following exposure to MPTP: Implications for Parkinson disease. *Free Radic Biol Med* 108: 236-246

Burbulla LF, Jeon S, Zheng J, Song P, Silverman RB, Krainc D (2019) A modulator of wild-type glucocerebrosidase improves pathogenic phenotypes in dopaminergic neuronal models of Parkinson's disease. *Sci Transl Med* 11

Burbulla LF, Song P, Mazzulli JR, Zampese E, Wong YC, Jeon S, Santos DP, Blanz J, Obermaier CD, Strojny C *et al* (2017) Dopamine oxidation mediates mitochondrial and lysosomal dysfunction in Parkinson's disease. *Science* 357: 1255-1261

Cabantous S, Terwilliger TC, Waldo GS (2005) Protein tagging and detection with engineered self-assembling fragments of green fluorescent protein. *Nature Biotechnology* 23: 102-107

Calì T, Ottolini D, Soriano ME, Brini M (2015) A new split-GFP-based probe reveals DJ-1 translocation into the mitochondrial matrix to sustain ATP synthesis upon nutrient deprivation. *Human Molecular Genetics* 24: 1045-1060

Caligiore D, Helmich RC, Hallett M, Moustafa AA, Timmermann L, Toni I, Baldassarre G (2016) Parkinson's disease as a system-level disorder. *npj Parkinson's Disease* 2: 16025

Calvo SE, Clauser KR, Mootha VK (2016) MitoCarta2.0: an updated inventory of mammalian mitochondrial proteins. *Nucleic Acids Research* 44: D1251-D1257

Chang D, Nalls MA, Hallgrímsdóttir IB, Hunkapiller J, van der Brug M, Cai F, Kerchner GA, Ayalon G, Bingol B, Sheng M *et al* (2017) A meta-analysis of genome-wide association studies identifies 17 new Parkinson's disease risk loci. *Nat Genet* 49: 1511-1516

Chartier-Harlin MC, Kachergus J, Roumier C, Mouroux V, Douay X, Lincoln S, Levecque C, Larvor L, Andrieux J, Hulihan M *et al* (2004) Alpha-synuclein locus duplication as a cause of

familial Parkinson's disease. *Lancet* 364: 1167-1169

Chen C, McDonald D, Blain A, Sachdeva A, Bone L, Smith ALM, Warren C, Pickett SJ, Hudson G, Filby A *et al* (2021) Imaging mass cytometry reveals generalised deficiency in OXPHOS complexes in Parkinson's disease. *npj Parkinson's Disease* 7: 39

Chiasserini D, Paciotti S, Eusebi P, Persichetti E, Tasegian A, Kurzawa-Akanbi M, Chinnery PF, Morris CM, Calabresi P, Parnetti L *et al* (2015) Selective loss of glucocerebrosidase activity in sporadic Parkinson's disease and dementia with Lewy bodies. *Mol Neurodegener* 10: 15

Cilia R, Tunesi S, Marotta G, Cereda E, Siri C, Tesei S, Zecchinelli AL, Canesi M, Mariani CB, Meucci N *et al* (2016) Survival and dementia in GBA-associated Parkinson's disease: The mutation matters. *Annals of Neurology* 80: 662-673

Clark LN, Chan R, Cheng R, Liu X, Park N, Parmalee N, Kisselev S, Cortes E, Torres PA, Pastores GM *et al* (2015) Gene-wise association of variants in four lysosomal storage disorder genes in neuropathologically confirmed Lewy body disease. *PLoS One* 10: e0125204

Clark LN, Kartsaklis LA, Wolf Gilbert R, Dorado B, Ross BM, Kisselev S, Verbitsky M, Mejia-Santana H, Cote LJ, Andrews H *et al* (2009) Association of Glucocerebrosidase Mutations With Dementia With Lewy Bodies. *Archives of Neurology* 66: 578-583

Cleeter MWJ, Chau K-Y, Gluck C, Mehta A, Hughes DA, Duchen M, Wood NW, Hardy J, Mark Cooper J, Schapira AH (2013) Glucocerebrosidase inhibition causes mitochondrial dysfunction and free radical damage. *Neurochemistry International* 62: 1-7

Concordet J-P, Haeussler M (2018) CRISPOR: intuitive guide selection for CRISPR/Cas9 genome editing experiments and screens. *Nucleic Acids Research* 46: W242-W245

Cooper JF, Machiela E, Dues DJ, Spielbauer KK, Senchuk MM, Van Raamsdonk JM (2017) Activation of the mitochondrial unfolded protein response promotes longevity and dopamine neuron survival in Parkinson's disease models. *Scientific reports* 7: 16441-16441

Cosden M, Jinn S, Yao L, Gretzula CA, Kandebo M, Toolan D, Hatcher NG, Ma L, Lemaire W, Adam GC *et al* (2021) A novel glucosylceramide synthase inhibitor attenuates alpha synuclein pathology and lysosomal dysfunction in preclinical models of synucleinopathy. *Neurobiol Dis* 159: 105507

Credle JJ, Forcelli PA, Delannoy M, Oaks AW, Permaul E, Berry DL, Duka V, Wills J, Sidhu A (2015) α-Synuclein-mediated inhibition of ATF6 processing into COPII vesicles disrupts UPR signaling in Parkinson's disease. *Neurobiol Dis* 76: 112-125

Dauer W, Przedborski S (2003) Parkinson's disease: mechanisms and models. *Neuron* 39: 889-909

Davis GC, Williams AC, Markey SP, Ebert MH, Caine ED, Reichert CM, Kopin IJ (1979) Chronic Parkinsonism secondary to intravenous injection of meperidine analogues. *Psychiatry Res* 1: 249-254

de Rus Jacquet A (2019) Preparation and Co-Culture of iPSC-Derived Dopaminergic Neurons and Astrocytes. *Current Protocols in Cell Biology* 85: e98

Defazio G, Berardelli A, Fabbrini G, Martino D, Fincati E, Fiaschi A, Moretto G, Abbruzzese G, Marchese R, Bonuccelli U *et al* (2008) Pain as a nonmotor symptom of Parkinson disease: evidence from a case-control study. *Arch Neurol* 65: 1191-1194

Devi L, Raghavendran V, Prabhu BM, Avadhani NG, Anandatheerthavarada HK (2008) Mitochondrial import and accumulation of alpha-synuclein impair complex I in human dopaminergic neuronal cultures and Parkinson disease brain. *The Journal of biological chemistry* 283: 9089-9100

Di Maio R, Barrett PJ, Hoffman EK, Barrett CW, Zharikov A, Borah A, Hu X, McCoy J, Chu CT, Burton EA *et al* (2016) α-Synuclein binds to TOM20 and inhibits mitochondrial protein import in Parkinson's disease. *Sci Transl Med* 8: 342ra378

Duran R, Mencacci NE, Angeli AV, Shoai M, Deas E, Houlden H, Mehta A, Hughes D, Cox TM, Deegan P *et al* (2013) The glucocerobrosidase E326K variant predisposes to Parkinson's disease, but does not cause Gaucher's disease. *Mov Disord* 28: 232-236

Durand M, Coué M, Croyal M, Moyon T, Tesse A, Atger F, Ouguerram K, Jacobi D (2021) Changes in Key Mitochondrial Lipids Accompany Mitochondrial Dysfunction and Oxidative Stress in NAFLD. *Oxid Med Cell Longev* 2021: 9986299

Edwards L, Quigley EMM, Hofman R, Pfeiffer RF (1993) Gastrointestinal symptoms in parkinson disease: 18-month follow-up study. *Movement Disorders* 8: 83-86

El-Beshlawy A, Tylki-Szymanska A, Vellodi A, Belmatoug N, Grabowski GA, Kolodny EH, Batista JL, Cox GF, Mistry PK (2017) Long-term hematological, visceral, and growth outcomes in children with Gaucher disease type 3 treated with imiglucerase in the International Collaborative Gaucher Group Gaucher Registry. *Mol Genet Metab* 120: 47-56

Erickson AH, Ginns EI, Barranger JA (1985) Biosynthesis of the lysosomal enzyme glucocerebrosidase. *J Biol Chem* 260: 14319-14324

Fang H, Ye X, Xie J, Li Y, Li H, Bao X, Yang Y, Lin Z, Jia M, Han Q *et al* (2021) A membrane arm of mitochondrial complex I sufficient to promote respirasome formation. *Cell Reports* 35

Fernandes HJ, Hartfield EM, Christian HC, Emmanoulidou E, Zheng Y, Booth H, Bogetofte H, Lang C, Ryan BJ, Sardi SP *et al* (2016) ER Stress and Autophagic Perturbations Lead to Elevated Extracellular α-Synuclein in GBA-N370S Parkinson's iPSC-Derived Dopamine Neurons. *Stem Cell Reports* 6: 342-356

Fishbein I, Kuo YM, Giasson BI, Nussbaum RL (2014) Augmentation of phenotype in a transgenic Parkinson mouse heterozygous for a Gaucher mutation. *Brain* 137: 3235-3247

Franken H, Mathieson T, Childs D, Sweetman GMA, Werner T, Tögel I, Doce C, Gade S, Bantscheff M, Drewes G *et al* (2015) Thermal proteome profiling for unbiased identification of direct and indirect drug targets using multiplexed quantitative mass spectrometry. *Nature Protocols* 10: 1567-1593

Galvagnion C, Marlet FR, Cerri S, Schapira AHV, Blandini F, Di Monte DA (2022) Sphingolipid changes in Parkinson L444P GBA mutation fibroblasts promote α-synuclein aggregation. *Brain* 145: 1038-1051

Gan-Or Z, Ozelius LJ, Bar-Shira A, Saunders-Pullman R, Mirelman A, Kornreich R, Gana-Weisz M, Raymond D, Rozenkrantz L, Deik A *et al* (2013) The p.L302P mutation in the lysosomal enzyme gene SMPD1 is a risk factor for Parkinson disease. *Neurology* 80: 1606-1610

Garrido-Gil P, Rodriguez-Perez AI, Dominguez-Meijide A, Guerra MJ, Labandeira-Garcia JL (2018) Bidirectional Neural Interaction Between Central Dopaminergic and Gut Lesions in Parkinson's Disease Models. *Molecular Neurobiology* 55: 7297-7316

Gegg ME, Verona G, Schapira AHV (2020) Glucocerebrosidase deficiency promotes release of α-synuclein fibrils from cultured neurons. *Hum Mol Genet* 29: 1716-1728

Goemans CG, Boya P, Skirrow CJ, Tolkovsky AM (2008) Intra-mitochondrial degradation of Tim23 curtails the survival of cells rescued from apoptosis by caspase inhibitors. *Cell Death & Differentiation* 15: 545-554

Goker-Alpan O, Lopez G, Vithayathil J, Davis J, Hallett M, Sidransky E (2008) The spectrum of parkinsonian manifestations associated with glucocerebrosidase mutations. *Arch Neurol* 65: 1353-1357

Goker-Alpan O, Schiffmann R, LaMarca ME, Nussbaum RL, McInerney-Leo A, Sidransky E (2004) Parkinsonism among Gaucher disease carriers. *J Med Genet* 41: 937-940

Goker-Alpan O, Stubblefield BK, Giasson BI, Sidransky E (2010) Glucocerebrosidase is present in α-synuclein inclusions in Lewy body disorders. *Acta Neuropathol* 120: 641-649

Gong T, Xiang Y, Saleh MG, Gao F, Chen W, Edden RAE, Wang G (2018) Inhibitory motor dysfunction in parkinson's disease subtypes. *J Magn Reson Imaging* 47: 1610-1615

González-Rodríguez P, Zampese E, Stout KA, Guzman JN, Ilijic E, Yang B, Tkatch T, Stavarache MA, Wokosin DL, Gao L *et al* (2021) Disruption of mitochondrial complex I induces progressive parkinsonism. *Nature*

Grace ME, Grabowski GA (1990) Human acid beta-glucosidase: glycosylation is required for catalytic activity. *Biochem Biophys Res Commun* 168: 771-777

Gramlich PA, Westbroek W, Feldman RA, Awad O, Mello N, Remington MP, Sun Y, Zhang W, Sidransky E, Betenbaugh MJ *et al* (2016) A peptide-linked recombinant glucocerebrosidase for targeted neuronal delivery: Design, production, and assessment. *J Biotechnol* 221: 1-12

Guarani V, Paulo J, Zhai B, Huttlin EL, Gygi SP, Harper JW (2014) TIMMDC1/C3orf1 functions as a membrane-embedded mitochondrial complex I assembly factor through association with the MCIA complex. *Mol Cell Biol* 34: 847-861

Guedes LC, Chan RB, Gomes MA, Conceição VA, Machado RB, Soares T, Xu Y, Gaspar P, Carriço JA, Alcalay RN *et al* (2017) Serum lipid alterations in GBA-associated Parkinson's disease. *Parkinsonism & Related Disorders* 44: 58-65

Gutbier S, Wanke F, Dahm N, Rümmelin A, Zimmermann S, Christensen K, Köchl F, Rautanen A, Hatje K, Geering B *et al* (2020) Large-Scale Production of Human iPSC-Derived Macrophages for Drug Screening. *Int J Mol Sci* 21

Halperin A, Elstein D, Zimran A (2006) Increased incidence of Parkinson disease among relatives of patients with Gaucher disease. *Blood Cells, Molecules, and Diseases* 36: 426-428

Harbauer AB, Zahedi RP, Sickmann A, Pfanner N, Meisinger C (2014) The protein import machinery of mitochondria-a regulatory hub in metabolism, stress, and disease. *Cell Metab* 19: 357-372

Hatano Y, Li Y, Sato K, Asakawa S, Yamamura Y, Tomiyama H, Yoshino H, Asahina M, Kobayashi S, Hassin-Baer S *et al* (2004) Novel PINK1 mutations in early-onset parkinsonism. *Annals of Neurology* 56

Henderson MX, Sedor S, McGeary I, Cornblath EJ, Peng C, Riddle DM, Li HL, Zhang B, Brown HJ, Olufemi MF *et al* (2020) Glucocerebrosidase Activity Modulates Neuronal Susceptibility to Pathological α-Synuclein Insult. *Neuron* 105: 822-836.e827

Hermanowicz N, Jones SA, Hauser RA (2019) Impact of non-motor symptoms in Parkinson's disease: a PMDAlliance survey. *Neuropsychiatr Dis Treat* 15: 2205-2212

Horowitz M, Wilder S, Horowitz Z, Reiner O, Gelbart T, Beutler E (1989) The human glucocerebrosidase gene and pseudogene: Structure and evolution. *Genomics* 4: 87-96

Hu D, Sun X, Liao X, Zhang X, Zarabi S, Schimmer A, Hong Y, Ford C, Luo Y, Qi X (2019) Alpha-synuclein suppresses mitochondrial protease ClpP to trigger mitochondrial oxidative damage and neurotoxicity. *Acta Neuropathol* 137: 939-960

Hughes LP, Pereira MMM, Hammond DA, Kwok JB, Halliday GM, Lewis SJG, Dzamko N (2021) Glucocerebrosidase Activity is Reduced in Cryopreserved Parkinson's Disease Patient Monocytes and Inversely Correlates with Motor Severity. *J Parkinsons Dis* 11: 1157-1165

Ishikawa K-I, Nonaka R, Akamatsu W (2021) Differentiation of Midbrain Dopaminergic NeuronsDopaminergic neurons from Human iPS Cells. In: *Experimental Models of Parkinson's Disease*, Imai Y. (ed.) pp. 73-80. Springer US: New York, NY

Janssen K, Bahnassawy L, Kiefer C, Korffmann J, Terstappen GC, Lakics V, Cik M, Reinhardt P (2019) Generating Human iPSC-Derived Astrocytes with Chemically Defined Medium for In Vitro Disease Modeling. *Methods Mol Biol* 1994: 31-39

Jesús S, Huertas I, Bernal-Bernal I, Bonilla-Toribio M, Cáceres-Redondo MT, Vargas-González L, Gómez-Llamas M, Carrillo F, Calderón E, Carballo M *et al* (2016) GBA Variants Influence Motor and Non-Motor Features of Parkinson's Disease. *PLoS One* 11: e0167749

Jo J, Xiao Y, Sun Alfred X, Cukuroglu E, Tran H-D, Göke J, Tan Zi Y, Saw Tzuen Y, Tan C-P, Lokman H *et al* (2016) Midbrain-like Organoids from Human Pluripotent Stem Cells Contain Functional Dopaminergic and Neuromelanin-Producing Neurons. *Cell Stem Cell* 19: 248-257

Jonsson LM, Murray GJ, Sorrell SH, Strijland A, Aerts JF, Ginns EI, Barranger JA, Tager JM, Schram AW (1987) Biosynthesis and maturation of glucocerebrosidase in Gaucher fibroblasts. *Eur J Biochem* 164: 171-179

Kahle M, Schäfer A, Seelig A, Schultheiß J, Wu M, Aichler M, Leonhardt J, Rathkolb B, Rozman J, Sarioglu H *et al* (2015) High fat diet-induced modifications in membrane lipid and mitochondrial-membrane protein signatures precede the development of hepatic insulin resistance in mice. *Mol Metab* 4: 39-50

Kanfer JN, Legler G, Sullivan J, Raghavan SS, Mumford RA (1975) The Gaucher mouse. *Biochemical and Biophysical Research Communications* 67: 85-90

Kent WJ, Hsu F, Karolchik D, Kuhn RM, Clawson H, Trumbower H, Haussler D (2005) Exploring relationships and mining data with the UCSC Gene Sorter. *Genome Research* 15: 737-741

Kilpatrick BS, Magalhaes J, Beavan MS, McNeill A, Gegg ME, Cleeter MW, Bloor-Young D, Churchill GC, Duchen MR, Schapira AH *et al* (2016) Endoplasmic reticulum and lysosomal Ca^{2+} stores are remodelled in GBA1-linked Parkinson disease patient fibroblasts. *Cell Calcium* 59: 12-20

Kim MJ, Jeon S, Burbulla LF, Krainc D (2018a) Acid ceramidase inhibition ameliorates α-synuclein accumulation upon loss of GBA1 function. *Hum Mol Genet* 27: 1972-1988

Kim S, Yun SP, Lee S, Umanah GE, Bandaru VVR, Yin X, Rhee P, Karuppagounder SS, Kwon S-H, Lee H *et al* (2018b) GBA1 deficiency negatively affects physiological α-synuclein tetramers and related multimers. *Proceedings of the National Academy of Sciences* 115: 798-803

Kinghorn KJ, Grönke S, Castillo-Quan JI, Woodling NS, Li L, Sirka E, Gegg M, Mills K, Hardy J, Bjedov I *et al* (2016) A Drosophila Model of Neuronopathic Gaucher Disease Demonstrates Lysosomal-Autophagic Defects and Altered mTOR Signalling and Is Functionally Rescued by Rapamycin. *J Neurosci* 36: 11654-11670

Kluenemann HH, Nutt JG, Davis MY, Bird TD (2013) Parkinsonism syndrome in heterozygotes for Niemann–Pick C1. *Journal of the Neurological Sciences* 335: 219-220

Koprivica V, Stone DL, Park JK, Callahan M, Frisch A, Cohen IJ, Tayebi N, Sidransky E (2000) Analysis and classification of 304 mutant alleles in patients with type 1 and type 3 Gaucher disease. *Am J Hum Genet* 66: 1777-1786

Kozlov G, Gehring K (2020) Calnexin cycle - structural features of the ER chaperone system. *Febs j* 287: 4322-4340

Kuo SH, Tasset I, Cheng MM, Diaz A, Pan MK, Lieberman OJ, Hutten SJ, Alcalay RN, Kim S, Ximénez-Embún P *et al* (2022) Mutant glucocerebrosidase impairs α-synuclein degradation by blockade of chaperone-mediated autophagy. *Sci Adv* 8: eabm6393

LaBelle DR, Walsh RR, Banks SJ (2017) Latent Cognitive Phenotypes in De Novo Parkinson's Disease: A Person-Centered Approach. *J Int Neuropsychol Soc* 23: 551-563

Lackova A, Beetz C, Oppermann S, Bauer P, Pavelekova P, Lorincova T, Ostrozovicova M, Kulcsarova K, Cobejova J, Cobej M *et al* (2022) Prevalence of Fabry Disease among Patients with Parkinson's Disease. *Parkinsons Dis* 2022: 1014950

Lancaster MA, Corsini NS, Wolfinger S, Gustafson EH, Phillips AW, Burkard TR, Otani T, Livesey FJ, Knoblich JA (2017) Guided self-organization and cortical plate formation in human brain organoids. *Nature Biotechnology* 35: 659-666

Latham T, Grabowski GA, Theophilus BD, Smith FI (1990) Complex alleles of the acid beta-glucosidase gene in Gaucher disease. *Am J Hum Genet* 47: 79-86

Lautenschläger J, Wagner-Valladolid S, Stephens AD, Fernández-Villegas A, Hockings C, Mishra A, Manton JD, Fantham MJ, Lu M, Rees EJ *et al* (2020) Intramitochondrial proteostasis is directly coupled to α-synuclein and amyloid β1-42 pathologies. *The Journal of biological chemistry* 295: 10138-10152

Lelieveld LT, Gerhardt S, Maas S, Zwiers KC, de Wit C, Beijk EH, Ferraz MJ, Artola M, Meijer AH, Tudorache C *et al* (2022) Consequences of excessive glucosylsphingosine in glucocerebrosidase-deficient zebrafish. *Journal of Lipid Research* 63

Lelieveld LT, Mirzaian M, Kuo C-L, Artola M, Ferraz MJ, Peter REA, Akiyama H, Greimel P, van den Berg RJBHN, Overkleeft HS *et al* (2019) Role of μ-glucosidase 2 in aberrant glycosphingolipid metabolism: model of glucocerebrosidase deficiency in zebrafish. *Journal of Lipid Research* 60: 1851-1867

Leonova T, Grabowski GA (2000) Fate and sorting of acid beta-glucosidase in transgenic mammalian cells. *Mol Genet Metab* 70: 281-294

Li Y, Xue Y, Xu X, Wang G, Liu Y, Wu H, Li W, Wang Y, Chen Z, Zhang W *et al* (2019) A mitochondrial FUNDC1/HSC70 interaction organizes the proteostatic stress response at the risk of cell morbidity. *Embo j* 38

Liu Y, Suzuki K, Reed JD, Grinberg A, Westphal H, Hoffmann A, Döring T, Sandhoff K, Proia RL (1998) Mice with type 2 and 3 Gaucher disease point mutations generated by a single insertion mutagenesis procedure. *Proc Natl Acad Sci U S A* 95: 2503-2508

Lobo-Jarne T, Pérez-Pérez R, Fontanesi F, Timón-Gómez A, Wittig I, Peñas A, Serrano-Lorenzo P, García-Consuegra I, Arenas J, Martín MA *et al* (2020) Multiple pathways coordinate assembly of human mitochondrial complex IV and stabilization of respiratory supercomplexes. *Embo j* 39: e103912

Lücking CB, Dürr A, Bonifati V, Vaughan J, De Michele G, Gasser T, Harhangi BS, Meco G, Denèfle P, Wood NW *et al* (2000) Association between Early-Onset Parkinson's Disease and Mutations in the Parkin Gene. *New England Journal of Medicine* 342: 1560-1567

Lunde KA, Chung J, Dalen I, Pedersen KF, Linder J, Domellöf ME, Elgh E, Macleod AD, Tzoulis C, Larsen JP *et al* (2018) Association of glucocerebrosidase polymorphisms and mutations with dementia in incident Parkinson's disease. *Alzheimer's & Dementia* 14: 1293-1301

Ma C, Zhang W, Cao M (2021) Role of the Peripheral Nervous System in PD Pathology, Diagnosis, and Treatment. *Front Neurosci* 15: 598457

Maegawa GH, Tropak MB, Buttner JD, Rigat BA, Fuller M, Pandit D, Tang L, Kornhaber GJ, Hamuro Y, Clarke JT *et al* (2009) Identification and characterization of ambroxol as an enzyme enhancement agent for Gaucher disease. *J Biol Chem* 284: 23502-23516

Malek N, Weil RS, Bresner C, Lawton MA, Grosset KA, Tan M, Bajaj N, Barker RA, Burn DJ, Foltynie T *et al* (2018) Features of GBA-associated Parkinson's disease at presentation in the UK Tracking Parkinson's study. *Journal of Neurology, Neurosurgery & Psychiatry* 89: 702-709

Malini E, Grossi S, Deganuto M, Rosano C, Parini R, Dominisini S, Cariati R, Zampieri S, Bembi B, Filocamo M *et al* (2014) Functional analysis of 11 novel GBA alleles. *Eur J Hum Genet* 22: 511-516

Maple-Grødem J, Dalen I, Tysnes OB, Macleod AD, Forsgren L, Counsell CE, Alves G (2021) Association of GBA Genotype With Motor and Functional Decline in Patients With Newly Diagnosed Parkinson Disease. *Neurology* 96: e1036-e1044

Marshall J, Sun Y, Bangari DS, Budman E, Park H, Nietupski JB, Allaire A, Cromwell MA, Wang B, Grabowski GA *et al* (2016) CNS-accessible Inhibitor of Glucosylceramide Synthase for Substrate Reduction Therapy of Neuronopathic Gaucher Disease. *Molecular Therapy* 24: 1019-1029

Mazzulli JR, Xu YH, Sun Y, Knight AL, McLean PJ, Caldwell GA, Sidransky E, Grabowski GA, Krainc D (2011) Gaucher disease glucocerebrosidase and α-synuclein form a bidirectional pathogenic loop in synucleinopathies. *Cell* 146: 37-52

Mazzulli JR, Zunke F, Isacson O, Studer L, Krainc D (2016a) α-Synuclein-induced lysosomal dysfunction occurs through disruptions in protein trafficking in human midbrain synucleinopathy models. *Proceedings of the National Academy of Sciences of the United States of America* 113: 1931-1936

Mazzulli JR, Zunke F, Tsunemi T, Toker NJ, Jeon S, Burbulla LF, Patnaik S, Sidransky E, Marugan JJ, Sue CM *et al* (2016b) Activation of β-Glucocerebrosidase Reduces Pathological α-Synuclein and Restores Lysosomal Function in Parkinson's Patient Midbrain Neurons. *J Neurosci* 36: 7693-7706

McNeill A, Magalhaes J, Shen C, Chau KY, Hughes D, Mehta A, Foltynie T, Cooper JM, Abramov AY, Gegg M *et al* (2014) Ambroxol improves lysosomal biochemistry in glucocerebrosidase mutation-linked Parkinson disease cells. *Brain* 137: 1481-1495

Migdalska-Richards A, Daly L, Bezard E, Schapira AHV (2016) Ambroxol effects in glucocerebrosidase and α-synuclein transgenic mice. *Annals of neurology* 80: 766-775

Mizuno Y, Ohta S, Tanaka M, Takamiya S, Suzuki K, Sato T, Oya H, Ozawa T, Kagawa Y (1989) Deficiencies in complex I subunits of the respiratory chain in Parkinson's disease. *Biochem Biophys Res Commun* 163: 1450-1455

Morabito G, Giannelli SG, Ordazzo G, Bido S, Castoldi V, Indrigo M, Cabassi T, Cattaneo S, Luoni M, Cancellieri C *et al* (2017) AAV-PHP.B-Mediated Global-Scale Expression in the Mouse Nervous System Enables GBA1 Gene Therapy for Wide Protection from Synucleinopathy. *Molecular Therapy* 25: 2727-2742

Muffat J, Li Y, Yuan B, Mitalipova M, Omer A, Corcoran S, Bakiasi G, Tsai L-H, Aubourg P, Ransohoff RM *et al* (2016) Efficient derivation of microglia-like cells from human pluripotent stem cells. *Nature Medicine* 22: 1358-1367

Mullin S, Smith L, Lee K, D'Souza G, Woodgate P, Elflein J, Hällqvist J, Toffoli M, Streeter A, Hosking J *et al* (2020) Ambroxol for the Treatment of Patients With Parkinson Disease With and Without Glucocerebrosidase Gene Mutations: A Nonrandomized, Noncontrolled Trial. *JAMA Neurology* 77: 427-434

Nègre-Pagès L, Regragui W, Bouhassira D, Grandjean H, Rascol O (2008) Chronic pain in Parkinson's disease: The cross-sectional French DoPaMiP survey. *Movement Disorders* 23: 1361-1369

Neudorfer O, Giladi N, Elstein D, Abrahamov A, Turezkite T, Aghai E, Reches A, Bembi B, Zimran A (1996) Occurrence of Parkinson's syndrome in type 1 Gaucher disease. *QJM: An International Journal of Medicine* 89: 691-694

Neumann J, Bras J, Deas E, O'Sullivan SS, Parkkinen L, Lachmann RH, Li A, Holton J, Guerreiro R, Paudel R *et al* (2009) Glucocerebrosidase mutations in clinical and pathologically proven Parkinson's disease. *Brain* 132: 1783-1794

Nilsson O, Svennerholm L (1982) Accumulation of glucosylceramide and glucosylsphingosine (psychosine) in cerebrum and cerebellum in infantile and juvenile Gaucher disease. *J Neurochem* 39: 709-718

Oeda T, Umemura A, Mori Y, Tomita S, Kohsaka M, Park K, Inoue K, Fujimura H, Hasegawa H, Sugiyama H *et al* (2015) Impact of glucocerebrosidase mutations on motor and nonmotor complications in Parkinson's disease. *Neurobiology of Aging* 36: 3306-3313

Okita K, Matsumura Y, Sato Y, Okada A, Morizane A, Okamoto S, Hong H, Nakagawa M, Tanabe K, Tezuka K-I *et al* (2011) A more efficient method to generate integration-free human iPS cells. *Nature Methods* 8: 409-412

Orvisky E, Park JK, LaMarca ME, Ginns EI, Martin BM, Tayebi N, Sidransky E (2002) Glucosylsphingosine accumulation in tissues from patients with Gaucher disease: correlation with phenotype and genotype. *Mol Genet Metab* 76: 262-270

Osellame Laura D, Rahim Ahad A, Hargreaves Iain P, Gegg Matthew E, Richard-Londt A, Brandner S, Waddington Simon N, Schapira Anthony HV, Duchen Michael R (2013) Mitochondria and Quality Control Defects in a Mouse Model of Gaucher Disease—Links to Parkinson's Disease. *Cell Metabolism* 17: 941-953

Pagliarini DJ, Calvo SE, Chang B, Sheth SA, Vafai SB, Ong SE, Walford GA, Sugiana C, Boneh A, Chen WK *et al* (2008) A mitochondrial protein compendium elucidates complex I disease biology. *Cell* 134: 112-123

Panicker LM, Miller D, Awad O, Bose V, Lun Y, Park TS, Zambidis ET, Sgambato JA, Feldman RA (2014) Gaucher iPSC-derived macrophages produce elevated levels of inflammatory mediators and serve as a new platform for therapeutic development. *Stem Cells* 32: 2338-2349

Panicker LM, Miller D, Park TS, Patel B, Azevedo JL, Awad O, Masood MA, Veenstra TD, Goldin E, Stubblefield BK *et al* (2012) Induced pluripotent stem cell model recapitulates pathologic hallmarks of Gaucher disease. *Proc Natl Acad Sci U S A* 109: 18054-18059

Park JK, Tayebi N, Stubblefield BK, LaMarca ME, MacKenzie JJ, Stone DL, Sidransky E (2002) The E326K mutation and Gaucher disease: mutation or polymorphism? *Clin Genet* 61: 32-34

Parker WD, Jr., Parks JK, Swerdlow RH (2008) Complex I deficiency in Parkinson's disease frontal cortex. *Brain research* 1189: 215-218

Parkin JL, Brunning RD (1982) Pathology of the Gaucher cell. *Prog Clin Biol Res* 95: 151-175

Pastores GM, Petakov M, Giraldo P, Rosenbaum H, Szer J, Deegan PB, Amato DJ, Mengel E, Tan ES, Chertkoff R *et al* (2014) A Phase 3, multicenter, open-label, switchover trial to assess the safety and efficacy of taliglucerase alfa, a plant cell-expressed recombinant human glucocerebrosidase, in adult and pediatric patients with Gaucher disease previously treated with imiglucerase. *Blood Cells, Molecules, and Diseases* 53: 253-260

Patnaik S, Zheng W, Choi JH, Motabar O, Southall N, Westbroek W, Lea WA, Velayati A, Goldin E, Sidransky E *et al* (2012) Discovery, Structure–Activity Relationship, and Biological Evaluation of Noninhibitory Small Molecule Chaperones of Glucocerebrosidase. *Journal of Medicinal Chemistry* 55: 5734-5748

Paul A, Jacoby G, Laor Bar-Yosef D, Beck R, Gazit E, Segal D (2021) Glucosylceramide Associated with Gaucher Disease Forms Amyloid-like Twisted Ribbon Fibrils That Induce α-Synuclein Aggregation. *ACS Nano* 15: 11854-11868

Pavelka L, Rauschenberger A, Landoulsi Z, Pachchek S, May P, Glaab E, Krüger R, Acharya G, Aguayo G, Alexandre M *et al* (2022) Age at onset as stratifier in idiopathic Parkinson's disease – effect of ageing and polygenic risk score on clinical phenotypes. *npj Parkinson's Disease* 8: 102

Peng Y, Liou B, Lin Y, Fannin V, Zhang W, Feldman RA, Setchell KDR, Grabowski GA, Sun Y (2021) Substrate Reduction Therapy Reverses Mitochondrial, mTOR, and Autophagy Alterations in a Cell Model of Gaucher Disease. *Cells* 10

Peterschmitt MJ, Crawford NPS, Gaemers SJM, Ji AJ, Sharma J, Pham TT (2021) Pharmacokinetics, Pharmacodynamics, Safety, and Tolerability of Oral Venglustat in Healthy Volunteers. *Clinical Pharmacology in Drug Development* 10: 86-98

Peterschmitt MJ, Saiki H, Hatano T, Gasser T, Isaacson SH, Gaemers SJM, Minini P, Saubadu S, Sharma J, Walbillic S *et al* (2022) Safety, Pharmacokinetics, and Pharmacodynamics of Oral Venglustat in Patients with Parkinson's Disease and a GBA Mutation: Results from Part 1 of the Randomized, Double-Blinded, Placebo-Controlled MOVES-PD Trial. *J Parkinsons Dis* 12: 557-570

Poewe W, Seppi K, Tanner CM, Halliday GM, Brundin P, Volkmann J, Schrag A-E, Lang AE (2017) Parkinson disease. *Nature Reviews Disease Primers* 3: 17013

Polissidis A, Koronaiou E, Nikolopoulou G, Viel C, Nikatou M, Bogiongko M, Sardi SP, Xilouri M, Vekrellis K, Stefanis L (2022) A double-hit in vivo model of GBA viral microRNA-mediated downregulation and human alpha-synuclein overexpression demonstrates nigrostriatal degeneration. *Neurobiol Dis* 163: 105612

Polymeropoulos MH, Lavedan C, Leroy E, Ide SE, Dehejia A, Dutra A, Pike B, Root H, Rubenstein J, Boyer R *et al* (1997) Mutation in the alpha-synuclein gene identified in families with Parkinson's disease. *Science* 276: 2045-2047

Puschmann A, Ross OA, Vilariño-Güell C, Lincoln SJ, Kachergus JM, Cobb SA, Lindquist SG, Nielsen JE, Wszolek ZK, Farrer M *et al* (2009) A Swedish family with de novo alpha-synuclein A53T mutation: evidence for early cortical dysfunction. *Parkinsonism Relat Disord* 15: 627-632

Quadri M, Fang M, Picillo M, Olgiati S, Breedveld GJ, Graafland J, Wu B, Xu F, Erro R, Amboni M *et al* (2013) Mutation in the SYNJ1 Gene Associated with Autosomal Recessive, Early-Onset Parkinsonism. *Human Mutation* 34: 1208-1215

Ramirez A, Heimbach A, Gründemann J, Stiller B, Hampshire D, Cid LP, Goebel I, Mubaidin AF, Wriekat AL, Roeper J *et al* (2006) Hereditary parkinsonism with dementia is caused by mutations in ATP13A2, encoding a lysosomal type 5 P-type ATPase. *Nat Genet* 38: 1184-1191

Ran FA, Hsu PD, Wright J, Agarwala V, Scott DA, Zhang F (2013) Genome engineering using the CRISPR-Cas9 system. *Nature Protocols* 8: 2281-2308

Rana AQ, Qureshi ARM, Shamli Oghli Y, Saqib Y, Mohammed B, Sarfraz Z, Rana R (2018) Decreased sleep quality in Parkinson's patients is associated with higher anxiety and depression prevalence and severity, and correlates with pain intensity and quality. *Neurol Res* 40: 696-701

Rath S, Sharma R, Gupta R, Ast T, Chan C, Durham TJ, Goodman RP, Grabarek Z, Haas ME, Hung WHW *et al* (2021) MitoCarta3.0: an updated mitochondrial proteome now with sub-organelle localization and pathway annotations. *Nucleic Acids Res* 49: D1541-d1547

Reczek D, Schwake M, Schröder J, Hughes H, Blanz J, Jin X, Brondyk W, Van Patten S, Edmunds T, Saftig P (2007) LIMP-2 is a receptor for lysosomal mannose-6-phosphate-independent targeting of beta-glucocerebrosidase. *Cell* 131: 770-783

Reinhardt P, Glatza M, Hemmer K, Tsytsyura Y, Thiel CS, Höing S, Moritz S, Parga JA, Wagner L, Bruder JM *et al* (2013) Derivation and Expansion Using Only Small Molecules of Human Neural Progenitors for Neurodegenerative Disease Modeling. *PLoS ONE* 8: e59252

Robak LA, Jansen IE, van Rooij J, Uitterlinden AG, Kraaij R, Jankovic J, Heutink P, Shulman JM (2017) Excessive burden of lysosomal storage disorder gene variants in Parkinson's disease. *Brain* 140: 3191-3203

Rocha EM, Smith GA, Park E, Cao H, Brown E, Hallett P, Isacson O (2015a) Progressive decline of glucocerebrosidase in aging and Parkinson's disease. *Annals of Clinical and Translational Neurology* 2: 433-438

Rocha EM, Smith GA, Park E, Cao H, Brown E, Hayes MA, Beagan J, McLean JR, Izen SC, Perez-Torres E *et al* (2015b) Glucocerebrosidase gene therapy prevents α-synucleinopathy of midbrain dopamine neurons. *Neurobiol Dis* 82: 495-503

Ron I, Horowitz M (2005) ER retention and degradation as the molecular basis underlying Gaucher disease heterogeneity. *Hum Mol Genet* 14: 2387-2398

Ron I, Horowitz M (2008) Intracellular cholesterol modifies the ERAD of glucocerebrosidase in Gaucher disease patients. *Mol Genet Metab* 93: 426-436

Ross OA, Braithwaite AT, Skipper LM, Kachergus J, Hulihan MM, Middleton FA, Nishioka K, Fuchs J, Gasser T, Maraganore DM *et al* (2008) Genomic investigation of alpha-synuclein multiplication and parkinsonism. *Ann Neurol* 63: 743-750

Ruan L, Zhou C, Jin E, Kucharavy A, Zhang Y, Wen Z, Florens L, Li R (2017) Cytosolic proteostasis through importing of misfolded proteins into mitochondria. *Nature* 543: 443-446

Ryan SK, Jordan-Sciutto KL, Anderson SA (2020) Protocol for Tri-culture of hiPSC-Derived Neurons, Astrocytes, and Microglia. *STAR Protoc* 1: 100190

Sánchez-Lanzas R, Castaño JG (2021) Mitochondrial LonP1 protease is implicated in the degradation of unstable Parkinson's disease-associated DJ-1/PARK 7 missense mutants. *Scientific Reports* 11: 7320

Schapansky J, Khasnavis S, DeAndrade MP, Nardozzi JD, Falkson SR, Boyd JD, Sanderson JB, Bartels T, Melrose HL, LaVoie MJ (2018) Familial knockin mutation of LRRK2 causes lysosomal dysfunction and accumulation of endogenous insoluble α-synuclein in neurons. *Neurobiol Dis* 111: 26-35

Schapira AH, Cooper JM, Dexter D, Clark JB, Jenner P, Marsden CD (1990a) Mitochondrial complex I deficiency in Parkinson's disease. *J Neurochem* 54: 823-827

Schapira AH, Mann VM, Cooper JM, Dexter D, Daniel SE, Jenner P, Clark JB, Marsden CD (1990b) Anatomic and disease specificity of NADH CoQ1 reductase (complex I) deficiency in Parkinson's disease. *J Neurochem* 55: 2142-2145

Schmitz M, Alfalah M, Aerts JM, Naim HY, Zimmer KP (2005) Impaired trafficking of mutants of lysosomal glucocerebrosidase in Gaucher's disease. *Int J Biochem Cell Biol* 37: 2310-2320

Schneider CA, Rasband WS, Eliceiri KW (2012) NIH Image to ImageJ: 25 years of image analysis. *Nature Methods* 9: 671-675

Schöndorf DC, Aureli M, McAllister FE, Hindley CJ, Mayer F, Schmid B, Sardi SP, Valsecchi M, Hoffmann S, Schwarz LK *et al* (2014) iPSC-derived neurons from GBA1-associated Parkinson's disease patients show autophagic defects and impaired calcium homeostasis. *Nature Communications* 5Schöndorf DC, Ivanyuk D, Baden P, Sanchez-Martinez A, De Cicco S, Yu C, Giunta I, Schwarz LK, Di Napoli G, Panagiotakopoulou V *et al* (2018) The NAD+ Precursor Nicotinamide Riboside Rescues Mitochondrial Defects and Neuronal Loss in iPSC and Fly Models of Parkinson's Disease. *Cell Rep* 23: 2976-2988

Schueler UH, Kolter T, Kaneski CR, Zirzow GC, Sandhoff K, Brady RO (2004) Correlation between enzyme activity and substrate storage in a cell culture model system for Gaucher disease. *J Inherit Metab Dis* 27: 649-658

Schulz C, Schendzielorz A, Rehling P (2015) Unlocking the presequence import pathway. *Trends in Cell Biology* 25: 265-275

Sechi A, Deroma L, Dardis A, Ciana G, Bertin N, Concolino D, Linari S, Perria C, Bembi B (2014) Long term effects of enzyme replacement therapy in an Italian cohort of type 3 Gaucher patients. *Mol Genet Metab* 113: 213-218

Shahmoradian SH, Lewis AJ, Genoud C, Hench J, Moors TE, Navarro PP, Castaño-Díez D, Schweighauser G, Graff-Meyer A, Goldie KN *et al* (2019) Lewy pathology in Parkinson's disease consists of crowded organelles and lipid membranes. *Nature Neuroscience* 22: 1099-1109

Shin C-S, Meng S, Garbis SD, Moradian A, Taylor RW, Sweredoski MJ, Lomenick B, Chan DC (2021) LONP1 and mtHSP70 cooperate to promote mitochondrial protein folding. *Nature Communications* 12: 265

Sidransky E, Bottler A, Stubblefield B, Ginns EI (1994) DNA mutational analysis of type 1 and type 3 gaucher patients: How well do mutations predict phenotype? *Human Mutation* 3: 25-28

Sidransky E, Nalls MA, Aasly JO, Aharon-Peretz J, Annesi G, Barbosa ER, Bar-Shira A, Berg D, Bras J, Brice A *et al* (2009) Multicenter analysis of glucocerebrosidase mutations in Parkinson's disease. *N Engl J Med* 361: 1651-1661

Simón-Sánchez J, Schulte C, Bras JM, Sharma M, Gibbs JR, Berg D, Paisan-Ruiz C, Lichtner P, Scholz SW, Hernandez DG *et al* (2009) Genome-wide association study reveals genetic risk underlying Parkinson's disease. *Nat Genet* 41: 1308-1312

Singleton AB, Farrer M, Johnson J, Singleton A, Hague S, Kachergus J, Hulihan M, Peuralinna T, Dutra A, Nussbaum R *et al* (2003) alpha-Synuclein locus triplication causes Parkinson's disease. *Science* 302: 841

Skidmore FM, Monroe WS, Hurt CP, Nicholas AP, Gerstenecker A, Anthony T, Jololian L, Cutter G, Bashir A, Denny T *et al* (2022) The emerging postural instability phenotype in idiopathic Parkinson disease. *npj Parkinson's Disease* 8: 28

Smith AL, Friedman DB, Yu H, Carnahan RH, Reynolds AB (2011) ReCLIP (reversible cross-link immuno-precipitation): an efficient method for interrogation of labile protein complexes. *PLoS One* 6: e16206

Soubannier V, Maussion G, Chaineau M, Sigutova V, Rouleau G, Durcan TM, Stifani S (2020) Characterization of human iPSC-derived astrocytes with potential for disease modeling and drug discovery. *Neuroscience Letters* 731: 135028

Steet RA, Chung S, Wustman B, Powe A, Do H, Kornfeld SA (2006) The iminosugar isofagomine increases the activity of N370S mutant acid β-glucosidase in Gaucher fibroblasts by several mechanisms. *Proceedings of the National Academy of Sciences* 103: 13813-13818

Stemmer M, Thumberger T, del Sol Keyer M, Wittbrodt J, Mateo JL (2015) CCTop: An Intuitive,

Flexible and Reliable CRISPR/Cas9 Target Prediction Tool. *PLOS ONE* 10: e0124633

Stenson PD, Ball EV, Mort M, Phillips AD, Shiel JA, Thomas NS, Abeysinghe S, Krawczak M, Cooper DN (2003) Human Gene Mutation Database (HGMD): 2003 update. *Hum Mutat* 21: 577-581

Stephens MC, Bernatsky A, Burachinsky V, Legler G, Kanfer JN (1978) The Gaucher mouse: differential action of conduritol B epoxide and reversibility of its effects. *J Neurochem* 30: 1023-1027

Stephens MC, Bernatsky A, Singh H, Kanfer JN, Legler G (1981) Distribution of conduritol B epoxide in the animal model for Gaucher's disease (Gaucher mouse). *Biochimica et Biophysica Acta (BBA) - General Subjects* 672: 29-32

Stone DL, Tayebi N, Orvisky E, Stubblefield B, Madike V, Sidransky E (2000) Glucocerebrosidase gene mutations in patients with type 2 Gaucher disease. *Hum Mutat* 15: 181-188

Straniero L, Asselta R, Bonvegna S, Rimoldi V, Melistaccio G, Soldà G, Aureli M, Della Porta M, Lucca U, Di Fonzo A *et al* (2020) The SPID-GBA study: Sex distribution, Penetrance, Incidence, and Dementia in GBA-PD. *Neurol Genet* 6: e523

Sun Y, Florer J, Mayhew CN, Jia Z, Zhao Z, Xu K, Ran H, Liou B, Zhang W, Setchell KD *et al* (2015) Properties of neurons derived from induced pluripotent stem cells of Gaucher disease type 2 patient fibroblasts: potential role in neuropathology. *PLoS One* 10: e0118771

Sun Y, Quinn B, Witte DP, Grabowski GA (2005) Gaucher disease mouse models: point mutations at the acid β-glucosidase locus combined with low-level prosaposin expression lead to disease variants. *Journal of Lipid Research* 46: 2102-2113

Swerdlow RH, Parks JK, Miller SW, Tuttle JB, Trimmer PA, Sheehan JP, Bennett JP, Jr., Davis RE, Parker WD, Jr. (1996) Origin and functional consequences of the complex I defect in Parkinson's disease. *Ann Neurol* 40: 663-671

Szklarczyk D, Gable AL, Lyon D, Junge A, Wyder S, Huerta-Cepas J, Simonovic M, Doncheva NT, Morris JH, Bork P *et al* (2019) STRING v11: protein-protein association networks with increased coverage, supporting functional discovery in genome-wide experimental datasets. *Nucleic Acids Res* 47: D607-d613

Taguchi YV, Liu J, Ruan J, Pacheco J, Zhang X, Abbasi J, Keutzer J, Mistry PK, Chandra SS (2017) Glucosylsphingosine Promotes α-Synuclein Pathology in Mutant GBA-Associated Parkinson's Disease. *J Neurosci* 37: 9617-9631

Takahashi K, Tanabe K, Ohnuki M, Narita M, Ichisaka T, Tomoda K, Yamanaka S (2007) Induction of Pluripotent Stem Cells from Adult Human Fibroblasts by Defined Factors. *Cell* 131: 861-872

Takahashi K, Yamanaka S (2006) Induction of Pluripotent Stem Cells from Mouse Embryonic and Adult Fibroblast Cultures by Defined Factors. *Cell* 126: 663-676

Tan Yun L, Genereux Joseph C, Pankow S, Aerts Johannes MFG, Yates John R, Kelly Jeffery W (2014) ERdj3 Is an Endoplasmic Reticulum Degradation Factor for Mutant Glucocerebrosidase Variants Linked to Gaucher's Disease. *Chemistry & Biology* 21: 967-976

Tayebi N, Callahan M, Madike V, Stubblefield BK, Orvisky E, Krasnewich D, Fillano JJ, Sidransky E (2001) Gaucher disease and parkinsonism: a phenotypic and genotypic characterization. *Mol Genet Metab* 73: 313-321

Tayebi N, Reissner KJ, Lau EK, Stubblefield BK, Klineburgess AC, Martin BM, Sidransky E (1998) Genotypic Heterogeneity and Phenotypic Variation among Patients with Type 2 Gaucher's Disease. *Pediatric Research* 43: 571-578

Tayebi N, Walker J, Stubblefield B, Orvisky E, LaMarca ME, Wong K, Rosenbaum H,

Schiffmann R, Bembi B, Sidransky E (2003) Gaucher disease with parkinsonian manifestations: does glucocerebrosidase deficiency contribute to a vulnerability to parkinsonism? *Mol Genet Metab* 79: 104-109

Thaler A, Bregman N, Gurevich T, Shiner T, Dror Y, Zmira O, Gan-Or Z, Bar-Shira A, Gana-Weisz M, Orr-Urtreger A *et al* (2018) Parkinson's disease phenotype is influenced by the severity of the mutations in the GBA gene. *Parkinsonism Relat Disord* 55: 45-49

Thirumal Kumar D, Eldous HG, Mahgoub ZA, George Priya Doss C, Zayed H (2018) Computational modelling approaches as a potential platform to understand the molecular genetics association between Parkinson's and Gaucher diseases. *Metab Brain Dis* 33: 1835-1847

Tomiyama H, Li Y, Funayama M, Hasegawa K, Yoshino H, Kubo S, Sato K, Hattori T, Lu CS, Inzelberg R *et al* (2006) Clinicogenetic study of mutations in LRRK2 exon 41 in Parkinson's disease patients from 18 countries. *Mov Disord* 21: 1102-1108

Tsuji S, Choudary PV, Martin BM, Winfield S, Barranger JA, Ginns EI (1986) Nucleotide sequence of cDNA containing the complete coding sequence for human lysosomal glucocerebrosidase. *J Biol Chem* 261: 50-53

Tybulewicz VLJ, Tremblay ML, LaMarca, Willemsen R, Stubblefield BK, Winfield S, Zablocka B, Sidransky E, Martin BM, Huang SP *et al* (1992) Animal model of Gaucher's disease from targeted disruption of the mouse glucocerebrosidase gene. *Nature* 357: 407-410

Vascellari S, Melis M, Palmas V, Pisanu S, Serra A, Perra D, Santoru ML, Oppo V, Cusano R, Uva P *et al* (2021) Clinical Phenotypes of Parkinson's Disease Associate with Distinct Gut Microbiota and Metabolome Enterotypes. *Biomolecules* 11

von Mering C, Jensen LJ, Snel B, Hooper SD, Krupp M, Foglierini M, Jouffre N, Huynen MA, Bork P (2005) STRING: known and predicted protein-protein associations, integrated and transferred across organisms. *Nucleic Acids Res* 33: D433-437

Wakabayashi K, Tanji K, Odagiri S, Miki Y, Mori F, Takahashi H (2013) The Lewy Body in Parkinson's Disease and Related Neurodegenerative Disorders. *Molecular Neurobiology* 47: 495-508

Wang P, Deng J, Dong J, Liu J, Bigio EH, Mesulam M, Wang T, Sun L, Wang L, Lee AY *et al* (2019a) TDP-43 induces mitochondrial damage and activates the mitochondrial unfolded protein response. *PLoS Genet* 15: e1007947

Wang T, Liu H, Itoh K, Oh S, Zhao L, Murata D, Sesaki H, Hartung T, Na CH, Wang J (2021) C9orf72 regulates energy homeostasis by stabilizing mitochondrial complex I assembly. *Cell Metab* 33: 531-546.e539

Wang X, Becker K, Levine N, Zhang M, Lieberman AP, Moore DJ, Ma J (2019b) Pathogenic alpha-synuclein aggregates preferentially bind to mitochondria and affect cellular respiration. *Acta Neuropathol Commun* 7: 41-41

Wang Y-X, Zhao J, Li D-K, Peng F, Wang Y, Yang K, Liu Z-Y, Liu F-T, Wu J-J, Wang J (2017) Associations between cognitive impairment and motor dysfunction in Parkinson's disease. *Brain and Behavior* 7: e00719

Welsh NJ, Gewinner CA, Mistry K, Koglin M, Cooke J, Butler M, Powney B, Roberts M, Staddon JM, Schapira AHV (2020) Functional assessment of glucocerebrosidase modulator efficacy in primary patient-derived macrophages is essential for drug development and patient stratification. *Haematologica* 105: e206-e209

Wen S, Aki T, Unuma K, Uemura K (2020) Chemically Induced Models of Parkinson's Disease: History and Perspectives for the Involvement of Ferroptosis. *Front Cell Neurosci* 14: 581191

Westbroek W, Nguyen M, Siebert M, Lindstrom T, Burnett RA, Aflaki E, Jung O, Tamargo R,

Rodriguez-Gil JL, Acosta W *et al* (2016) A new glucocerebrosidase-deficient neuronal cell model provides a tool to probe pathophysiology and therapeutics for Gaucher disease. *Dis Model Mech* 9: 769-778

Wie J, Liu Z, Song H, Tropea TF, Yang L, Wang H, Liang Y, Cang C, Aranda K, Lohmann J *et al* (2021) A growth-factor-activated lysosomal K(+) channel regulates Parkinson's pathology. *Nature* 591: 431-437

Wiedemann N, Pfanner N (2017) Mitochondrial Machineries for Protein Import and Assembly. *Annual Review of Biochemistry* 86: 685-714

Winder-Rhodes SE, Evans JR, Ban M, Mason SL, Williams-Gray CH, Foltynie T, Duran R, Mencacci NE, Sawcer SJ, Barker RA (2013) Glucocerebrosidase mutations influence the natural history of Parkinson's disease in a community-based incident cohort. *Brain* 136: 392-399

Wong YC, Ysselstein D, Krainc D (2018) Mitochondria-lysosome contacts regulate mitochondrial fission via RAB7 GTP hydrolysis. *Nature* 554: 382-386

Woodard CM, Campos BA, Kuo SH, Nirenberg MJ, Nestor MW, Zimmer M, Mosharov EV, Sulzer D, Zhou H, Paull D *et al* (2014) iPSC-derived dopamine neurons reveal differences between monozygotic twins discordant for Parkinson's disease. *Cell Rep* 9: 1173-1182

Wooten GF, Currie LJ, Bovbjerg VE, Lee JK, Patrie J (2004) Are men at greater risk for Parkinson's disease than women? *Journal of Neurology, Neurosurgery & Psychiatry* 75: 637-639

Xu YH, Xu K, Sun Y, Liou B, Quinn B, Li RH, Xue L, Zhang W, Setchell KD, Witte D *et al* (2014) Multiple pathogenic proteins implicated in neuronopathic Gaucher disease mice. *Hum Mol Genet* 23: 3943-3957

Yang SY, Gegg M, Chau D, Schapira A (2020) Glucocerebrosidase activity, cathepsin D and monomeric α-synuclein interactions in a stem cell derived neuronal model of a PD associated GBA1 mutation. *Neurobiol Dis* 134: 104620

Young JC, Hoogenraad NJ, Hartl FU (2003) Molecular Chaperones Hsp90 and Hsp70 Deliver Preproteins to the Mitochondrial Import Receptor Tom70. *Cell* 112: 41-50

Ysselstein D, Nguyen M, Young TJ, Severino A, Schwake M, Merchant K, Krainc D (2019) LRRK2 kinase activity regulates lysosomal glucocerebrosidase in neurons derived from Parkinson's disease patients. *Nature Communications* 10: 5570

Yun SP, Kim D, Kim S, Kim S, Karuppagounder SS, Kwon S-H, Lee S, Kam T-I, Lee S, Ham S *et al* (2018) α-Synuclein accumulation and GBA deficiency due to L444P GBA mutation contributes to MPTP-induced parkinsonism. *Molecular neurodegeneration* 13: 1-1

Zhang Y, Shu L, Zhou X, Pan H, Xu Q, Guo J, Tang B, Sun Q (2018) A Meta-Analysis of GBA-Related Clinical Symptoms in Parkinson's Disease. *Parkinsons Dis* 2018: 3136415

Zimprich A, Benet-Pagès A, Struhal W, Graf E, Eck SH, Offman MN, Haubenberger D, Spielberger S, Schulte EC, Lichtner P *et al* (2011) A mutation in VPS35, encoding a subunit of the retromer complex, causes late-onset Parkinson disease. *Am J Hum Genet* 89: 168-175

Zimprich A, Biskup S, Leitner P, Lichtner P, Farrer M, Lincoln S, Kachergus J, Hulihan M, Uitti RJ, Calne DB *et al* (2004) Mutations in LRRK2 cause autosomal-dominant parkinsonism with pleomorphic pathology. *Neuron* 44: 601-607

Zunke F, Moise AC, Belur NR, Gelyana E, Stojkovska I, Dzaferbegovic H, Toker NJ, Jeon S, Fredriksen K, Mazzulli JR (2018) Reversible Conformational Conversion of α-Synuclein into Toxic Assemblies by Glucosylceramide. *Neuron* 97: 92-107.e110

9 Appendix

9.1 Detailed list of materials

In the following sections the materials used for the thesis are listed. If a material was already described in a previous section, the details are not repeated.

9.1.1 Cloning constructs into plasmid

Material	Manufacturer	Catalogue N°
Accutase	Sigma-Aldrich	A6964-100 ml
AflII (10 U/µl) and 10x Buffer O	Thermo Fisher Scientific Inc.	ER0831
ALLin™ RPH Polymerase	highQu	HLE0101
Ampicillin sodium salt	Gibco	11593027
BactoTM Agar	BD	214010
Coverslip (round Ø 12 MM NR.1)	VWR	31-1577
DNeasy Blood & Tissue kit	Qiagen	69504
EcoRI (10 U/µl)	Thermo Fisher Scientific Inc.	ER0271
EndoFree Plasmid Maxi Kit (10)	Qiagen	12362
HEK 293	/	/
Ingenio electroporation solution	Mirus	MIR 50111
Matrigel® Growth Factor Reduced (GFR) Basement Membrane Matrix, 10mL	Corning	354230
Moonlab® Petrischale, Ø: 90 mm, Höhe: 15 mm, 3 Nocken, klar, steril, PS, 50 x 10	neolab	4-0085
Natrium Chloride	Merck	1.06404.1000
One Shot™ TOP10 Chemically Competent E. coli with SOC medium	Invitrogen™	C404003
Paraformaldehyde powder, 95%	Sigma-Aldrich	158127-500G
pcDNA™3.0	Invitrogen™	n.a.
pcDNA™5/FRT/TO	Invitrogen™	V652020
Polyethylenimine 25kD linear (dissolved to 1mg/ml in Milli-Q H_20)	Polysciences	23966-2
QIAprep Spin Miniprep Kit (250)	Qiagen	27106
QIAquick Gel extraction Kit	Qiagen	28706
QuikChange II XL Site-Directed Mutagenesis Kit, 10 Rxn	Agilent	200521
SeaKem LE Agarose	Lonza	50001
T4 DNA ligase and buffer	New England BioLabs inc. (NEB)	M0202S
Trypton/Pepton from Casein	Carl Roth	8952.4
XhoI (10 U/µL) and 10 x Tango Buffer	Thermo Fisher Scientific Inc.	ER0691
Yeast extract BioChemica	PanReac AppliChem	A1552,1000

LB medium preparation: 10 g Tryptone, 10g NaCl, 5 g yeast extract were mixed, and Milli-Q water was added to reach a volume of 1L. The mixture was autoclaved for sterilization. After cooling to RT, the LB medium was stored at 4°C.

LB Agar plates: 15 g Agar was added to the LB medium mix and Milli-Q water was added to 1L volume followed by autoclaving. When the sterilized LB Agar reached about body temperature, the antibiotics (50 µg/ml) were added and mixed. Then the 10cm dishes were poured and left to cool down. The plates were then stored upside down at 4°C.

9.1.2 PCR and sequencing analysis

Material	Manufacturer	Catalogue N°
1x Phosphate Buffered Saline (PBS)	Sigma-Aldrich	D8537-500ML
BigDye v3.1 kit incl. Buffer	Thermo Fisher Scientific Inc.	4337455
Boric acid	Carl Roth	P010.2
DMSO for cell culture	Sigma-Aldrich	D4540-1L
dNTS	Thermo Fisher Scientific Inc.	R0182
Ethanol absolute ≥99,8%	VWR Chemicals	20821330
Ethylenediamine tetraacetic acid disodium salt dihydrate (EDTA)	Carl Roth	8043.2
GeneRuler DNA Ladder Mix	Thermo Fisher Scientific Inc.	SM0331
GoTaq II Polymerase kit with 5X Green GoTaq® Reaction Buffer	Promega	M3005
Hi-Di™ Formamide	Applied Biosystems™	4401457
Midori Green Advance	NIPPON Genetics	M604
QuickExtract DNA extraction solution	Epicentre	QE09050
Sodium acetate trihydrate	Carl Roth	6779.2
Sodium hydroxide	Merck	1.06462.1000
Tris Pufferan	Carl Roth	AE15.3

TBE buffer: For TBE buffer 108g Tris Pufferan, 55 g boric acid, 40 ml of 0.5 M EDTA (pH8) was mixed. Then the volume was filled up to 1 L with Milli-Q H_2O.

0.5 M EDTA (pH 8): 93.05 g EDTA powder was mixed with 300 ml H_2O. NaOH is added until EDTA starts to dissolve. Then pH is adjusted to 8 using HCl or NaOH and the total volume to 500 ml with Milli-Q H_2O.

Sodium acetate buffer: Mix 1 ml 3M sodium acetate with 24 ml pure Ethanol.

9.1.3 T-Rex HEK cell culture and transfection

Material	Manufacturer	Catalogue N°
Calcium chloride	Carl Roth	CN93.1
HEK 293	/	/
HEPES	Sigma-Aldrich	H4034-25G
Sodium chloride	Sigma-Aldrich	S7653-250G
Sodium phosphate dibasic	Sigma-Aldrich	S5136-100G
T-REx™-293 cell line	Invitrogen™	R78007
Venor GEM Classic (Mycoplasma Detection Kit)	Minerva Biolabs	11-1100

2x HBS: 28 ml of 5M sodium chloride, 11.9g HEPES, 750 µl 1M Na_2HPO_4 were mixed with about 350 ml Milli-Q H_2O. After adjustment of pH to 7.1 with NaOH, the volume was adjusted to 500 ml and sterile filtered.

9.1.4 Immunoprecipitation

10x TBS: In 1.5 L Milli-Q H_2O, 121.14 g Tris Pufferan and 175.32 g of NaCl are dissolved. When everything is dissolved, the pH is adjusted to 7.4 with HCl and the volume adjusted to 2L with Milli-Q H_2O.

6x Laemmli buffer: 3.12 ml of 2 M Tris/HCl (pH 6.8) was mixed with 2 g SDS, 10 ml Glycerin, 0.01 g Bromophenol blue, 2.5 ml ß-Mercaptoethanol and then filled with Milli-Q H_2O up to 20 ml.

Material	Manufacturer	Catalogue N°
Anti- GBA MaxPab (Rabbit) antibody	Abnova	H00002629-D01
Anti-Flag M2 Affinity Gel	Sigma-Aldrich	A2220
Flag Peptide	Sigma-Aldrich	F3290
Glycerin	Carl Roth	3783.1
HCl	Merck	1.00316.1000
HPLC-grade Water for MS	Merck Millipore	1153331000
IGEPAL® CA-630 (NP40)	Sigma-Aldrich	I8896-50ML
Microspin™ Columns	GE Healthcare	27-3565-01
normal rabbit IgG	Enzo Life Sciences	CVL-PAB01004-P
Pierce™ BCA Protein Assay Kit	Thermo Fisher Scientific Inc.	23225
Protease and Phosphatase Inhibitor	Thermo Fisher Scientific Inc.	A32959
Protein G agarose fast flow beads	Merck Millipore	16-266
SDS	Carl Roth	CN30.3
ß-Mercaptoetha**nol**	Sigma-Aldrich	805740
Tween-20	Carl Roth	9127.1
Water for chromatography	Merck Millipore	1153331000

9.1.5 Mass spectrometry measurement

Material	Manufacturer	Catalogue N°
Benzonase® Nuclease	Sigma-Aldrich	E1014-5KU

9.1.6 Generation of iPSC

Material	Manufacturer	Catalogue N°
(10x) Trypsin (1:250)/EDTA-Lösung (0,5 %/0,2 %)	Biochrom	L2153
Amaxa nucleofection kit for human dermal fibroblasts	Lonza	VPD-100
BD regular Bevel Needles 26 G 0,45x23 mm	Terumo	AN2623R1
pCXLE-hOct3/4	Addgene	27076
pCXLE-hSK	Addgene	27078
pCXLE-hUL	Addgene	27080
Rock inhibitor (Y27632)	Selleckchem	S1049
Sodium butyrate	Sigma-Aldrich	B5887-1G
Vitronectin XF™	StemCell™ Technologies	100-0763

9.1.7 Gene-correction

Material	Manufacturer	Catalogue N°
Alt-R Cas9 Nuclease V3 100 ug	IDT	1081058
Atto550 labelled tracrRNA	IDT	1075928
Falcon® 40µm Cell Strainer, Sterile	Corning	352340
G418	InvivoGen	ant-gn-1

9.1.8 Differentiation of iPSC into NPC and midbrain DA neurons

Material	Manufacturer	Catalogue N°
B27 without Vitamin A	Gibco	12587010
BDNF	PeproTech	450-02
CHIR99021	Sigma-Aldrich	SML1046
Corning® Matrigel® Growth Factor Reduced (GFR) Basement Membrane Matrix, 10mL	Corning	354230
dbcAMP	PanReac AppliChem	A0455,1000

Material	Manufacturer	Catalogue N°
DMEM Knockout Medium	Gibco	10829018
DMEM/ Hams F12 without HEPES	Gibco	11320033
Dorsomorphin	Sigma-Aldrich	P5499
FGF8B	PeproTech	100-25
GDNF	PeproTech	450-10
Knockout-Serum-Replacement	Gibco	10828028
N2	Gibco	17502048
NEEA	Gibco	11140-035
Neurobasal	Gibco	21103049
PMA	Merck	540220-5MG
SB431542	Selleckchem	S1067
TGF-ß3	PeproTech	100-36E-50uG

9.1.9 Western blot analysis

Material	Manufacturer	Catalogue N°
Acrylamide - Solution 40%	PanReac AppliChem	A3658-1000
Anti-mouse IgG, HRP linked Antibody	Cell Signaling Technology	7076S
Anti-rabbit IgG, HRP linked Antibody	Cell Signaling Technology	7074S
ECL western blot HRP Substrate	Millipore	WBKLS0500
Glycine	Carl Roth	3908.3
Immobilon PVDF	Life Technologies	IPVH00010
Methanol	VWR	20847,307
Nonfat dried milk powder	PanReac AppliChem	A0830
NuPAGE™ 4-12% Bis-Tris Protein Gels, 1.5 mm, 10-well	Thermo Fisher Scientific Inc.	NP0335BOX
NuPAGE™ 4-12% Bis-Tris Protein Gels, 1.5 mm, 15-well	Thermo Fisher Scientific Inc.	NP0336BOX
NuPAGE™ MOPS SDS Running Buffer (20X)	Thermo Fisher Scientific Inc.	NP0001
Precision Plus Protein™ Dual Color Standards	BioRad	1610374
SignalFire™ Elite ECL Reagent	Cell Signaling technology	12757S
TEMED	Carl Roth	2367.1
Tris/Cl	Carl Roth	9090.3
UltraCruz® Autoradiography Film	Santa Cruz	sc-201697
Western Blocking Reagent, Roche	Sigma-Aldrich	11921681001

10% APS: 5 g of APS are dissolved in 50 ml Milli-Q H_2O.

Lower Buffer: 45.43 g of Tris Pufferan is mixed with 1 g of SDS, and Milli-Q H_2O was added. When everything was dissolved, the pH was adjusted to 8.8. Then the total volume was topped up to 250 ml.

Upper Buffer: 15.14 g Tris Pufferan and 1 g SDS were added to Milli-Q H_2O. After adjustment of the pH to 6.8 with HCl, the total volume was adjusted to 250 ml with Milli-Q H_2O.

10x Running buffer: 60.6 g Tris Pufferan, 290 g Glycine and 20 g SDS were weighted in. Milli-Q H_2O was added and when everything was dissolved it was topped up to 2L.

Strong stripping buffer: 7.57 g of Tris Pufferan was mixed with 20 g SDS and 7.18 g ß-Mercaptoethanol. The total volume was filled to 1 L.

Soft stripping buffer: 3.8 g Glycine, 0.5 g SDS, 5 ml Tween-20 where mixed with Milli-Q H_2O. The pH was adjusted to 2.2 with HCl and the volume adjusted to 250 ml with Milli-Q H_2O.

10x Transfer buffer: 60.56 g Tris Pufferan and 288.16 g Glycine were dissolved in Milli-Q H_2O. At the end, the volume was filled with Milli-Q H_2O up to 2L.

9.1.10 Immunofluorescent staining

Material	Manufacturer	Catalogue N°
Alexa Fluor 488 goat anti-mouse	Invitrogen	A-11001
Alexa Fluor 488 goat anti-rabbit	Invitrogen	A-11008
Alexa Fluor 568 goat anti-mouse	Invitrogen	A-11004
Alexa Fluor 568 goat anti-rabbit	Invitrogen	A-11011
Dako Mounting Medium	Agilent	S302380-2
DAPI (4',6-Diamidino-2-Phenylindole, Dihydrochloride)	Biolegend	422801
Normal goat serum	Biozol	VEC-S-1000
Objektträger SuperFrost Ultra Plus	OmniLab	5429581
Triton-X 100	Carl Roth	3051.4

9.1.11 PLA

Material	Manufacturer	Catalogue N°
Duolink In Situ Red Starter Kit Mouse/Rabbit	Sigma-Aldrich	DUO92101-1KT
Nunc™ Lab-Tek™ Chamber Slide System (16-well)	Fisher Scientific	178599PK

9.1.12 RNA isolation, reverse transcription, and qRT-PCR

Material	Manufacturer	Catalogue N°
MicroAmp™ Optical 384-Well Reaction Plate with Barcode	Applied Biosystems™	4309849
QuantiTect Rev. Transcription Kit (200)	Qiagen	205313
QuantiTect SYBR Green PCR Kit	Qiagen	204145
RNaseZAP™	Sigma-Aldrich	R2020-250ML
RNeasy Mini Kit (250)	Qiagen	74106

9.1.13 Lentiviral KD in T-Rex HEK cells

Material	Manufacturer	Catalogue N°
Lenti-X™ GoStix™ Plus	TaKaRa	631280
Opti-MEM™ I Reduced Serum Medium, no phenol red	Gibco	11058021
pMD2.G	Addgene	12259
psPAX2	Addgene	12260
Puromycin	InvivoGen	Ant-pr-1
Syringe Filter PVDF 33mm 0.45µm STR	Fisher Scientific	15191499
TRANSIT™-X2 DYNAMIC DELIVERY	Mirus	MIR-6004
Vivaspin 20 centrifugal concentrator (Sartorius VS2042)	Sigma-Aldrich	Z614688-48EA

9.1.14 GBA activity assay

Material	Manufacturer	Catalogue N°
4-methylumbelliferyl-β-D-glucopyranoside	Glycosynth	44059
Citric Acid monohydrate	Sigma-Aldrich	C1909-500G
Conduritol B Epoxide	Calbiochem	234599-100MG
Microplates for Fluorescence-based Assays, 96-well	Thermo Fisher Scientific Inc.	M33089
Taurocholic acid sodium salt hydrate	Sigma-Aldrich	T4009

Sodium citrate phosphate buffer: 2.3 g citric acid monohydrate and 1.42 g Sodium phosphate

dibasic were added to separate tubes and H^2O was added to 50 ml total volume. 25 ml of each solution were transferred to a common tube and the pH was adjusted to 5.4.

MUB-Glc solution: 0.0169 g MUB-Glc were dissolved in 10 ml sodium citrate phosphate buffer

Taurocholic acid solution: 0.025 g taurocholic acid was resuspended in 10 ml Milli-Q H_2O. Then 100 µl Triton-X 100 was added and mixed. The 300 µl of the resulting solution was distributed into 2 ml tubes and where dried at 37°C.

9.1.15 Seahorse analysis

Material	Manufacturer	Catalogue N°
Antimycin A from *Streptomyces* sp.	Sigma-Aldrich	A8674-25MG
Carbonyl cyanide 4-(trifluoromethoxy)phenylhydrazone	Sigma-Aldrich	C2920-10MG
Oligomycin A, ≥95% (HPLC)	Sigma-Aldrich	75351-5MG
Rotenone	Sigma-Aldrich	R8875-1G
Seahorse XF 1.0 M glucose solution, 50 mL	Agilent	103577-100
Seahorse XF 100 mM pyruvate solution	Agilent	103578-100
Seahorse XF DMEM medium, pH 7.4, 500 mL	Agilent	103575-100
Seahorse XFe96 FluxPak	Agilent	102601-100

9.1.16 Split GFP materials

Material	Manufacturer	Catalogue N°
Ibidi USA U SLIDE 8 WELL IBITREAT	Ibidi	80826
MitoTracker™ Red CM-H2Xros	Invitrogen™	M7513
Opti-MEM™ I Reduced Serum Medium, no phenol red	Thermo Fisher Scientific Inc.	11058021
ViaFect Transfection Reagent	Promega	E4981

9.1.17 General plasticware

Material	Manufacturer	Catalogue N°
0.5 mL SafeLock Tube	Eppendorf	0030 121.023
1 mL Syringe	Santa Cruz	sc-358901
1.5 mL SafeLock Tube	Eppendorf	0030 120.086
100x17mm Dish, Nunclon™ Delta 100 x 20 mm Optilux (Falcon)	Schubert und Weiss	FALC353003
12-well plate	Greiner	665180
15 ml CellStar tube	Greiner Bio-One	188271
150x21mm Dish, Nunc™ Cell culture dishes	Thermo Fisher Scientific Inc.	168381
2 mL SafeLock Tube	Eppendorf	0030 121 880
2.5 µl SafeSeal tips	Biozym	690005X
24-well plate	Greiner	662160
48-well plate	Greiner	677180
50 ml CellStar tube	Greiner Bio-One	227261
6-well plate	Greiner	657160
96-well flat bottom	Greiner	655101
Cell scraper	Sarstedt	831830
Corning 10 ml Stripette	Corning	4101
Corning 25 ml Stripette	Corning	4251
Corning 5 ml Stripette	Corning	4051
Corning 50 ml Stripette	Corning	4501
Injekt® 20 ml, Luer-Ansatz, exzentrisch	Braun	4606205V
Millex filter unit, 33mm Pes 0.22 um	Merck	SLGP033RS
Nunc Cryotube Vial	Thermo Fisher Scientific Inc.	368632
Nunc Easy Flask 175 Filter	Thermo Fisher Scientific Inc.	156499

Material	Manufacturer	Catalogue N°
PCR stripes	VWR	732-4802
SurPhob 10 µl sterile tips	Biozym	VT0200
SurPhob 100 µl sterile tips	Biozym	VT0230
SurPhob 1000 µl sterile tips	Biozym	VT0260
SurPhob 200 µl sterile tips	Biozym	VT0240
Vakuum Filtersystem	Corning	CORN431097

9.2 Sequences of constructs

first base after leader sequence
V5 sequence
Overlap V5 and Flag sequence
Flag sequence
Repetition of GCase sequence
Mitochondrial targeting sequence from COX8A
GFP 1-10
GFP s11ß

9.2.1 V5-Flag-tag control sequence

GCCGCCACCATGATCCCTAACCCTCTCCTCGGTCTCGATTACAAGGATGACGACGATAAGTGA

9.2.2 WT GBA1

GCCGCCACCATGGAGTTTTCAAGTCCTTCCAGAGAGGAATGTCCCAAGCCTTTGAGTAGGGTAA
GCATCATGGCTGGCAGCCTCACAGGATTGCTTCTACTTCAGGCAGTGTCGTGGGCATCAGGTGC
CCGCCCCTGCATCCCTAAAAGCTTCGGCTACAGCTCGGTGGTGTGTGTCTGCAATGCCACATACT
GTGACTCCTTTGACCCCCCGACCTTTCCTGCCCTTGGTACCTTCAGCCGCTATGAGAGTACACGC
AGTGGGCGACGGATGGAGCTGAGTATGGGGCCCATCCAGGCTAATCACACGGGCACAGGCCTG
CTACTGACCCTGCAGCCAGAACAGAAGTTCCAGAAAGTGAAGGGATTTGGAGGGGCCATGACAG
ATGCTGCTGCTCTCAACATCCTTGCCCTGTCACCCCCTGCCCAAAATTTGCTACTTAAATCGTACT
TCTCTGAAGAAGGAATCGGATATAACATCATCCGGGTACCCATGGCCAGCTGTGACTTCTCCATC
CGCACCTACACCTATGCAGACACCCCTGATGATTTCCAGTTGCACAACTTCAGCCTCCCAGAGGA
AGATACCAAGCTCAAGATACCCCTGATTCACCGAGCCCTGCAGTTGGCCCAGCGTCCCGTTTCA
CTCCTTGCCAGCCCCTGGACATCACCCACTTGGCTCAAGACCAATGGAGCGGTGAATGGGAAGG
GGTCACTCAAGGGACAGCCCGGAGACATCTACCACCAGACCTGGGCCAGATACTTTGTGAAGTT
CCTGGATGCCTATGCTGAGCACAAGTTACAGTTCTGGGCAGTGACAGCTGAAAATGAGCCTTCTG
CTGGGCTGTTGAGTGGATACCCCTTCCAGTGCCTGGGCTTCACCCCTGAACATCAGCGAGACTT
CATTGCCCGTGACCTAGGTCCTACCCTCGCCAACAGTACTCACCACAATGTCCGCCTACTCATGC
TGGATGACCAACGCTTGCTGCTGCCCCACTGGGCAAAGGTGGTACTGACAGACCCAGAAGCAGC
TAAATATGTTCATGGCATTGCTGTACATTGGTACCTGGACTTTCTGGCTCCAGCCAAAGCCACCCT
AGGGGAGACACACCGCCTGTTCCCCAACACCATGCTCTTTGCCTCAGAGGCCTGTGTGGGCTCC
AAGTTCTGGGAGCAGAGTGTGCGGCTAGGCTCCTGGGATCGAGGGATGCAGTACAGCCACAGC
ATCATCACGAACCTCCTGTACCATGTGGTCGGCTGGACCGACTGGAACCTTGCCCTGAACCCCG
AAGGAGGACCCAATTGGGTGCGTAACTTTGTCGACAGTCCCATCATTGTAGACATCACCAAGGAC
ACGTTTTACAAACAGCCCATGTTCTACCACCTTGGCCACTTCAGCAAGTTCATTCCTGAGGGCTC
CCAGAGAGTGGGGCTGGTTGCCAGTCAGAAGAACGACCTGGACGCAGTGGCACTGATGCATCC
CGATGGCTCTGCTGTTGTGGTCGTGCTAAACCGCTCCTCTAAGGATGTGCCTCTTACCATCAAGG
ATCCTGCTGTGGGCTTCCTGGAGACAATCTCACCTGGCTACTCCATTCACACCTACCTGTGGCGT
CGCCAGTGA

9.2.3 V5-Flag-tagged GBA1

GCCGCCACCATGGAGTTTTCAAGTCCTTCCAGAGAGGAATGTCCCAAGCCTTTGAGTAGGGTAA
GCATCATGGCTGGCAGCCTCACAGGATTGCTTCTACTTCAGGCAGTGTCGTGGGCATCAGGTGC
CCGCCCCATCCCTAACCCTCTCCTCGGTCTCGATTACAAGGATGACGACGATAAGGCCCGCCCC
TGCATCCCTAAAAGCTTCGGCTACAGCTCGGTGGTGTGTGTCTGCAATGCCACATACTGTGACTC
CTTTGACCCCCCGACCTTTCCTGCCCTTGGTACCTTCAGCCGCTATGAGAGTACACGCAGTGGG
CGACGGATGGAGCTGAGTATGGGGCCCATCCAGGCTAATCACACGGGCACAGGCCTGCTACTG
ACCCTGCAGCCAGAACAGAAGTTCCAGAAAGTGAAGGGATTTGGAGGGGCCATGACAGATGCTG
CTGCTCTCAACATCCTTGCCCTGTCACCCCCTGCCCAAAATTTGCTACTTAAATCGTACTTCTCTG

AAGAAGGAATCGGATATAACATCATCCGGGTACCCATGGCCAGCTGTGACTTCTCCATCCGCACC
TACACCTATGCAGACACCCCTGATGATTTCCAGTTGCACAACTTCAGCCTCCCAGAGGAAGATAC
CAAGCTCAAGATACCCCTGATTCACCGAGCCCTGCAGTTGGCCCAGCGTCCCGTTTCACTCCTTG
CCAGCCCCTGGACATCACCCACTTGGCTCAAGACCAATGGAGCGGTGAATGGGAAGGGGTCACT
CAAGGGACAGCCCGGAGACATCTACCACCAGACCTGGGCCAGATACTTTGTGAAGTTCCTGGAT
GCCTATGCTGAGCACAAGTTACAGTTCTGGGCAGTGACAGCTGAAAATGAGCCTTCTGCTGGGC
TGTTGAGTGGATACCCCTTCCAGTGCCTGGGCTTCACCCCTGAACATCAGCGAGACTTCATTGCC
CGTGACCTAGGTCCTACCCTCGCCAACAGTACTCACCACAATGTCCGCCTACTCATGCTGGATGA
CCAACGCTTGCTGCTGCCCCACTGGGCAAAGGTGGTACTGACAGACCCAGAAGCAGCTAAATAT
GTTCATGGCATTGCTGTACATTGGTACCTGGACTTTCTGGCTCCAGCCAAAGCCACCCTAGGGGA
GACACACCGCCTGTTCCCCAACACCATGCTCTTTGCCTCAGAGGCCTGTGTGGGCTCCAAGTTCT
GGGAGCAGAGTGTGCGGCTAGGCTCCTGGGATCGAGGGATGCAGTACAGCCACAGCATCATCA
CGAACCTCCTGTACCATGTGGTCGGCTGGACCGACTGGAACCTTGCCCTGAACCCCGAAGGAGG
ACCCAATTGGGTGCGTAACTTTGTCGACAGTCCCATCATTGTAGACATCACCAAGGACACGTTTT
ACAAACAGCCCATGTTCTACCACCTTGGCCACTTCAGCAAGTTCATTCCTGAGGGCTCCCAGAGA
GTGGGGCTGGTTGCCAGTCAGAAGAACGACCTGGACGCAGTGGCACTGATGCATCCCGATGGC
TCTGCTGTTGTGGTCGTGCTAAACCGCTCCTCTAAGGATGTGCCTCTTACCATCAAGGATCCTGC
TGTGGGCTTCCTGGAGACAATCTCACCTGGCTACTCCATTCACACCTACCTGTGGCGTCGCCAGT
GA

9.2.4 Mito-GFP 1-10 construct

GCCGCCACCATGTCCGTCCTGACGCCGCTGCTGCTGCGGGGCTTGACAGGCTCGGCCCGGCG
GCTCCCAGTGCCGCGCGCCAAGATCCATTCGTTGTCCAAAGGAGAAGAACTGTTTACCGGTGTT
GTGCCAATTTTGGTTGAACTCGATGGTGATGTCAACGGACATAAGTTCTCAGTGAGAGGCGAAGG
AGAAGGTGACGCCACCATTGGAAAATTGACTCTTAAATTCATCTGTACTACTGGTAAACTTCCTGT
ACCATGGCCGACTCTCGTAACAACGCTTACGTACGGAGTTCAGTGCTTTTCGAGATACCCAGACC
ATATGAAAAGACATGACTTTTTTAAGTCGGCTATGCCTGAAGGTTACGTGCAAGAAAGAACAATTT
CGTTCAAAGATGATGGAAAATATAAAACTAGAGCAGTTGTTAAATTTGAAGGAGATACTTTGGTTA
ACCGCATTGAACTGAAAGGAACAGATTTTAAAGAAGATGGTAATATTCTTGGACACAAACTCGAAT
ACAATTTTAATAGTCATAACGTATACATCACTGCTGATAAGCAAAAGAACGGAATTAAAGCGAATTT
CACAGTACGCCATAATGTAGAAGATGGCAGTGTTCAACTTGCCGACCATTACCAACAAAACACCC
CTATTGGAGACGGTCCGGTACTTCTTCCTGATAATCACTACCTCTCAACACAAACAGTCCTGAGC
AAAGATCCAAATGAAAAAGGAACATAA

9.2.5 Mitochondrial targeted GBA1

ATGGAGTTTTCAAGTCCTTCCAGAGAGGAATGTCCCAAGCCTTTGAGTAGGGTAAGCATCATGGC
TGGCAGCCTCACAGGATTGCTTCTACTTCAGGCAGTGTCGTGGGCATCAGGTGCCCGCCCCTCC
GTCCTGACGCCGCTGCTGCTGCGGGGCTTGACAGGCTCGGCCCGGCGGCTCCCAGTGCCGCG
CGCCAAGATCCATTCGTTGGCCCGCCCCTGCATCCCTAAAAGCTTCGGCTACAGCTCGGTGGTG
TGTGTCTGCAATGCCACATACTGTGACTCCTTTGACCCCCCGACCTTTCCTGCCCTTGGTACCTT
CAGCCGCTATGAGAGTACACGCAGTGGGCGACGGATGGAGCTGAGTATGGGGCCCATCCAGGC
TAATCACACGGGCACAGGCCTGCTACTGACCCTGCAGCCAGAACAGAAGTTCCAGAAAGTGAAG
GGATTTGGAGGGGCCATGACAGATGCTGCTGCTCTCAACATCCTTGCCCTGTCACCCCCTGCCC
AAAATTTGCTACTTAAATCGTACTTCTCTGAAGAAGGAATCGGATATAACATCATCCGGGTACCCA
TGGCCAGCTGTGACTTCTCCATCCGCACCTACACCTATGCAGACACCCCTGATGATTTCCAGTTG
CACAACTTCAGCCTCCCAGAGGAAGATACCAAGCTCAAGATACCCCTGATTCACCGAGCCCTGCA
GTTGGCCCAGCGTCCCGTTTCACTCCTTGCCAGCCCCTGGACATCACCCACTTGGCTCAAGACC
AATGGAGCGGTGAATGGGAAGGGGTCACTCAAGGGACAGCCCGGAGACATCTACCACCAGACC
TGGGCCAGATACTTTGTGAAGTTCCTGGATGCCTATGCTGAGCACAAGTTACAGTTCTGGGCAGT
GACAGCTGAAAATGAGCCTTCTGCTGGGCTGTTGAGTGGATACCCCTTCCAGTGCCTGGGCTTC
ACCCCTGAACATCAGCGAGACTTCATTGCCCGTGACCTAGGTCCTACCCTCGCCAACAGTACTCA
CCACAATGTCCGCCTACTCATGCTGGATGACCAACGCTTGCTGCTGCCCCACTGGGCAAAGGTG
GTACTGACAGACCCAGAAGCAGCTAAATATGTTCATGGCATTGCTGTACATTGGTACCTGGACTT
TCTGGCTCCAGCCAAAGCCACCCTAGGGGAGACACACCGCCTGTTCCCCAACACCATGCTCTTT
GCCTCAGAGGCCTGTGTGGGCTCCAAGTTCTGGGAGCAGAGTGTGCGGCTAGGCTCCTGGGAT
CGAGGGATGCAGTACAGCCACAGCATCATCACGAACCTCCTGTACCATGTGGTCGGCTGGACCG
ACTGGAACCTTGCCCTGAACCCCGAAGGAGGACCCAATTGGGTGCGTAACTTTGTCGACAGTCC
CATCATTGTAGACATCACCAAGGACACGTTTTACAAACAGCCCATGTTCTACCACCTTGGCCACTT
CAGCAAGTTCATTCCTGAGGGCTCCCAGAGAGTGGGGCTGGTTGCCAGTCAGAAGAACGACCTG
GACGCAGTGGCACTGATGCATCCCGATGGCTCTGCTGTTGTGGTCGTGCTAAACCGCTCCTCTA
AGGATGTGCCTCTTACCATCAAGGATCCTGCTGTGGGCTTCCTGGAGACAATCTCACCTGGCTAC

TCCATTCACACCTACCTGTGGCGTCGCCAGGGCGACGGCGGCAGCGGCGGCGGCAGCCGGGA
CCACATGGTGCTGCACGAGTACGTGAACGCCGCCGGCATCACATGA

9.2.6 GBA1-GFP s11ß

ATGGAGTTTTCAAGTCCTTCCAGAGAGGAATGTCCCAAGCCTTTGAGTAGGGTAAGCATCATGGC
TGGCAGCCTCACAGGATTGCTTCTACTTCAGGCAGTGTCGTGGGCATCAGGTGCCCGCCCCTGC
ATCCCTAAAAGCTTCGGCTACAGCTCGGTGGTGTGTGTCTGCAATGCCACATACTGTGACTCCTT
TGACCCCCCGACCTTTCCTGCCCTTGGTACCTTCAGCCGCTATGAGAGTACACGCAGTGGGCGA
CGGATGGAGCTGAGTATGGGGCCCATCCAGGCTAATCACACGGGCACAGGCCTGCTACTGACC
CTGCAGCCAGAACAGAAGTTCCAGAAAGTGAAGGGATTTGGAGGGGCCATGACAGATGCTGCTG
CTCTCAACATCCTTGCCCTGTCACCCCCTGCCCAAAATTTGCTACTTAAATCGTACTTCTCTGAAG
AAGGAATCGGATATAACATCATCCGGGTACCCATGGCCAGCTGTGACTTCTCCATCCGCACCTAC
ACCTATGCAGACACCCCTGATGATTTCCAGTTGCACAACTTCAGCCTCCCAGAGGAAGATACCAA
GCTCAAGATACCCCTGATTCACCGAGCCCTGCAGTTGGCCCAGCGTCCCGTTTCACTCCTTGCC
AGCCCCTGGACATCACCCACTTGGCTCAAGACCAATGGAGCGGTGAATGGGAAGGGGTCACTCA
AGGGACAGCCCGGAGACATCTACCACCAGACCTGGGCCAGATACTTTGTGAAGTTCCTGGATGC
CTATGCTGAGCACAAGTTACAGTTCTGGGCAGTGACAGCTGAAAATGAGCCTTCTGCTGGGCTGT
TGAGTGGATACCCCTTCCAGTGCCTGGGCTTCACCCCTGAACATCAGCGAGACTTCATTGCCCGT
GACCTAGGTCCTACCCTCGCCAACAGTACTCACCACAATGTCCGCCTACTCATGCTGGATGACCA
ACGCTTGCTGCTGCCCCACTGGGCAAAGGTGGTACTGACAGACCCAGAAGCAGCTAAATATGTT
CATGGCATTGCTGTACATTGGTACCTGGACTTTCTGGCTCCAGCCAAAGCCACCCTAGGGGAGA
CACACCGCCTGTTCCCCAACACCATGCTCTTTGCCTCAGAGGCCTGTGTGGGCTCCAAGTTCTG
GGAGCAGAGTGTGCGGCTAGGCTCCTGGGATCGAGGGATGCAGTACAGCCACAGCATCATCAC
GAACCTCCTGTACCATGTGGTCGGCTGGACCGACTGGAACCTTGCCCTGAACCCCGAAGGAGGA
CCCAATTGGGTGCGTAACTTTGTCGACAGTCCCATCATTGTAGACATCACCAAGGACACGTTTTA
CAAACAGCCCATGTTCTACCACCTTGGCCACTTCAGCAAGTTCATTCCTGAGGGCTCCCAGAGAG
TGGGGCTGGTTGCCAGTCAGAAGAACGACCTGGACGCAGTGGCACTGATGCATCCCGATGGCT
CTGCTGTTGTGGTCGTGCTAAACCGCTCCTCTAAGGATGTGCCTCTTACCATCAAGGATCCTGCT
GTGGGCTTCCTGGAGACAATCTCACCTGGCTACTCCATTCACACCTACCTGTGGCGTCGCCAGG
GCGACGGCGGCAGCGGCGGCGGCAGCCGGGACCACATGGTGCTGCACGAGTACGTGAACGCC
GCCGGCATCACATAA

9.2.7 GBA1-ΔMTS

GAATTCGCCGCCACCATGGAGTTTTCAAGTCCTTCCAGAGAGGAATGTCCCAAGCCTTTGAGTAG
GGTAAGCATCATGGCTGGCAGCCTCACAGGATTGCTTCTACTTCAGGCAGTGTCGTGGGCATCA
GGTGCCCGCCCCTGCATCCCTAAAAGCTTCGGCTACAGCTCGGTGGTGTGTGTCTGCAATGCCA
CATACTGTGACTCCTTTGACCCCCCGACCTTTCCTGCCCTTGGTACCTTCAGCCGCTATGAGAGT
ACACGCAGTGGGCGACGGATGGAGCTGAGTATGGGGCCCATCCAGGCTAATCACACGGGCACA
GGCCTGCTACTGACCCTGCAGCCAGAACAGAAGTTCCAGAAAGTGAAGGGATTTGGAGGGGCCA
TGACAGATGCTGCTGCTCTCAACATCCTTGCCCTGTCACCCCCTGCCCAAAATTTGCTACTTAAAT
CGTACTTCTCTGAAGAAGGAATCGGATATAACATCATCCGGGTACCCATGGCCAGCTGTGACTTC
TCCATCCGCACCTACACCTATGCAGACACCCCTGATGATTTCCAGTTGCACAACTTCAGCCTCCC
AGAGGAACTGCAGTTGGCCCAGCGTCCCGTTTCACTCCTTGCCAGCCCCTGGACATCACCCACT
TGGCTCAAGACCAATGGAGCGGTGAATGGGAAGGGGTCACTCAAGGGACAGCCCGGAGACATC
TACCACCAGACCTGGGCCAGATACTTTGTGAAGTTCCTGGATGCCTATGCTGAGCACAAGTTACA
GTTCTGGGCAGTGACAGCTGAAAATGAGCCTTCTGCTGGGCTGTTGAGTGGATACCCCTTCCAG
TGCCTGGGCTTCACCCCTGAACATCAGCGAGACTTCATTGCCCGTGACCTAGGTCCTACCCTCG
CCAACAGTACTCACCACAATGTCCGCCTACTCATGCTGGATGACCAACGCTTGCTGCTGCCCCAC
TGGGCAAAGGTGGTACTGACAGACCCAGAAGCAGCTAAATATGTTCATGGCATTGCTGTACATTG
GTACCTGGACTTTCTGGCTCCAGCCAAAGCCACCCTAGGGGAGACACACCGCCTGTTCCCCAAC
ACCATGCTCTTTGCCTCAGAGGCCTGTGTGGGCTCCAAGTTCTGGGAGCAGAGTGTGCGGCTAG
GCTCCTGGGATCGAGGGATGCAGTACAGCCACAGCATCATCACGAACCTCCTGTACCATGTGGT
CGGCTGGACCGACTGGAACCTTGCCCTGAACCCCGAAGGAGGACCCAATTGGGTGCGTAACTTT
GTCGACAGTCCCATCATTGTAGACATCACCAAGGACACGTTTTACAAACAGCCCATGTTCTACCA
CCTTGGCCACTTCAGCAAGTTCATTCCTGAGGGCTCCCAGAGAGTGGGGCTGGTTGCCAGTCAG
AAGAACGACCTGGACGCAGTGGCACTGATGCATCCCGATGGCTCTGCTGTTGTGGTCGTGCTAA
ACCGCTCCTCTAAGGATGTGCCTCTTACCATCAAGGATCCTGCTGTGGGCTTCCTGGAGACAATC
TCACCTGGCTACTCCATTCACACCTACCTGTGGCGTCGCCAGGGCGACGGCGGCAGCGGCGGC
GGCAGCCGGGACCACATGGTGCTGCACGAGTACGTGAACGCCGCCGGCATCACATAA

9.3 Off-target Heidelberg (Stemmer et al., 2015)

Off-target sequence and PAM		position	Location
AAGGTGGTGTCTCTTCCCTACGG		Intergenic	FGF16
CAGTGTCTGTGTCTTCCCTAAGG		Intergenic	SRRM1
GAGCCAGTCTGTCTTCCCTATGG		Intergenic	NA
CATGCAATCTGTCTTCCCTAGGG		Intergenic	AC099791.1
AAGAGGGTGTGCCTTCCCTAAGG		Intergenic	RP1-159A19.3
CAAACGCTGTCTCTTCCCTAAGG		Exonic	NUDCD3
CAGGCGGTGTGTCTCCCCTAGGG		Exonic	GBA
CAGAAGTTGTTTCTTCCCTAAGG		Intronic	CDH4
CAGTAGGTCAGTCTTCCCTAGGG		Intergenic	RP11-448N11.1
CAGAGGGAGTTTCTTCCCTAAGG		Intronic	THSD4
TAAGCTGTGTGTATTCCCTAAGG		Intergenic	RGS4
CTGTCTGTGTGTCCTCCCTATGG		Intronic	ATP6AP1L
CCTGCGCTGTGTCCTCCCTAAGG		Intronic	RP11-619F23.2
CAGGTGTTGGATCTTCCCTAGGG		Intronic	RP11-839D17.3
CGGGCACTGTGTCCTCCCTATGG		Intronic	TMEM105
CGGGTGGGGTGTCCTCCCTAGGG		Intronic	RBFADN
CAGGCAGCGGGCCTTCCCTA	GGG	Intronic	THEM6
GAGGTGATGTGTCTTACCTA	AGG	Intronic	E2F2
CAGGAGGTGGGTCTTGCCTA	AGG	Intronic	RP11-236J17.6
CAGGGTATGTGTCTTTCCTA	TGG	Intergenic	AC134698.1
CAGGGGCTGGGTCTCCCCTA	GGG	Intronic	RP11-326I19.3
CTGGGGGTGTGCCTGCCCTA	GGG	Intergenic	HNRNPA1P23
CAGGCCTTGTGCCGTCCCTA	TGG	Intronic	CCDC37
CTGGCAGTGTGACTGCCCTA	TGG	Intergenic	RP11-114H21.2
AAGGAGGTGTGTTTCCCCTA	GGG	Intronic	SEMA4D
CATGAGCTGTGTCTTCTCTA	GGG	Intronic	ASTN2
CAGCAGGTGTGTTTACCCTA	TGG	Intergenic	KLF14
CAGGAGGGATGTCTTCACTA	GGG	Intronic	PTP4A1P7
GAGGAGGTGTGGCTTCACTA	GGG	Intergenic	CDK1
CAGGCGGGGTGCCTTCGCTA	GGG	Intronic	RP11-98L4.1
CAGGCCATGTTTCTTCGCTA	GGG	Exonic	WDR1
CAGCAGGTGTTTCTTCCTTA	TGG	Intronic	ABCC6
CAGGCCCTGTGTTTTCTCTA	GGG	Intergenic	RP11-323A7.1
CAGGTGGTCTGTCTTCCCCA	TGG	Intergenic	C1QL2
CAGGAGGAGGGTCTTCCTTA	AGG	Exonic	BBS9
CAGGGTGCGTGTCTTCCCCA	CGG	Intergenic	NA
CAGGGTGCGTGTCTTCCCGA	CGG	Intergenic	NA
CTGGCGCTGTGTCTGCTCTA	TGG	Intergenic	IGLC6
CAGGCACTATGTCTTCCCCA	AGG	Intronic	AC108142.1
CCGGCGGAGGGTCTTCCCCA	AGG	Intronic	IL33
GAGCTGGTGTGTCTTCCCTG	GGG	Intergenic	POLD2P1
CAGGGGCTGGGTCTTCCCCA	GGG	Intergenic	ZBTB32
CAGGTGGTGTGTCTCCCTTA	GGG	Exonic	GBAP1

CAGGCAATGAGTCTTCCCCA	GGG	Intergenic	AC016831.6
CAGGAGCTGTTTCTTCCCCA	GGG	Intronic	RP11-1134I14.4
GAGGGGATGTGTCTTCCCTG	AGG	Intronic	MEGF11
CAGGCAGTGTGTGTTCCCCA	CGG	Intergenic	RP11-1338A24.1
CAGTGTGTGTGTCTTCCCTG	TGG	Intronic	SDC1
CAAGCACTGTGTCTTCCCTC	TGG	Intronic	MYOF
CAAGAGGAGTGTCTTCCCTT	TGG	Intronic	RIC3
CAGCCGGGGTGTCTCCCTTA	GGG	Exonic	RP11-576I22.2
CAGGTGATGTGTTTTCCCCA	TGG	Intronic	EML5
CAGGGTGTTTGTCTTCCCTC	TGG	Intronic	KRT13
AAGGCAGTGTTTCTTCCCTC	AGG	Intronic	RP11-467L24.1
CTGGCTGTGTCTCTTCCCTT	TGG	Intronic	TTC39A
CAGGAAGTGTGTCTTGCATA	CGG	Intergenic	NA
CAGGAAGTGTGTCTTGCATA	GGG	Intergenic	NA
CAGGCCCTGAGTCTTCCCTG	AGG	Intronic	ZNF816
CCGGAGGTGTGGCTTCCCTG	TGG	Intronic	BBC3
CAGGGTGTGTGTCTGCCCCA	AGG	Intronic	CAMK2B
CAAGGGGTGTGTTTTCCCTT	GGG	Intronic	snoU13
GAGGCGTTGTGTCTTGCCCA	AGG	Intronic	RP11-67L3.2
CAGGAGGCGTGTTTTCCCTG	AGG	Intronic	SCN5A
CAGCCAGTGTGTCGTCCCTG	GGG	Exonic	IFNA12P
CAGGCTGAGTGTCTTACCTT	AGG	Intronic	FAM185A
CATGAGGTGTGTCTTCTCTT	TGG	Intronic	CLDN11
CAGGTGCTGTGTCTTCACTG	AGG	Intronic	TMEM143
CAGGCCGTGTGTCTTCCCGG	CGG	Intergenic	RP11-862G15.1
GAGGGGGTGTGTCTTCCCCT	TGG	Intronic	C1orf21

9.4 CRISPOR off-targets list (Concordet & Haeussler, 2018)

Off-target Sequence	Position and gene name
GAGGTGATGTGTCTTACCTAAGG	intron: E2F2
AAGAGGGTGTGCCTTCCCTAAGG	intergenic: FGR-RP1-159A19.3
CAGGCAGCGGGCCTTCCCTAGGG	intergenic: THEM6/CTD-2292P10.2-THEM6
GAGGGGATGTGTCTTCCCTGAGG	intergenic: MEGF11-MIR4311
CAGGCTGAGTGTCTTACCTTAGG	intron: FAM185A
CAGGCCCTGAGTCTTCCCTGAGG	intergenic: ZNF816-ZNF321P/ZNF816/ZNF321P-ZNF816-ZNF321P/ZNF816
CAGGAGGCGTGTTTTCCCTGAGG	intron: SCN5A
CAGGCGGTGTGTCTCCCCTAGGG	exon: GBA
AAGGTGGTGTCTCTTCCCTACGG	intergenic: FGF16-ATRX
CATGCAATCTGTCTTCCCTAGGG	intergenic: NFIA-AC099791.1
AAGGCGGTGTGATTTCTCTAAGG	intergenic: PSKH1-PSKH1/CTRL/CTC-479C5.12
GAGCCAGTCTGTCTTCCCTATGG	intergenic:RP11-174E22.2-PCDH7
CAGGCAATGAGTCTTCCCCAGGG	intergenic:AC016831.6-AC016831.7
GAGCTGGTGTGTCTTCCCTGGGG	intergenic: POLD2P1-NR2F1-AS1
TAGGCGGTGTGTCCTACCTGTGG	intergenic:RP11-65J21.1-RP11-65J21.4
CAAGAGGAGTGTCTTCCCTTTGG	intron: RIC3
CAAACGCTGTCTCTTCCCTAAGG	exon: NUDCD3

TAAGCTGTGTGTATTCCCTAAGG	intergenic:RP11-331H2.3-RGS4
CAAGGGGTGTGTTTTCCCTTGGG	intergenic: CCDC64-snoU13
CAGGTGTTGGATCTTCCCTAGGG	intron:RP11-839D17.3
CCGGAGGTGTGGCTTCCCTGTGG	intergenic: BBC3/MIR3191-BBC3
CAGAGGGAGTTTCTTCCCTAAGG	intron: THSD4
CGGGCACTGTGTCCTCCCTATGG	intron: TMEM105
CAGGTGCTGTGTCTTCACTGAGG	intron: TMEM143
CAGGCCCTGTGTTTTCTCTAGGG	intergenic:RP11-323A7.1-RP11-470F18.1
CAGGCTGTGTGCCTTTCCTGAGG	intergenic:RP11-469N6.1-RP11-555G19.1
CAGGAGGAGGGTCTTCCTTAAGG	exon: BBS9
CAGGCAGTCTGTATTCCTTAGGG	intergenic:RP11-459O1.2-RNGTT
CAGGCCGTGTGTCTTCCCGGCGG	intergenic: GOLGA5-RP11-862G15.1
CAGGAGGGATGTCTTCACTAGGG	intergenic: PTP4A1P7-PAPPA2
CTGGCTGTGTCTCTTCCCTTTGG	intron: TTC39A
CAGGGTATGTGTCTTTCCTATGG	intergenic:AC134698.1-RP11-643N23.2
CAGGAGGTGTTATTTCCCTATGG	intron: FOLR4
CAGGTGATGTGTTTTCCCCATGG	intron:EML5
CAGCAGGTGTGTTTACCCTATGG	intergenic: TSGA13-KLF14
CAGGCACTATGTCTTCCCCAAGG	intergenic:RP11-402C9.1/AC108142.1-MIR1305
GAGGAGGTGTGGCTTCACTAGGG	intergenic: CDK1-RHOBTB1
CAAGCACTGTGTCTTCCCTCTGG	intron: MYOF
CAGAAGTTGTTTCTTCCCTAAGG	intron: CDH4
CAGGTGGTGTGTCTCCCTTAGGG	exon: GBAP1
CAGTGTGTGTGTCTTCCCTGTGG	intron: SDC1
CAGGGTGCGTGTCTTCCCCACGG	intergenic: KRT8P17-RP11-3D23.1
AAGGAGGTGTGTTTCCCCTAGGG	intron: SEMA4D
CGGGTGGGGTGTCCTCCCTAGGG	intergenic: RBFADN-RP11-795F19.5/RBFADN
CAGGCCGTGTGACTTTCCTTTGG	intergenic:GM2AP1-RPL21P39
CAGTGTCTGTGTCTTCCCTAAGG	intergenic: SRRM1-CLIC4
CAGGGTGCGTGTCTTCCCGACGG	intergenic: KRT8P17-RP11-3D23.1
CAGTAGGTCAGTCTTCCCTAGGG	intergenic:RP11-448N11.1-RP11-448N11.2
CAGGTGGTCTGTCTTCCCCATGG	intergenic: MARCO-C1QL2
CATGAGCTGTGTCTTCTCTAGGG	intron: ASTN2
GAGGGGGTGTGTCTTCCCCTTGG	intron:C1orf21
AAGGCAGTGTTTCTTCCCTCAGG	intron:RP11-467L24.1
CCGGCGGAGGGTCTTCCCCAAGG	intron:IL33
CATGAGGTGTGTCTTCTCTTTGG	intergenic: SLC7A14/CLDN11-CLDN11
CAGGCTGTCTGCCTTCCCTCAGG	intron: PLIN4
CCTGCGCTGTGTCCTCCCTAAGG	intron:RP11-619F23.2
CAGCAGGTGTTTCTTCCTTATGG	intron: ABCC6
CAGCCGGGGTGTCTCCCTTAGGG	exon:RP11-576I22.2
CAGCCGGTGTGATTTCCCTCAGG	intergenic: CTB-95D12.1-RNA5SP199
CAGGCAGTGTGGCTTCACAATGG	intergenic:AL096864.1-NRG3
CAGGGGCTGGGTCTTCCCCAGGG	intergenic:AC002314.4-ZBTB32
CAGGGGCTGGGTCTCCCCTAGGG	intron:RP11-326I19.3
CAGGAGGTCTGTTTTCCCGAAGG	intron:AC090505.6
CAGGGGGTGAGTGTTCCCTGGGG	exon: CDH23
CAGACGGTGTCTGTTACCTACGG	intron:RP4-753D10.5
CTGTCTGTGTGTCCTCCCTATGG	intron: ATP6AP1L
CAGGTGGTTTTTATTCCCTATGG	intergenic: YPEL2-MIR4729

CAGGGTGTTTGTCTTCCCTCTGG	intergenic: KRT13-KRT13/AC019349.5
CAGGAAGTGTGTCTTGCATAGGG	intergenic: RNU6-184P-SURF6P1
CAGGAAGTGTGTCTTGCATACGG	intergenic: RNU6-184P-SURF6P1
CAGGAGGTGGGTCTTGCCTAAGG	intergenic:RP11-236J17.6/TUB-RP11-236J17.5
CAGGCGGAGAGTCTCCCCTCAGG	intergenic: GNA12-AC006028.11
CAGGAGCTGTTTCTTCCCCAGGG	intergenic: NDUFA5P12-RP11-1134I14.4
CAGGCTGTGTGTTTTTCCAAGGG	intergenic: SLC35B3-HULC
CAGGCGGGGTGCCTTCGCTAGGG	intergenic:RP11-98L4.1-HMGN1P33
CAGGCAGTGTGTGTTCCCCACGG	intergenic: CPZ/GPR78-RP11-1338A24.1
GAGGCGGTGTGAGTTTCCTAAGG	intergenic: SPARCL1-RP11-742B18.1
CTGGCAGTGTGACTGCCCTATGG	intergenic:RP11-114H21.2-CTB-1I21.1
GAGGCGTTGTGTCTTGCCCAAGG	intergenic:RP11-67L3.2-TTC22
CTGGGGGTGTGCCTGCCCTAGGG	intergenic: CASR-HNRNPA1P23
CAGGCGGTGTTTATTCTCCATGG	intron: PTPRT
CAGGCGGTGTGTCCCTCCTGGGG	intron: FAM120B
CAGGCTGTGTGTCCTGCCTTGGG	intergenic:AC090103.1-EBF2
CAGCCGGTGTTTCTCCCCAAAGG	intron: GRAMD4
CAGGCCATGTTTCTTCGCTAGGG	exon: WDR1
CAGGCAGTGAGTCTGCCCCAGGG	intron: FAM19A5
CTGGCGCTGTGTCTGCTCTATGG	intergenic: IGLJ6-IGLC6
CAGGAGGTGTGTCCTGCCCACGG	intergenic: CTB-60B18.17-CGB5
CAGGAGGTGTGTCCTGCCCATGG	intergenic: CGB-NTF6A
CAGGGTGTGTGTCTGCCCCAAGG	intron: CAMK2B
CAGGCGGTTTCTCTGCCCCAGGG	intergenic: NSG2-CTC-229L21.1
CAGGCGGTGGGTCTGGCCCAGGG	exon: CCDC155
CAGGCCTTGTGCCGTCCCTATGG	intron: CCDC37
CAGCCAGTGTGTCGTCCCTGGGG	exon: IFNA12P
CAGGAGGTGTGTAGTCCATAGGG	intergenic: RN7SKP191-RP11-112N13.1

10 Acknowledgments

First I would like to thank Michela for the chance to do my PhD in this interesting field. Furthermore, I would like to thank everyone that I met during the journey.

I would like to as well point out some unique people I met along the way and who became friends for life. The first one in the row is Silvia, who taught me many techniques in the lab and with whom I enjoyed hanging out during free time. Furthermore, I would like to specially thank Vasiliki for her support in every situation. I appreciate that I can count on both anytime. Steffi who was always a pleasure to work with.

Next I would like to thank all my friends, with whom I am not always in touch, but with whom it is always as no time passed since we last met.

I would like to thank Markus, an important person who went with me through heights and lows and my cute Mona that made me happy every day.

I would like to thank my whole family, that I see far too few times. I would like to specially thank my parents who enabled me studying in my dream destinations and helped in this way pave my future. I am grateful to have such supportive parents.